Fraunhofer IFAM

Universität Bremen

Scanning Kelvin Probe study of electrochemical delamination in adhesively bonded joints

Dissertation

approved for the degree of
Doctor in Engineering
– Dr.-Ing –

Faculty of Production Engineering
Department of Production Engineering
University of Bremen

by

Barbara Priscila Andreon

Bremen, November 2019

Fraunhofer IFAM

Universität Bremen

Scanning Kelvin Probe study of electrochemical delamination in adhesively bonded joints

Vom Fachbereich Produktionstechnik

der

Universität Bremen

zur Erlangung des Grades

Doktor-Ingenieur

genehmigte

Dissertation

von

Barbara Priscila Andreon

Bremen, November 2019

1. Referee

Prof. Dr. –Ing. Lucio Colombi Ciacchi

Universität Bremen - Faculty of Production Engineering (FB4)

Am Fallturm 1 | 28359 Bremen - Germany

2. Referee

Prof. Dr. Fabio La Mantia

Universität Bremen - Faculty of Production Engineering (FB4)

Wiener Straße 12 | 28359 Bremen - Germany

Day of the oral test: 21.10.2019

Eidesstattliche Versicherung

Hiermit versichere ich, Barbara Priscila Andreon, dass ich diese Arbeit ohne unerlaubte fremde Hilfe angefertigt habe, keine anderen als die von mir angegebenen Quellen und Hilfsmittel benutzt habe und die den benutzten Werken wörtlich oder inhaltlich entnommenen Stellen als solche kenntlich gemacht habe.

Bremen, 27.11.2019

Ort, Datum

Unterschrift

I would like to dedicate this doctoral dissertation to my beloved mother Kathia R. H. Andreon

Abstract

Adhesive bonding is a key technology for the construction of lightweight components and its interest in the industry is increasing due to the several advantages when compared to other joining technologies. A major concern is the long-term stability of adhesive joints, especially for metallic substrates exposed to corrosive media. The aim of this work is to investigate the delamination mechanisms occurring in a real closed adhesive joint geometry. To achieve this purpose, the potential distribution at the metal/polymer interface was measured by means of Scanning Kelvin Probe (SKP) through a thin layer of glass. Quantitative measurements of the delamination kinetics were performed, accompanied by XPS inspection of the fracture surfaces. The delamination rate was found to be hundred times slower than in an open joint geometry. Furthermore, the delamination-limiting step for the open joint is the transport of cations, whereas for the closed joint is limited by the ingress of oxygen along the interphase. The cathodic delamination was the mechanism taking place in both cases, however depending on the geometry of the closed joint also the anodic undermining mechanism was found to occur.

Keywords: Dispersion adhesives; Ageing behaviour; Lifetime prediction; Scanning Kelvin Probe; Cathodic delamination; Anodic undermining

Zusammenfassung

Die Klebtechnik ist eine Schlüsseltechnologie für die Herstellung von Leichtbauteilen und das industrielle Interesse an ihr steigt aufgrund der vielen Vorteile gegenüber anderen Fügetechnologien. Ein großer liegt in der Langzeitstabilität von Klebverbindungen, insbesondere für metallische Substrate, welche korrosiven Medien ausgesetzt sind. Ziel dieser Arbeit ist es, die Delaminationsmechanismen zu untersuchen, die in einer geschlossenen Klebverbindungsgeometrie auftreten. Zu diesem Zweck wurde die Potentialverteilung an der Metall-Polymer-Grenzfläche mittels Kelvinsonde durch eine dünne Glasschicht gemessen. Es wurden quantitative Messungen der Delaminationskinetik durchgeführt, begleitet von einer XPS-Inspektion der Bruchflächen. Die Delaminationsrate war dabei ca. 100 x langsamer als bei einer offenen Fugengeometrie. Darüber hinaus ist der Transport von Kationen der delaminationslimitierende Schritt für die offene Verbindung, während für die geschlossene Verbindung das Eindringen von Sauerstoff entlang der Interphase begrenzend ist. Die kathodische Delamination war der Mechanismus, der in beiden Fällen stattfand, aber abhängig von der Geometrie der geschlossenen Verbindung wurde auch der anodische Untergrabungsmechanismus festgestellt.

Stichwörter: Dispersionsklebstoffe; Alterungsverhalten; Lebensdauervorhersage; Kelvinsonde; Kathodische Delamination; Anodische Untergrabung

Acknowledgements

I would like to express my sincere gratitude to my advisor Prof. Dr. –Ing. Lucio Colombi Ciacchi for his immense support throughout the course of this work. I would like to thank Prof. Dr. rer. nat Bernd Mayer for the opportunity of developing this work at the Fraunhofer IFAM. I would like to thank Prof. Dr. Fabio La Mantia for his kind acceptance of the invitation to be part of this examination committee.

I am truly grateful to Dr. Peter Plagemann for all the time spent on discussions and sharing of ideas as well as his constant motivation and guidance, without which, this work would not have been possible. I am grateful to the technicians and researchers of the OE418 for their support and scientific inputs. Special thanks to Dr. Olga Yezerska for always helping with great scientific ideas and help for solving experimental issues and, of course, my thanks also go to all colleagues of the Corrosion Protection and Electrochemistry working group. My special thanks to Dr. Stefan Dieckhoff for providing me opportunities and resources allowing me to attend conferences and qualification trainings, which were relevant not only for this thesis but for my professional formation.

I would like to express my deepest gratitude to Dr. Welchy Leite Cavalcanti and to Dr. Michael Noeske for being my second family in Germany, for all the encouragement, trust and opportunities provided in a personal and professional level. Not to mention the great scientific support with key discussions and suggestions. I would like to thank Barbara Guenther for her assistance, patience and enthusiasm and for her great work. I would like also to thank my friend Vinicius Beber for his support with scientific writing.

I would like to thank the support and love of my family even from far away. My infinite gratitude to my parents, Kathia and Acacio, for giving me always the best since the day I was born and for making me believe in my dreams; to my sister Bianca and my brother Eduardo for their unconditional love. Special thanks to my boyfriend Esteban for being always there for me providing immense support, care and love.

Finally, I would like to thank the financial support of the Brazilian Government (National Council for Scientific and Technological Development-CNPq) in the frame of the Science without Borders Program (234307/2014-5).

Table of contents

List of Acronyms

Acronym	Definition
ASTM	American Society for Testing and Materials
BASF	Badische Anilin & Soda Fabrik
CAE	Constant Analyser Energy Mode
CPD	Contact Potential Difference
DIN	Deutsches Institut Für Normung
DVS	Dynamic Vapour Sorption
ISO	International Organization for Standardization
LSCM	Laser Scanning Confocal Microscopy
MFFT	Minimum Film Formation Temperature
SAE	Society of Automotive Engineers
SHE	Standard Hydrogen Electrode
SKP	Scanning Kelvin Probe
Tg	Glass Transition Temperature
WA	Thermodynamic Work of Adhesion
XPS	Photoelectron Spectroscopy

List of Figures

List of Tables

1. INTRODUCTION

1.1. BACKGROUND

Adhesive bonding has nowadays become a key technology for the production of new products made of heterogeneous materials, most notably in the aerospace, automotive, construction, and electronics industry sectors (Silva et al. 2011a; Pethrick 2014; Silva und Sato 2013). In comparison with other joining methods, the main advantages of adhesive bonding are its ability to bond dissimilar materials, to guarantee an efficient load transfer, and to preserve the integrity of the joined parts (as opposed, e.g. to riveting (Adams 2005; Beber et al. 2017)). In addition, adhesive bonding is in many cases the most convenient and cost-effective joining technique and, in fact, the bonding process can often be automated.

Several industrial applications require the adhesive joint to withstand mechanical loads under harsh environmental conditions, such as high moisture, or extreme temperatures. Predicting the lifetime of adhesively bonded joints in such environments is crucial to tailor their properties for the respective application demand, and the performance and durability of an adhesive bond is critically dependent on its quality and environmental stability (Pethrick 2014; Kinloch 1982). The loss of strength in a joint might occur, for instance, due to hydrodynamic displacement of adhesive from the substrate, adhesive plasticization, or substrate corrosion (Lu et al. 2011; Kinloch et al. 2007). Once a deep fundamental understanding of the physical and chemical phenomena that may lead to bond degradation is achieved, interphases between adhesively bonded materials can be designed with increased stability and decreased complexity.

A major concern is, in particular, the long-term loss of mechanical performance of adhesive joints between metallic substrates exposed to aqueous environments. Studies revealed that the interphase between the substrate and the polymeric adhesive is susceptible to corrosive attack (Kropka et al. 2015; Kinloch et al. 2000; Weiss et al. 2016). Investigations on the degradation of adhesive joints exposed to moisture are typically performed by means of salt spray or immersion tests followed by destructive mechanical testing methods with different joint geometries, e.g. peel test, single-lap shear test and wedge test (Zhang et al. 2013; Sørensen et al. 2010a; Kinloch et al. 2007; Abrahami et al. 2017; Brémont und Brockmann 1996). These mechanical tests are sometimes accompanied by analytical methods, such as X-ray photoelectron spectroscopy and electron microscopy techniques, which are great tools to identify the locus of joint failure and the mechanisms of environmental attack (Brémont und Brockmann 1996). Gravimetric methods are also common for bulk polymer and joint specimens

(Al-Harthi et al. 2007). However, in the latter the accuracy is poor (due to the very low adhesive/substrate mass ratio) and no local information is obtained as the whole joint is measured (Weiss et al. 2016).

The delamination mechanisms of organic coatings from metals are well understood as a result of studies using the scanning Kelvin probe (SKP) technique (Leng et al. 1998a; Posner et al. 2010; Nazarov et al. 2018; Leng et al. 1998c, 1998e), which is a powerful tool developed three decades ago by Stratmann *et al.* (Stratmann et al. 1991). This technique detects and follows the delamination of a coated metal in a non-contact and non-destructive manner, with a high spatial resolution (McMurray und Williams 2002; Wicinski et al. 2016). SKP enables the measurement of the potential distribution at a metallic surface even through an insulating material such as a polymer coating. In principle, the Kelvin probe measures the Volta potential difference between a sample and a reference using the vibrating condenser method. The measured potential differences are determined by the electrode potentials in the interfacial region, thus changes at the interface such as the ingression of ions or changes in the oxide/hydroxide structure of metal surfaces can be detected. The theory behind the SKP technique has been described elsewhere in detail (Grundmeier und Stratmann 2005).

This technique, however, has not yet been used for closed joint geometries, in which an adhesive film is sandwiched between two solid substrates, which block the diffusion of moisture and gases along directions perpendicular to the joint's plane. In this case, the geometric constraints strongly influence both the hardening process and possible chemical degradation mechanisms of the substrate/adhesive interphases. The transport kinetics of hydrated alkali ions along a closed adhesive/iron interphase has been studied with SKP by Wapner *et al.* (Wapner et al. 2006). Here, an aluminum foil has been used as a second substrate, which was chemically removed in order to allow the SKP measurements to be performed.

In this work, we present a novel application of SKP to investigate the delamination kinetics of closed adhesive joint geometries *in situ*, using a similar approach as for the delamination of coatings (Leng et al. 1998c). In order to probe with SKP the local interfacial potentials at a buried metal/metal-oxide/polymer interphase, a second substrate made of thin borosilicate glass is employed. This does act as a diffusion barrier layer, but still allows SKP measurements to be performed. However, the interpretation of the measured Volta potentials is not straightforward, since the electrostatic charging, thickness, and relative permittivity of the barrier layer must be taken into account (Salerno und Dante 2018; Orihuela et al. 2017). In addition to SKP measurements, chemical details of the delamination mechanisms taking place at the interphase

are analyzed a posteriori by means of X-ray photoelectron spectroscopy (XPS), after the removal of the adhesive layer.

1.2. STATE OF THE ART

In this chapter a comprehensive literature review is presented regarding the following topics: adhesive bonding technology (**Section 1.2.1**), water uptake on polymers (**Section 1.2.2**), de-adhesion processes (**Section 1.2.3)**, and scanning Kelvin probe technique (**Section 1.2.4)**.

1.2.1. Adhesive bonding technology

Adhesively bonded joints are an increasing alternative to mechanical joints in engineering applications. The main advantages of adhesive bonding over conventional mechanical fasteners are for instance, the capability of joining different materials and complex-shaped components, more efficient load transfer, no damage to the substrate materials, function integration such as optimised corrosion and sealing properties. On the other hand, as any technology, adhesive bonding shows some limitations which include: reduced long-term resistance due to ageing mechanisms, the difficulty to predict the lifetime, the requirement of surface preparation and, fixture devices are often needed during the waiting period for operating strength (Adams et al. 1997). For metallic materials, adhesive bonding is an indispensable industrial technology, especially in the construction of aircrafts and cars. However, there are still important technological problems which are left unsolved, including the loss of adhesion strength in the presence of humidity and corrosive media and lack of non-destructive testing (Silva und Sato 2013).

According to the norm DIN EN 923 (DIN EN 923) an adhesive is “a non-metallic substance which can join two substrates together via bonding to the substrate surfaces (adhesion) and via its own internal strength (cohesion)”. Adherends are the substrates which are joined by the adhesive. The elements of an adhesively bonded joint are shown in Figure 1.1. The adhesive layer comprises the bulk area and the so-called interphase, which has different structure when compared to the bulk due to the interactions with the substrate.

Figure 1.1 - Elements of an adhesively bonded joint

The interphase is a region with finite volume and a distinct physical gradient in properties (Leidheiser und Deck 1988). Its structure and mechanical properties also differ both from the adherend and from the adhesive (Lee 1994). The interphase between the bulk adhesive and substrate might be composed by different constituents, such as oxide layer from the metallic substrate, adsorbed water and contaminants, a layer of low-molecular constituents, which is also called a "weak-boundary layer" (Habenicht 2006) and a layer in which the functional groups of the adhesive adhere to the oxide layer of the metal. The model of the interphase used in this work is shown in Figure 1.2.

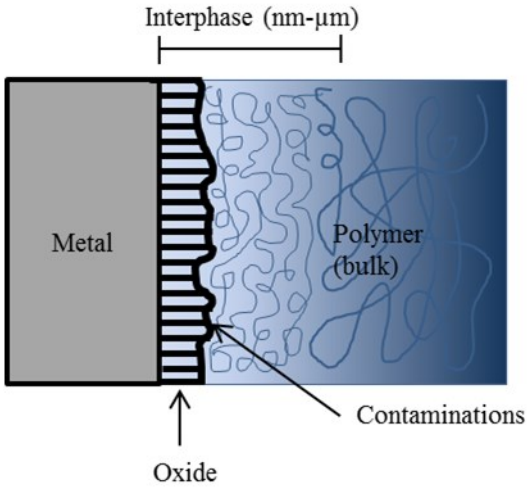

Figure 1.2 - Polymer/oxide/metal interphase. Adapted from (Lee 1994)

Adhesion and cohesion forces

The binding forces in adhesive bonds can be differentiated in adhesion and cohesion forces. Cohesion describes the sum of all individual forces inside an adhesive or adherend that hold them together, the stronger the inner cohesion of the molecules stronger are the materials. Adhesion is the sum of all individual forces that act between the surfaces of two different materials that hold them together.

The binding forces arise due to different types of interactions in and between condensed phases. It distinguishes between chemical bonds, physical interactions, and mechanical interlocking. Mechanical interlocking is understood as the mechanical anchoring that results from the penetration of the liquid adhesive into depressions in the substrate and subsequent hardening. Chemical bonds include covalent, ionic and metallic bonds. The physical interactions, include the Van der Waals forces (dipole, induction, and dispersion forces) (Habenicht 2006).

Theories of adhesion

Adhesion is one of the main factors acting on the strength of an adhesive joint since interactions involving adhesion are stronger than the cohesive strength of the adhesive (Adams et al. 1997). Several models are available to explain the phenomenon of adhesion, which in practice always occur in combination. Some of the known adhesion theories are summarised below:

- Mechanical adhesion model: this theory assumes that the adhesive penetrates into the pores or unevenness of the substrate and forms a positive connection after curing. The mechanical interlocking prevents the adhesive from detaching from the substrate. Thus, the mechanical theory is commonly related to the effect of surface roughness on the adhesion strength.
- Diffusion theory (Vojuckij 1963): this model is explained based on the micro-Brownian molecular motion. Adhesion only occurs when molecules or molecular segments have sufficient energy to diffuse into the respective joining partners. The interdiffusion will depend on the chain mobility and polymer compatibility. The diffusion theory can explain the adhesion to non-polar phases.
- Electrostatic theory (Derjaguin und Smilga 1967): this theory describes that a difference in the thermodynamic potential between the polymer and metal leads to carrier-state diffusion in the boundary layer. A so-called electric double layer forms between the donor and the acceptor, which is held responsible for the adhesion.
- Polarization theory: in this theory, it is assumed that both contact surfaces have polar groups that cause the adhesion of a bond via dipole interactions (Habenicht 2006). In addition to the dipole interactions, hydrogen bonds can form between polymers and the oxide layers on metals, which can be characterized by the acid-base interactions. With the help of the de Bruyne polarization model, however, adhesion to non-polar substrates cannot be explained.
- Thermodynamic theory: the basis for this theory is that the adhesion is considered as a wetting process on surfaces. The surface energy is the most important parameter, which

may be defined as the excess energy at the surface of a material compared to the bulk, or it is the work required to build an area of a particular surface. Extensive and fundamental investigations have been carried out (Zisman 1963; Fowkes 1964; F. M. Fowkes, in R. L. Patrick, 1967; Good 1975, 1964) with the aim of accurately determining the specific surface and interfacial energies of the contacting phases.

- Chemical Adhesion Theory: according to this theory covalent bonds are formed at the interfaces in addition to the physical, intermolecular forces (van der Waals forces). An interesting addition to the chemical adhesion model is the so-called micro-electrolyte model. Here, the potentials of metals is used as a basis to describe the processes taking place at the phase boundary between positively and negatively charged ions. Bishof et al. (Bischof et al. 1989) assume that micro-electrolytes form on surfaces with negative electrode potentials due to adsorbed water, since metal ions go into solution.

Water dispersion adhesives

Waterborne adhesives currently represent the largest consumed type of adhesive, representing about 49% of overall worldwide demand in terms of tonnage (Ceresana 2017; Silva et al. 2011b). Emulsion polymerization is used to prepare water dispersion adhesives, mostly made of acrylics, chloroprene, and polyvinyl acetate. The water solvent needs to be absorbed or evaporated for bonding, on nonporous substrates water usually must be removed prior to bonding (Silva et al. 2011b).

In addition to its value in terms of safety, toxicity and environment, water dispersion adhesives present some advantages, such as low cost, long shelf life, good solvent resistance, non-flammability, high molecular weight dispersions with high solids content and low viscosity. On the other hand, they have slow curing, limited heat resistance, poor creep and water resistance. Water can adsorb at the substrate surface and form layers with no cohesion. Furthermore it can accumulate near the polar groups of polymer joints, weakening the adhesive interactions and potentially lead to the deterioration in the long term through hydrolysis, for instance. The ability of the water dispersion-based adhesives to solve safety and protection of the environment problems, and the inherent challenges due to the use of dispersions, is leading to highly active research, both theoretical and applied (Silva et al. 2011b).

Acrylic adhesives

In this work, one technically relevant aqueous dispersion of a styrene acrylic copolymer is investigated. Copolymers of hydrophobic monomers like styrene, alkyl acrylates, acrylonitrile, and small amounts (1-10%) of polar unsaturated carboxylated monomers are the products of commercial interest due to their applications in paints and adhesives (Bajaj et al. 1994; Mathakiya et al. 2001). Generally, the emulsion or the emulsifier free-emulsion polymerization technique is used for synthesizing the above-mentioned acrylic copolymers (Shouldice et al. 1994). The molecular structure of monomers for the synthesis of styrene-acrylic copolymer are shown in the figure below (Figure 1.3).

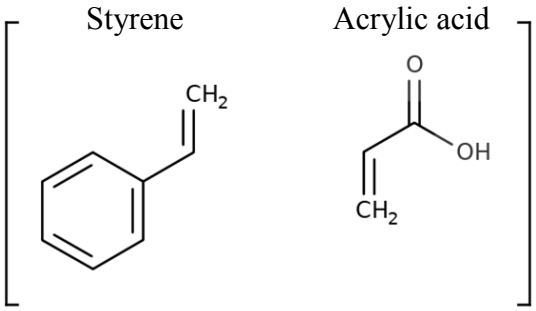

Figure 1.3 – Monomers styrene and acrylic acid

The binder in water-reducible acrylic resin polymeric materials is dispersed in water. After application, the liquid is converted to a dry (*i.e.*, solid) film. The chemical and physical changes that occur in this process are called film formation. The film formation takes place by evaporation of water and coalescence (fusion) of the dispersed binder particles. For a given polymer, the lowest temperature at which coalescence occurs sufficiently to form a continuous film is called its minimum film formation temperature (MFFT). This process is irreversible, *i. e.* these films are not water soluble after drying. The drying time depends on the air movement, the relative humidity and the temperature (Wicks 2007)(DIN EN ISO 12944-5).

The film formation mechanism is divided into three overlapping steps:

i) Evaporation of water and water-soluble solvents that leads to a close packed layer of polymeric particles,

ii) Deformation of the particles from their spherical shape that leads to a more or less continuous but weak film,

iii) Coalescence a relatively slow process in which the polymer molecules interdiffuse across the particle boundaries and entangle, strengthening the film.

Failure modes of adhesively bonded joints

Adhesive joints may fail adhesively or cohesively. The types of failure modes can be classified as shown in Figure 1.4. Adhesive failure occurs at the interface between adhesive and adherend, whereas cohesive failure occurs within the adhesive layer, allowing adhesive to remain on both adherend surfaces. A combination of adhesive and cohesive failure is classified as mixed failure. Furthermore, cohesive failure of the substrate can occur; in this case the adherend fails before the adhesive. The ideal failure is a 100% cohesive failure in the adhesive layer (Ebnesajjad und Landrock 2015).

The type of failure is strongly dependent on the adhesive type, adherend type and its surface state, type of loading and environmental conditions. The analysis of the failure mode can be extremely useful tool in determining whether the failure was due to weak boundary layer or due to improper surface preparation, for instance. Nevertheless, the failure mode should not be the only criterion for a stable joint; the ultimate joint strength is generally the most important criterion to be considered.

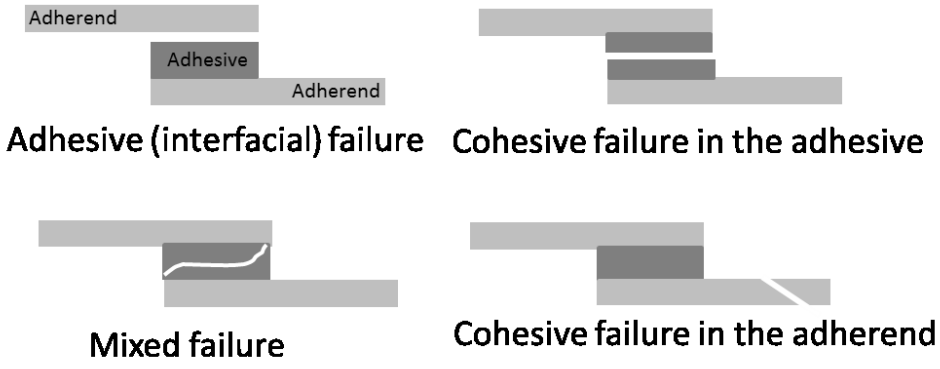

Figure 1.4 - Failure modes of adhesively bonded joints

Design of adhesive joints

The ultimate joint strength is highly dependent on the geometry of the joint. Design guidelines can increase the joint strength by minimizing the stress concentrations, e.g. use a thin adhesive layer, use a large bonded area and inclusion of a spew fillet (see Figure 1.5).

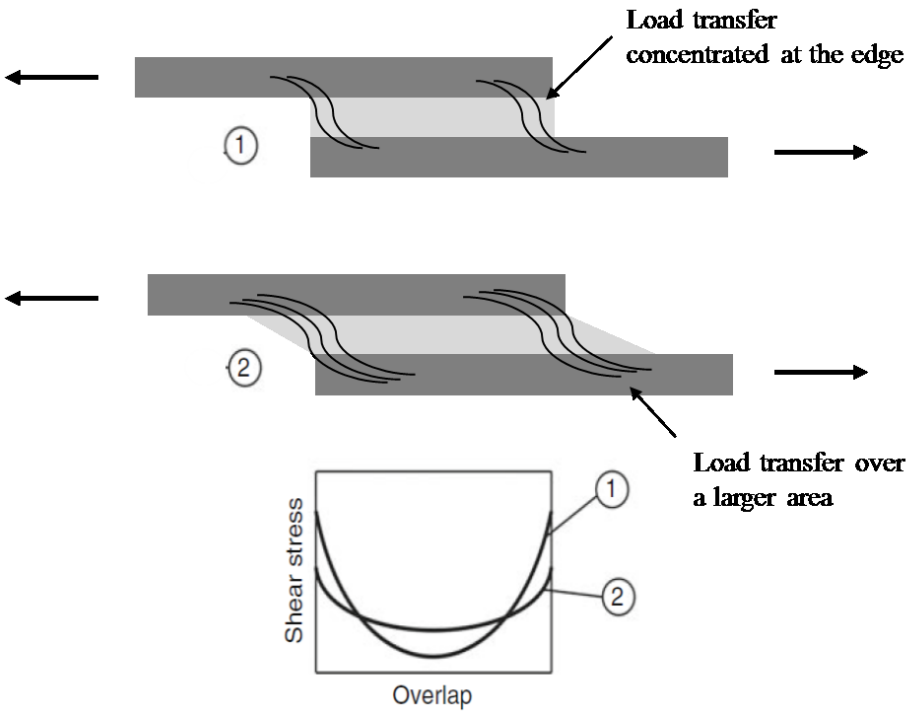

Figure 1.5 – Load transfer and shear stress distribution in single-lap joints with and without fillet

The fillet is especially interesting for this work because it can be useful in the design of joints that are exposed to corrosive environment, improving the corrosion resistance of the joint. One example of the functionality of the fillet is shown in Figure 1.6 where, besides increasing the joint strength, it prevents water to accumulate at the joint edges.

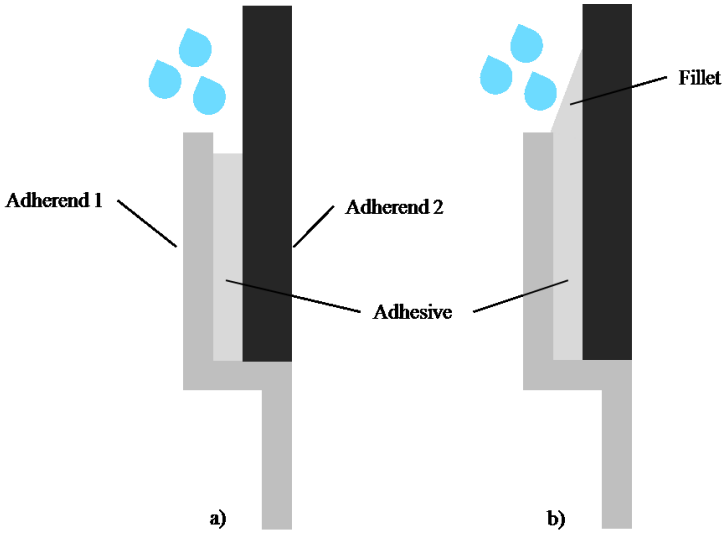

Figure 1.6 – Example of joint design in corrosive environment - a) without fillet and b) with fillet

1.2.2. Water uptake in polymers

A major limitation encountered in the use of adhesives is the damaging effect that moisture may have upon the strength of a bonded joint (Kinloch 1982). Moisture ingress during service is believed to be responsible for several examples of premature joint failure. Water can be transported either by bulk diffusion or along an interphase (Silva et al. 2011b). Considering the materials (polymer and metallic substrates), geometries (open and closed joint geometries) and environmental conditions (humidity and aggressive media) studied in this work, it is relevant to discuss about the water uptake not only on adhesives joints but also on coated metals. Furthermore, the literature available on the mechanisms of degradation of coatings can be used as base for understanding the processes occurring in a joint. Therefore, the following sections summarize the effects of water and possible electrochemical processes occurring in a bulk polymer and at the interphase between polymers and metals.

General concept of ageing

Ageing is the totality of all irreversible chemical and physical processes in a material over the course of time . Operating environmental factors (*e. g.* heat and moisture) are capable of degrading an adhesive joint in various ways. The combined effect of such factors acting on a joint leads to a synergistic result of reducing the joint strength (Habenicht 2016). Ageing may affect cohesive and/or adhesive interactions in a bonded structure and different ageing mechanisms can occur:

i. mechanical ageing (environmental stress cracking, creeping, fatigue),
ii. chemical ageing (thermal ageing, photo-oxidation, chemical degradation),
iii. corrosion,

(chemical ageing and corrosion may overlap to a great extend) (Habenicht 2006).

Effect of water in bulk adhesive

Absorbed water may affect the material in several ways:

- dimensional changes (swelling),
- reduction in the glass transition temperature, T_g,
- reduction of mechanical and physical properties (*i. e.* stiffness, strength and hardness).

The penetration of moisture is one of the strongest damaging mechanism for ageing of adhesive bonds (Habenicht 2006). One can distinguish between migration by capillary forces and

diffusion. The first occurs due to the existence of cracks, pores and crevices inside de adhesive. The diffusion into a polymer can be described by the one-dimensional case of the second Fick's law in the following form:

Equation 1

$$\frac{\partial c}{\partial t} = D\left(\frac{\partial^2 c}{\partial x^2}\right)$$

with c = concentration, D = diffusion coefficient, x= distance inside the polymer and t = time.

The diffusion of water in polymers obeys the Arrhenius relation, which means that the rate of diffusion increases strongly with temperature (Silva et al. 2011b; Dillard 2010):

Equation 2

$$D(T) = D_0^{\,-E_a/RT}$$

where: D_0 a constant pre-exponential factor (at infinite temperature; in m^2/s),

T temperature in (K),

R gas-law constant, 8.31446 (J/(mol·K)),

E_a activation energy for diffusion (in J/mol).

The moisture uptake of the adhesives is strongly dependent on the type of polymer. For instance, typical values of D are in the range of $3x10^{-13}$ to $5x10^{-12}$ m^2s^{-1} for epoxy resins (Ding et al. 2001; Al-Harthi et al. 2007; Legghe et al. 2009).

Effect of water at the interphase

It is often observed that, while the locus of failure of well-prepared joints is by cohesive fracture in the adhesive layer, after environmental attack an interfacial failure is commonly observed between the adhesive (or primer) and substrate (Kinloch 1982). This highlights the importance of the interphase when considering environmental failure mechanisms. The thermodynamic work of adhesion, W_A, required to separate unit area of two phases forming an interface may be related to the surface free energies by the Dupre equation (Kinloch 1980). The reversible work of adhesion, WA, in an inert medium may be expressed by

Equation 3

$$W_A = \gamma_a + \gamma_b - \gamma_{ab},$$

where γ_a and γ_b are the surface energies of the two phases and γ_{ab} is the interfacial free energy. In the presence of a liquid (L), the work of adhesion, W_{AL}, is

Equation 4

$$W_{AL} = \gamma_{aL} + \gamma_{bL} - \gamma_{ab}.$$

For a polymer-substrate interface the work of adhesion, W_A, in an inert atmosphere, is usually a positive value, suggesting thermodynamic stability of the interface. However, in the presence of a liquid the thermodynamic work of adhesion, W_{AL}, may be a negative value and this provides the driving force for the displacement of the adhesive from the substrate surface by the liquid. Thus, knowing the terms W_A and W_{AL} may enable the prediction of the environmental stability of the interface (Kinloch 1980, 1982). It has to be noted that the thermodynamics stated in Equation 3 and Equation 4 do not consider chemisorption, interdiffusion and mechanical interlocking.

In the situation of a metallic substrate, when the water is present at the metal/polymer interface and contains sufficient number of molecules to have the properties of bulk water, the conditions exist for the electrochemical reactions to occur that are involved in a corrosion process. The electrochemical de-adhesion processes which might occur at a metal/polymer interface are discussed in the following sections.

1.2.3. De-adhesion Processes

De-adhesion processes at polymer/oxide/metal interfaces are generally connected to the interfacial ingress of water and hydrated ions. For instance, water molecules adsorbed on the oxide surface can substitute electrostatic interactions and thereby reduce the adhesion between the polymer and the substrate (Posner et al. 2011).

In the literature (McCafferty 2010), three possible modes of failure for the de-adhesion, or delamination, of coatings are recognized.

(i) The dissolution of the oxide film in the formed local alkaline environment,
(ii) the degradation of the polymer in the local alkaline environment, and
(iii) loss of adhesion at the organic coating/oxide-coated metal interface.

The locus of failure occurs, respectively, within the oxide, within the polymer or at the oxide/polymer interface. Figure 1.7 represents the different planes in the interfacial regions of

a metal/organic polymer system. The type of electrochemical de-adhesion process and the plane along which delamination occurs is a function of the system and the environmental conditions.

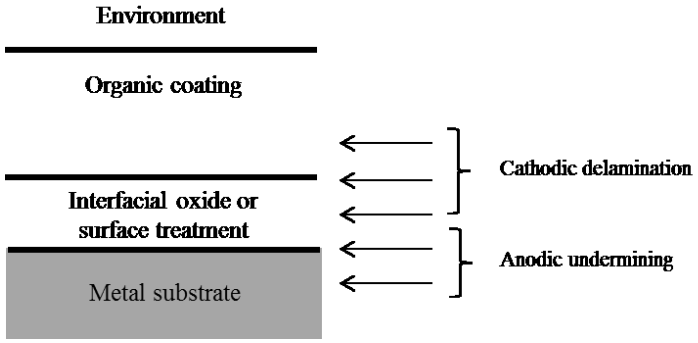

Figure 1.7 - Planes along which de-adhesion of an organic coating may occur. Adapted from (Leidheiser 1982)

Considering the adhesion at a metal/polymer interface in the sense of a chemical definition of adhesion, a loss of adhesion can be interpreted as a bond breaking at the interface. Depending on the prevailing adhesion mechanism at the interface, this may occur, for example, by displacement of adsorbed species by water, by mechanical forces, or by chemical or electrochemical reactions.

An essential prerequisite for electrochemical damage at room temperature is the presence of corrosive media (e.g. water containing ions, oxygen) in combination with a reactive metal substrate (e.g. iron, zinc, aluminium). In the case of a metal/polymer joint, it is necessary that mobile charge-bearing species can first advance to the interface and, as a consequence, cause a reaction at the metal surface, which may require the possibility of electron transfer reactions or ion transfer reactions at the interface.

Electrochemical processes occurring on the substrate and at the interphase can also have an influence on the strength of adhesively bonded parts. For instance, the contact of adhesively bonded steel samples with salt water or salt spray or with electrically conductive adhesives bonded with metals has been able to document the existence of corrosion (Gledhill und Kinloch 2006). On the surface of aluminium and aluminium alloys, hydrolysis of the oxide layer was observed as water penetrated at the bondline. The resulting hydroxides have a very low strength and in many cases this leads to failure of the adhesive bond (Kinloch et al. 2000; Venables 1984; Davis et al. 1995).

In the following, cathodic delamination, anodic undermining and crevice corrosion are described. These electrochemical mechanisms may occur among the conditions used in this work (e.g. room temperature, corrosive media, iron substrates).

Cathodic delamination

Electrochemical reactions occurring at the substrate/electrolyte and substrate/polymer interfaces of coated and bonded metals are responsible for the cathodic delamination and this mechanism is usually dominant on iron, steel, and zinc substrates. When an electrolyte reaches a metallic substrate, e.g. through a defect in a coating, the transport of hydrated ions along a polymer/oxide/metal interface might be observed in humid air. The rate of delamination is determined by the transport of oxygen and water across the polymer, or electrolyte cations along the metal/polymer interface (Leidheiser et al. 1983).

The proposed model for delamination is shown in Figure 1.8, explaining the formation of the galvanic element (Leng et al. 1998d). According to this model, at the uncoated steel the metal dissolution predominates and shows more negative potentials (local anode) whereas at the intact zone under the polymer metal dissolution and oxygen reduction are strongly inhibited and potentials are more positive due to an increase in Fe^{2+} states within the oxide layer. Within the delaminated zone only oxygen reduction takes place (local cathode), the hydroxide species generated increase the pH of the interface and cations are transported from the defect to the delaminated area for charge compensation.

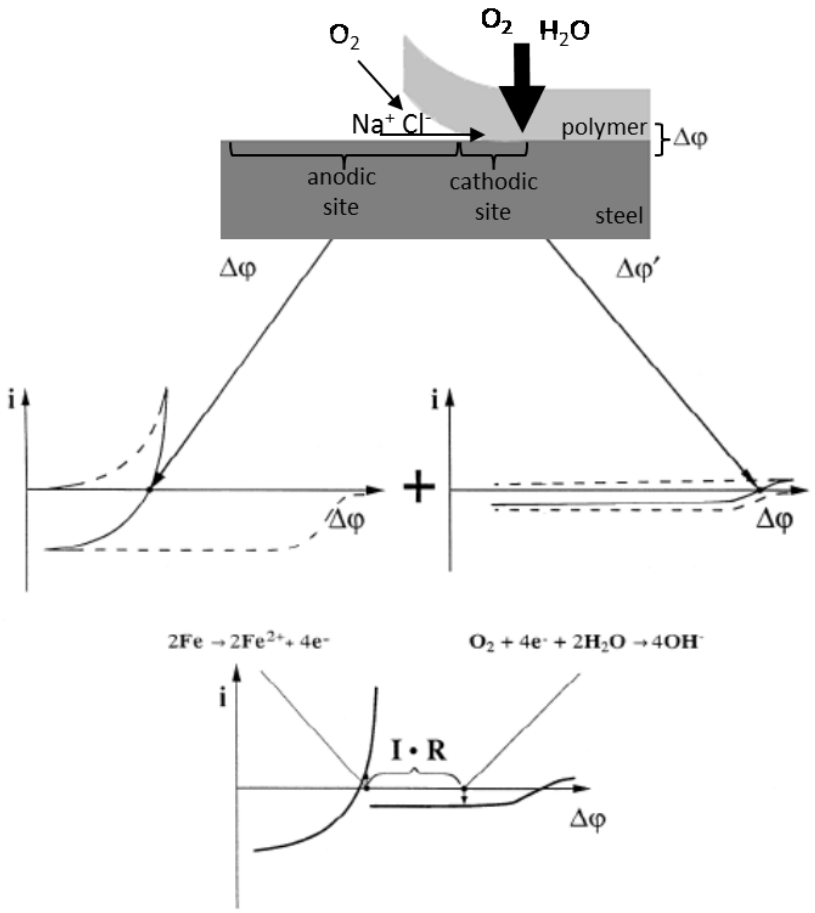

Figure 1.8 – Cathodic delamination model. Adapted from (Leng et al. 1998d)

The alkaline pH at the interface will stabilize (e.g. iron) or destabilize (e.g. zinc) the oxide layer under the delaminated zone. The de-adhesion of the polymer is usually explained by chemical bond breaking between polymer and metal oxide. It is believed (Wroblowa 1992; Grundmeier et al. 1998) that reactive intermediates are formed during oxygen reduction, such as $^{-}O_2H$, OH and $^{-}O_2$ which might degrade the polymer. The following reaction scheme for the oxidative degradation of the organic coating by reactive intermediates of oxygen reduction was postulated:

Chain start: $$O_2^- + R - H \rightarrow R^{\cdot} + HO_2^-$$

Chain reaction: $$R^{\cdot} + O_2 \rightarrow ROO^{\cdot}$$

$$ROO^{\cdot} + R - H \rightarrow ROOH + R^{\cdot}$$

Anodic undermining

In general, most of the failure at a polymer/metal interface are due to cathodic delamination and anodic undermining starting from a mechanical defect at the polymer (Fürbeth und Stratmann

2001b, 2001c). Cathodic delamination usually takes place under immersions conditions whereas anodic undermining or filiform corrosion occurs under atmospheric corrosion exposures (Watson et al. 2014; Bautista 1996; Leblanc und Frankel 2004). Furthermore, the nature of the electrolyte can lead to an alternative change of the corrosion delamination mode, cathodic delamination will tend to occur under high water electrolyte thickness and high ionic species concentration, whereas anodic undermining will take place in the case of low surface contamination and under thin water layers (Nazarov und Thierry 2010).

Anodic undermining can be a major type of failure for coated steel, it occurs when the potential at the defect is higher than under the intact polymer and is influenced by precipitation of corrosion products, humidity and salt deposition. This type of delamination represents the class of corrosion reactions underneath an organic coating in which the major separation process is the anodic corrosion reaction occurring under the coating. Galvanic effects and principles which apply to crevice corrosion provide a suitable explanation for observed cases of anodic undermining (Leidheiser 1982). Generally, it is agreed that differential aeration cells are created and maintained (Watson et al. 2014; Saraby-Reintjes 1972).

While cathodic delamination is interpreted in terms of cationic transport from defect towards the intact coating, anodic undermining is interpreted as a form of metal or metal oxide dissolution beneath the coating, which involves transport of the anion. Both mechanisms can be the result of a differential aeration cell. According to Nazarov *et al.* (Nazarov et al. 2018) anodic undermining requires the formation of differently aerated areas while cathodic delamination mechanism is working also without. Depending on the oxygen transport path to the metal interface, the separation of anodic and cathodic reaction sites take place in different ways (Lenderink 1995). In the case of anodic undermining, as shown in Figure 1.9 the anodic front propagates from the defect, the galvanic cell consists in the cathodic area (e.g. defect) and the anodic location (delamination front).

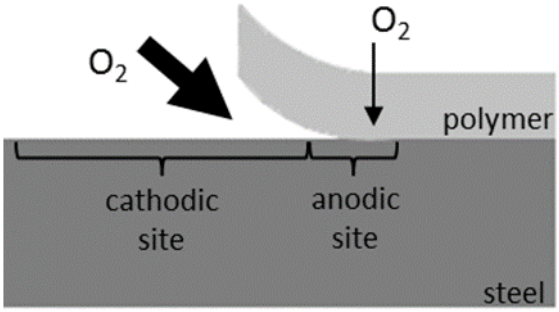

Figure 1.9 – Anodic undermining mechanism. Oxygen transport paths are shown

Anodic undermining can occur in the form of filiform corrosion (Bautista 1996) and can be preceded by cathodic delamination under certain conditions, such as the presence of group I cations at the defect (Williams und McMurray 2003). Besides that, Doherty and Sykes have shown that for a painted mild steel, after a certain time of exposure the defect changed from anode to cathode due to the formation of corrosion products blocking the defect area (Doherty und Sykes 2004). For iron substrates, green rust was found to be stable in the anodic site, this type of oxide is a result of the low oxygen concentration. The iron oxide identification supports the mechanism of differential aeration that is referenced in the literature for filiform corrosion (Cambier et al. 2014).

Crevice corrosion

Crevice corrosion is a form of localized corrosion occurring in zones of restricted flow where a small part of metallic material is in contact with a volume of confined, stagnant liquid whereas most of the material surface is exposed to the bulk environment (Marcus 2002). Crevice corrosion is caused by a change of the local environment inside the crevice zone into more aggressive conditions.

The characteristics of a crevice zone (shown in Figure 1.10) are the limited mass transport (Φ) by diffusion and convection between the inside of the crevice and the bulk environment, the small solution volume in contact with large surface area (L/h), the presence of large external surfaces (Se) exposed to the bulk environment, and, in many cases, the significant solution resistance (*IR* drop) between the inside and the outside of the crevice.

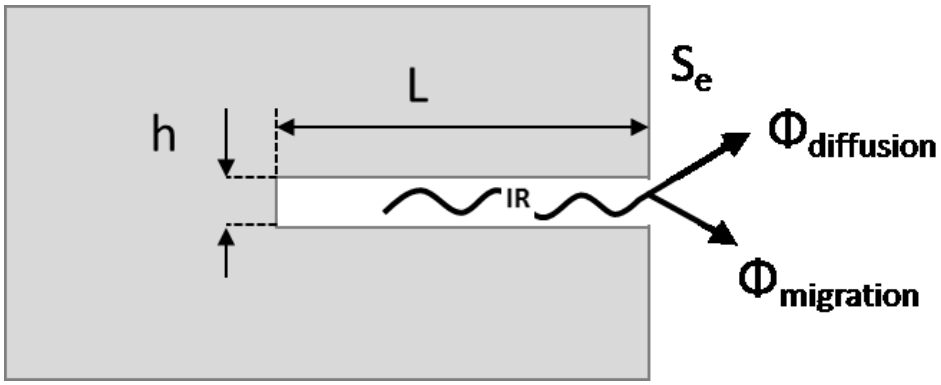

Figure 1.10 – Characteristics of a crevice zone

1.3. RESEARCH AIM

Within the background previously provided, the aim of the present research work is:

- To investigate the effect of corrosive media on the delamination of adhesive joints by means of scanning Kelvin probe technique with focus on understanding the corrosion mechanisms occurring at the interphase polymer/metal.

1.3.1. Specific objectives

In order to achieve the proposed research aim, the following specific objectives were set:

i. To develop a novel non-destructive experimental set-up capable to monitor and capture the progression of delamination of real closed joint geometries;
ii. To generate electrochemical experimental data of the delamination of coatings and adhesive joints under different corrosive environment;
iii. To assess the effect of electrolyte type and concentration on the delamination kinetics and fracture behaviour of adhesive joints;
iv. To assess the effect of the geometry on the delamination behaviour of adhesive joints with regards to the corrosion mechanisms;
v. To evaluate the relationship between potential distribution at the polymer/metal interphase, fracture pattern and substrates surface chemistry on adhesive joints;
vi. To describe the effect of delamination on the electrode potential distribution;
vii. To propose a model for the delamination mechanisms occurring in closed joint geometries;
viii. To propose an efficient, accurate and reliable approach based on the SKP method for the early stage detection and estimation of the delamination of closed joint specimens under different levels of corrosive media.

1.3.2. Research methodology

A research methodology was followed to ensure that results of the present research work were valid and reliable for several cases of delamination involving adhesive joints. During the planning of the methodology some aspects were taken into account including:

a) Use of specimens as shown in Figure 1.11: this geometry allows the comparison between coated (open joint geometry) and bonded structure (closed geometry) and simulates;

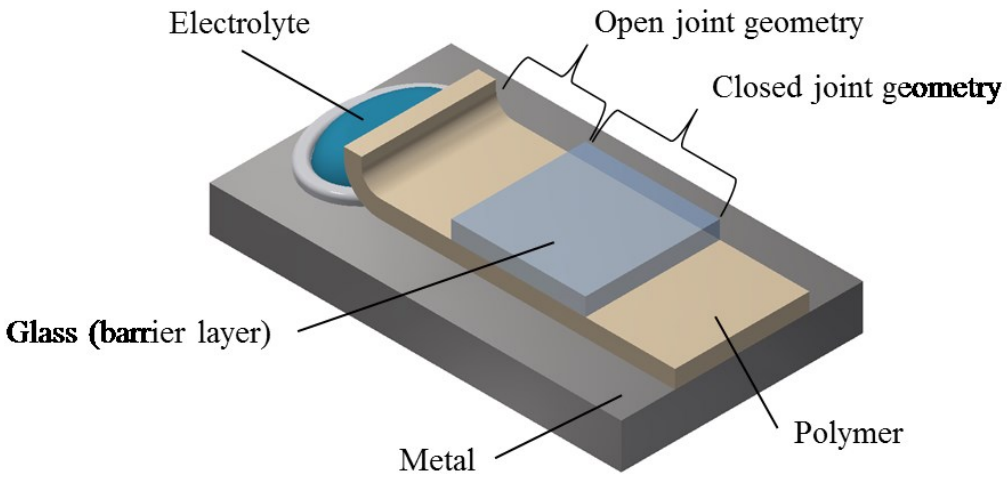

Figure 1.11 – Scheme of the sample specimen used in this work. Showing the two parts of the sample: open and closed joint geometry.

b) Use of a polymer system that suitable for application as a coating and as an adhesive joint: validate the electrochemical model for the delamination of coatings proposed in literature and compare with a joint;
c) Use of a commercial polymer system: additional industrial relevance for the findings
d) Use of a weak system (water based polymer and non-alloyed steel): obtain results in a shorter timeframe;
e) Use of a polymeric system with near ambient conditions curing (low temperature/pressure), fast curing, easy to apply: important for the specimen preparation using extremely thin glass layer (30 μm);
f) Use of a polymeric system which allows the SKP measurements: low dielectric constant, low charges, uniform film thickness after curing;
g) Use of free standing films: compare diffusion coefficients of species through the film thickness and along the interphase;
h) Use of thin glasses as second substrate: act as a barrier the diffusion of oxygen and water, while it does not block the SKP signal;
i) Use of an epoxy system for comparison and validation of the novel delamination testing methodology;
j) Use of different types of corrosive media and atmosphere: understand the mechanisms of delamination and rate controlling steps.

A summary of the applied methodology is described in Figure 1.12:

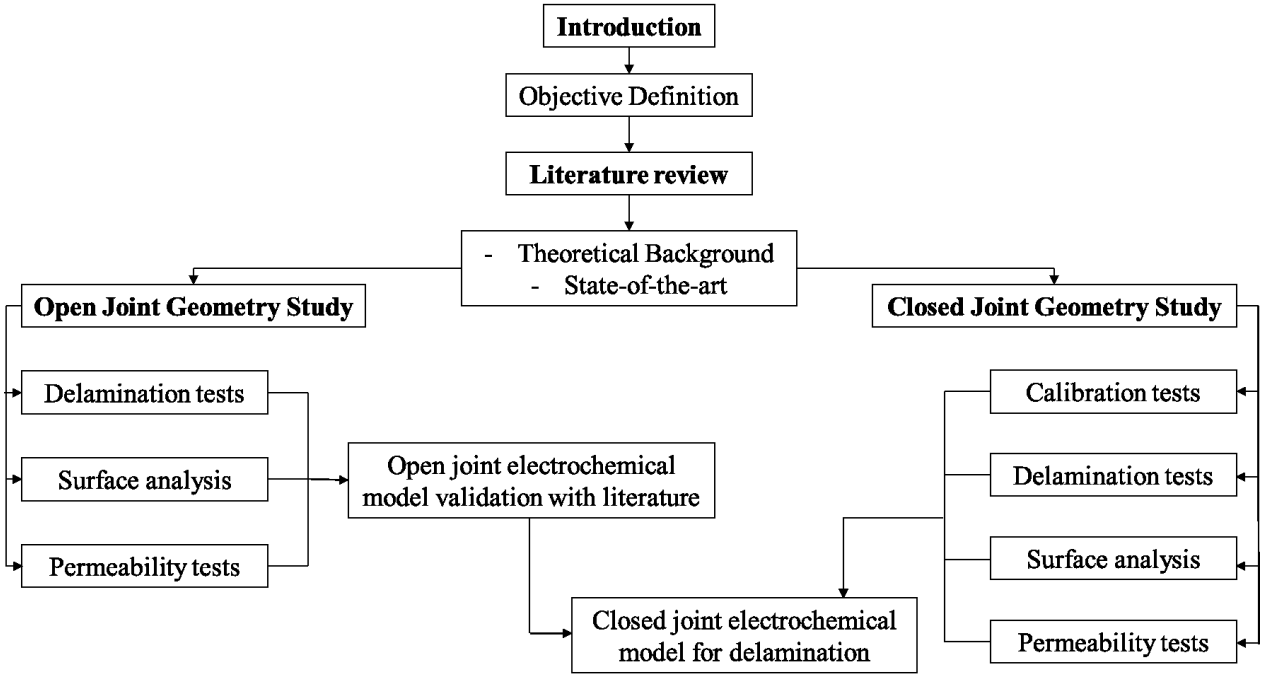

Figure 1.12 – Summary of the methodology applied in the present research work

1.4. THESIS OUTLINE

The present research work is divided in five chapters which are summarised below:

- **Chapter 1** "Introduction". This chapter is concerned with a comprehensive literature review aiming to: (i) establish the theoretical framework for the investigation, (ii) describe key terminology/definitions, and (iii) evaluate the state-of-the-art on the mechanisms and experimental testing of delamination of coatings and adhesive joints.

- **Chapter 2** "Experimental methodology". This chapter is focused on the description of applied experimental methodology, which includes: selection of adhesives and substrates, manufacturing of samples, and experimental set-up for electrochemical tests. Calibration of the SKP". In this chapter the theory related to the scanning Kelvin probe technique applied in the present research work is described and the results of the calibration experiments are presented.

- **Chapter 3** "Open joint geometry delamination". This chapter is focused on the investigations regarding the delamination behaviour of adhesives in an open joint geometry under the different corrosive media. Findings regarding the mechanisms occurring at the polymer/metal interphase were validated with the literature.

- **Chapter 4** "Closed joint geometry delamination". This chapter is concerned with the understanding the delamination behaviour of adhesives in a closed joint geometry. Bonded

specimens were analysed by means of SKP using a thin borosilicate glass as a barrier layer. The electrochemical model for the delamination established in Chapter 5 for the open joint geometry was used as a base and for comparison with a closed joint geometry in Chapter 6.

- **Chapter 5** "Discussions and outlook". This final chapter has the purpose of reviewing the main findings of previous chapters whilst highlighting the novel contributions of the present research work to the field of the delamination of adhesive joints. Finally, some suggestions about topics for future research are given.

1.5. SUMMARY

In the present section the key concepts and terminologies related to adhesive bonding technology, ageing, water uptake on polymers, deadhesion and electrochemical processes occurring in coatings and adhesive joints were revised. The technological relevance of adhesives was presented. The effect of water in bulk adhesive and at the interphase between polymer and metals was revised and discussed. Furthermore, the effects of corrosive media exposure on coated and bonded metals were considered.

State-of-the art literature research showed that the once present, water molecules can cause a modification in the adhesive mechanical properties, for example, by plasticization or by a reduction in the glass transition temperature. Alternatively, it is proposed that interfacial bonds can be disrupted or modification of the adherend surface can result, for example, by hydration of a metal. Water diffusion via free volume or directly through the polymer matrix itself takes place even for defect-free films. Water diffusion coefficients and the water uptake of the polymer films are often used to characterize their barrier properties.

The exposure to corrosive media leads to de-adhesion processes at polymer/oxide/metal interfaces. The main electrochemical mechanisms occurring at the interfaces are the cathodic delamination and anodic undermining. The occurrence, type and extent of corrosion processes are not only extremely dependent on the environmental conditions but also of the system, i.e. the type of substrate, surface treatment, polymer and geometry.

Finally, the research objectives and thesis outline were described.

2. EXPERIMENTAL METHODOLOGY

The present chapter contains the description of the experimental methodology applied for achieving the objectives set in **Chapter 1**. The present description was divided into the following topics: adhesive selection, sample manufacturing and experimental set-up of delamination tests, surface analysis and diffusion tests. An overview of the experimental methodology is shown in Figure 2.1.

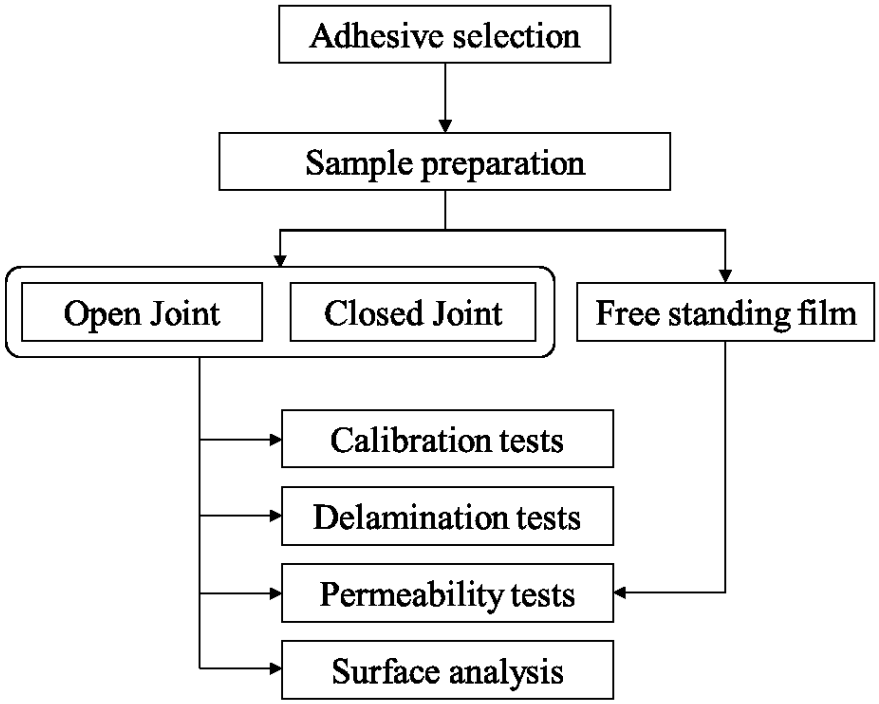

Figure 2.1 – Overview of experimental methodology

2.1. SELECTION OF POLYMER

The commercial aqueous dispersion of a styrene acrylic copolymer was employed for the present research work. Throughout the next chapters this polymer will be named: Acronal (commercial name Acronal® S 790 from BASF). Among others, it was designed for architectural coatings, textured finishes, interior paints and primers. The idea behind using this commercial system is to ensure that results found in this work are relevant for industrial applications. Furthermore, this system was chosen considering the sensibility of the experimental method (SKP) to charging effects of the polymer and its limitations regarding the sample dimensions (*e.g.* film thickness in the range of 50 μm). Other important aspects considered were the polymer's medium viscosity, curing conditions and applicability as both coating and adhesive.

Regarding the curing conditions it is a single component coating/adhesive with minimum film forming temperature (MFFT) of approximately 20°C. More information regarding the polymer is available in Table 2-1.

Table 2-1 – Technical data and main characteristics of the polymer - Acronal

Technical Data - Acronal	
Solids content	approx. 50%
pH value	approx. 7.5 – 9.0
Viscosity (DIN EN ISO 3219 (23°C, 100 1/s))	approx. 700 – 1.500mPa.s
Average particle size	approx. 0.1 μm
MFFT	approx. 20°C
Specific gravity (dispersion)	approx. 1.04 g/cm^3
Specific gravity (dry polymer)	approx. 1.08 g/cm^3
Dispersion type	anionic

Furthermore, for comparison with the Acronal system, one experiment was also performed with a 2 component Epoxy system, more technical information is shown in Table 2-2 below.

Table 2-2 – Technical data and main characteristics of the polymer - Epoxy

Technical Data - Epoxy	
Component A (no fillers)	Epoxy resin – Bisphenol F with 5%wt of reactive diluent Butanediol diglycidyl ether
Component B (no fillers)	Ancamine® 1922A (low viscosity, moderately reactive room temperature curing agent)
Mixing ratio	A:B = 3.06 : 1 (w/w)
Open time	1 – 2h
Curing time	2 days (at RT)

2.2. SAMPLE PREPARATION

The samples were prepared using cold-rolled steel plates of 45 x 27 x 1 mm^3 as the substrate (DC04, material number: 1.0338 (SAE designation)). Before bonding, they were polished using 80 and 500 grit abrasive paper and cleaned in deionised water and pure ethanol in an ultrasonic bath during 5 min. The preparation of the sample is illustrated in Figure 2.2. Part of the sample was protected with a pressure-sensitive adhesive tape and then the whole sample was covered with Acronal. Immediately after applying the adhesive, a 30 µm thick borosilicate glass foil (with lateral dimensions of 15 x 20 mm^2) was bonded to the rest of the sample, starting at about 7 mm from the edge of the adhesive tape.

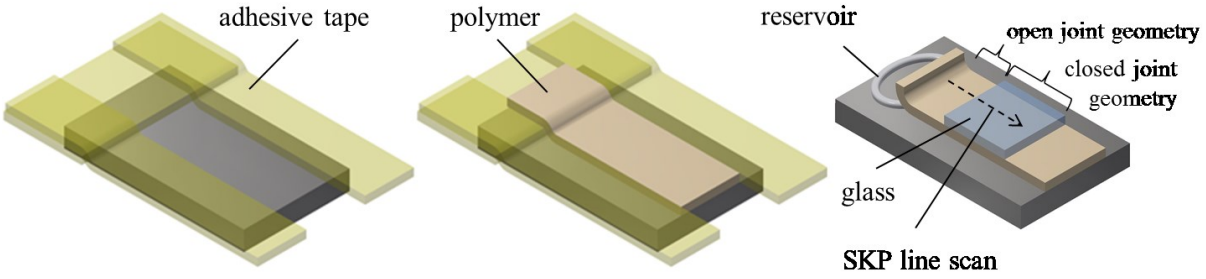

Figure 2.2 - Scheme of the sample preparation for the delamination experiments

The glass acts as a barrier layer to the diffusion of water and gases in the direction perpendicular to the adhesive joint's plane. After curing for two days at 40° C, the adhesives with layer thicknesses of about 30 – 50 µm were lifted off the adhesive tape, which was also removed from the metallic surface. By this procedure, a defined defect was created, where the metallic surface remained exposed and limited towards the adhesive and glass area by the polymer film itself. Strong film adhesion was observed through the whole sample; it was not possible to remove the film with a scalpel. An electrolyte reservoir was formed using a two-component epoxy paste. In addition, following similar preparation, other two specimen geometries were produced, as shown in Figure 2.3.

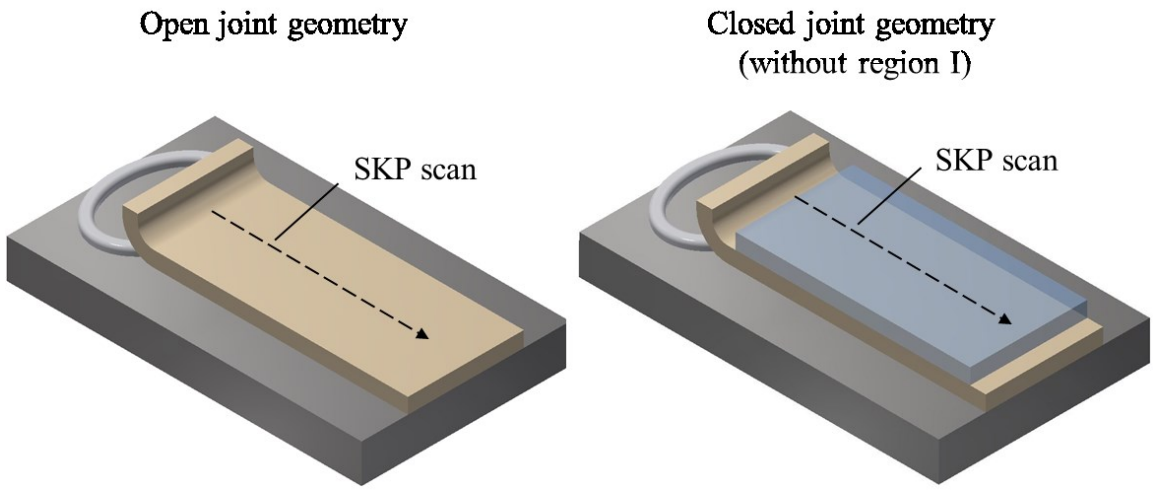

Figure 2.3 - Scheme of the open and closed joint geometry (without region I) samples

2.3. EXPERIMENTAL SET-UP

2.3.1. Laser scanning confocal microscopy (LCSM)

Laser scanning confocal microscopy (LSCM) is a non-contact measurement technique for obtaining high-resolution optical images with depth selectivity of transparent and non-transparent surfaces within several minutes. The key feature of confocal microscopy is its ability to acquire in-focus images from selected depths, a process known as optical sectioning. Images are acquired point-by-point and reconstructed by computer allowing three-dimensional reconstructions of topologically-complex objects. Cutaway views and roughness parameters are determinate from the generated topographies.

Laser scanning confocal microscopy (LSCM) uses a laser beam irradiated from a light source that passes through the scanning object lens and focuses on the sample. The reflected light is focused onto a pinhole in front of the detector. This detector aperture (pinhole) obstructs the light that is not coming from the focal point. By measuring the position of the tuning fork, which moves the object lens, the distance to the object can be accurately measured. This technique allows a height information for every measuring point in focus and results sharper images than those from conventional microscopy techniques.

The LSCM-measurements were performed on a Keyence VK-9700 system. The step size in Z-direction was 0,02 µm. The observation range was 270 µm x 202 µm. Regarding the roughness measurement ((JISB 0601:2001),(ISO 4287:1997)) following filter were used: λ_s : none; λc : none; λf : none.

2.3.2. X-ray photoelectron spectroscopy (XPS)

The X-ray Photoelectron Spectroscopy (XPS) investigations were carried out with a Thermo K-Alpha K1102 system. The parameters used were: acceptance angle of the photoelectrons 0°, monochromatized AlKα excitation, Constant Analyzer Energy-Mode (CAE) with 150 eV matching energy in overview spectra and 40 eV in energetically high-resolution line spectra, spot size diameter of 400 μm. The neutralization of electrically non-conductive samples was carried out by a combination of low-energy electrons and low-energy argon ions.

2.3.3. Gas permeability tests

To validate the SKP-based estimation of the oxygen diffusion coefficient, we also measured the oxygen diffusion coefficient by means of a gas permeability test following the manometric principle (Tester type GDP-C from Brugger). To this aim, free standing polymer films were prepared by applying the adhesive on a smooth Teflon surface. The experiments were performed according to ISO 15105/1 and ASTM D1434 standards (ISO 15105-1:2007; ASTM D1434).

2.3.4. Dynamic vapour sorption (DVS)

The diffusion coefficient of water in free-standing polymer films was measured gravimetrically. The experiments were carried out in a DVS automated moisture sorption instrument at 20 ºC. The free-standing films were initially dried under a continuous flow of air, then exposed to a water partial pressure profile in which the chamber's humidity first changed abruptly from 0% to 95% RH and then decreased again to 0% RH.

2.3.5. Scanning Kelvin probe (SKP)

The Kelvin probe was introduced in 1898 by William Thomson (Lord Kelvin) (Kelvin 2009), is an established and versatile method that allows the non-contact measurement of contact potentials and work function. Historically, a real breakthrough for testing the delamination of coated metals occurred around the 90's with the new technique presented by Stratmann *et al.* (Stratmann et al. 1991). Using a scanning Kelvin probe (picture in Figure 2.4), the authors measured for the first time the corrosion potential below polymer films in a non-contact and non-destructive manner. With this approach the delamination of coated metals can be monitored *in situ* with a local resolution of some μm. Furthermore temporal information can be obtained and therefore, the delamination rate can be calculated for different coating systems.

Since three decades, the method of the scanning Kelvin probe has been particularly useful for the measurement of the corrosive stability of coated substrates on a variety of substrates such as iron, zinc, or magnesium alloys (Leng et al. 1998d; Fürbeth und Stratmann 2001a).

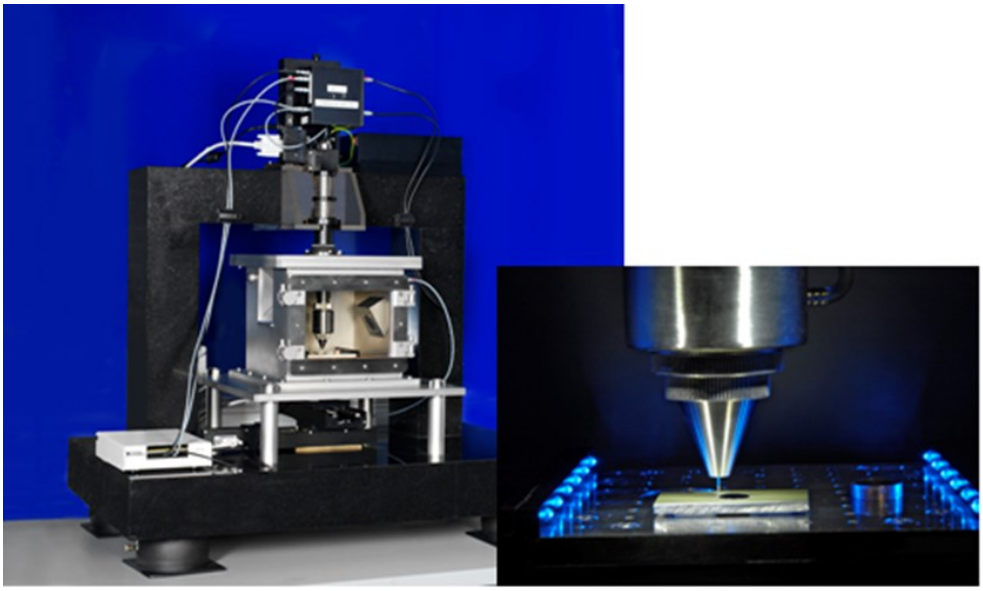

Figure 2.4 – SKP equipment

The contact potential difference CPD (also called Volta potential) measured with the SKP is determined by the interfacial electrode potential and is highly sensitive to changes in interfacial structures, such as surface modification, membrane polarization, adsorption, and redox state. Thus SKP is ideal for studying corrosion (Yee 1991; Fürbeth und Stratmann 1995; Williams et al. 2001a; Williams et al. 2001b; Williams und Grace 2011), especially the atmospheric corrosion of metals where electrochemical reactions occur in thin films of electrolyte and where metal-oxides formed by chemical reactions exhibit distinguishing electronic properties. Other applications are the study of semiconductor doping (Koley und Spencer 2001; Jacobs et al. 1997), organic semiconductors (Heil et al. 2001), biological systems (Heinz und Hoh 1999), surface reactivity (Camp et al. 1991; Ilie et al. 2000) and organic monolayers (Pfeiffer et al. 1996; Taylor 2000).

The measurement of the work function of a metallic sample under ultra-high-vacuum is the simplest system that which be investigated by means of the SKP. Under these conditions, the SKP measures the difference between a reference (Kelvin probe) the work function of the sample and the Kelvin probe reference (which under the experimental conditions should have a constant and by calibration determinable work function).

More complex system is when the sample surface is covered by other phases such as an aqueous electrolyte or a polymer. The potential difference measured by the SKP (Volta potential difference) between the sample and the reference ("Ref") will be sum of the work function from the substrate and the potentials of all occurring phases and phase boundaries. The potential distributions for different systems can be found in (Grundmeier et al. 2006), one relevant system for this work is an intact coated metal, the potential distribution over the interfaces metal/metal oxide/polymer/humid air/reference is shown in Figure 2.5. Where

$\Delta\phi_{Ox}^{Me}$ – Galvani potential difference across the inner metal/oxide interface

$\Delta\phi_{Ox}$ – Galvani potential distribution over the oxide scale due to varying composition of the oxide from the inner to the outer interface

$\Delta\phi_{Pol}^{Ox}$ – Galvani potential difference across the inner oxide/polymer interface

χ_{Pol} – dipole potential of the polymeric phase, for non-highly oriented polymers this potential is rather small

$\Delta\Psi_{Ref}^{Pol}$ – the Volta potential difference and measurable quantity

$-\chi_{Ref}$ – The surface potential of the reference itself, having a negative sign as the interface is crossed from the gas phase into the metal.

$\Delta\phi_{Ref}^{Me}$ – Galvani potential difference between the sample and the probe (sum of the potential differences of all interfaces)

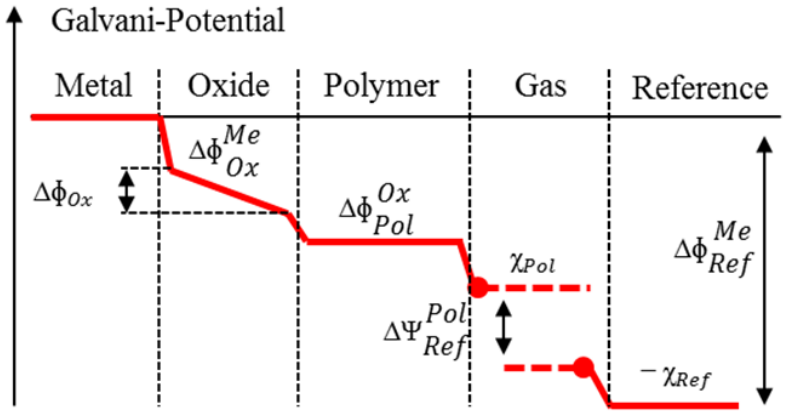

Figure 2.5 – Potential distribution over the system metal/metal oxide/polymer/humid air/reference. Adapted from (Grundmeier et al. 2006)

Grundmeier *et al.* (Grundmeier et al. 2006) showed that the Volta potential is given by

Equation 5

$$\Delta\Psi_{Ref}^{Pol} = \Delta\phi_{Ox}^{Me} + \Delta\phi_{Ox} + \Delta\phi_{Pol}^{Ox} - \frac{1}{F}\mu_e^{Me} - \frac{W_{Ref}}{F} + \chi_{Pol}$$

F – Faraday's constant

μ_e^{Me} – chemical potential of the electron in the metal

W_{Ref} – work function of the reference electrode

If the Volta potential drop over the oxide layer is substituted by the corresponding change in chemical composition, then for an iron substrate

Equation 6

$$\Delta\Psi_{Ref}^{Pol} = \frac{\Delta\mu^0_{Fe^{3+}/Fe^{3+}}}{F} + \Delta\phi_{Pol}^{Ox} - \frac{W_{Ref}}{F} + \chi_{Pol} + \frac{RT}{F} ln \frac{[Fe^{3+}]"}{[Fe^{2+}]"}$$

where $[Fe^{3+}]"\ and\ [Fe^{2+}]"$ are the activities of $Fe^{2+}\ and\ Fe^{2+}$ at the outer interface, respectively. Hence, for this system the Volta potential difference represents the oxidation states within the oxide surface. For a delaminated interface the typical system is metal/metal oxide/electrolyte/polymer/humid air/reference, a new element is present over the electrolyte/polymer interface, the Donnan potential, $\Delta\phi_D$. This potential is directly associated with the preferential incorporation of ions into the polymeric matrix and is usually of significance only for polymers with high density of fixed charges or for very dilute electrolytes (Doblhofer und Armstrong 1988; Cappadonia et al. 1988; Leng et al. 1998d).

The corrosion potential is, in general, defined by the rate of electrochemical reactions, which reflects the kinetics of electron and ion transfer reactions. Stratmann and Streckel (Stratmann und Streckel 1990a) showed that there is a simple linear correlation between the Volta potential difference measured by the SKP and the corrosion potential E_{Corr}. The corrosion potential (relative to the standard hydrogen electrode (SHE)) is given by

Equation 7

$$E_{Corr} = \varepsilon_{1/2}^{Sample} - \varepsilon_{1/2}^{Ref}$$

with

$\varepsilon_{1/2}^{Sample}$ the half-cell potential of the sample and $\varepsilon_{1/2}^{Ref}$ the half-cell potential of the reference electrode, a correlation can be derived to the Volta potential difference for the delaminated interface:

Equation 8

$$E_{Corr} = \frac{W_{Ref}}{F} - \chi_{Pol} - \varepsilon_{1/2}^{Ref} + \Delta\phi_D + \Delta\Psi_{Pol}^{Ref}$$

In most circumstances the Volta potential difference is only offset to the corrosion potential by a constant term, which is accessible by calibration experiments (Leng et al. 1998d).

SKP equipment measuring principle

The SKP measures the contact potential difference between the tip (Kelvin probe) and a conducting or semi-conducting surface in a non-contact fashion through the vibrating capacitor technique (Stratmann et al. 1994; Kohlrausch 2014). The Kelvin probe is a needle like probe made from an inert metal wire (Pt, Cr/Ni) and is tapered to have a flat end.

Figure 2.6 sketches measurement of the CDP with the SKP, one end of the probe is connected to a support via a pin connector; the other end is positioned in close proximity of the sample surface. When the two components are brought in electrical contact thought an external circuit, their Fermi levels equalize. With this, electrons will flow from the metal with the higher work function to the one with lower work function leading to oppositely charged surfaces forming a contact potential difference.

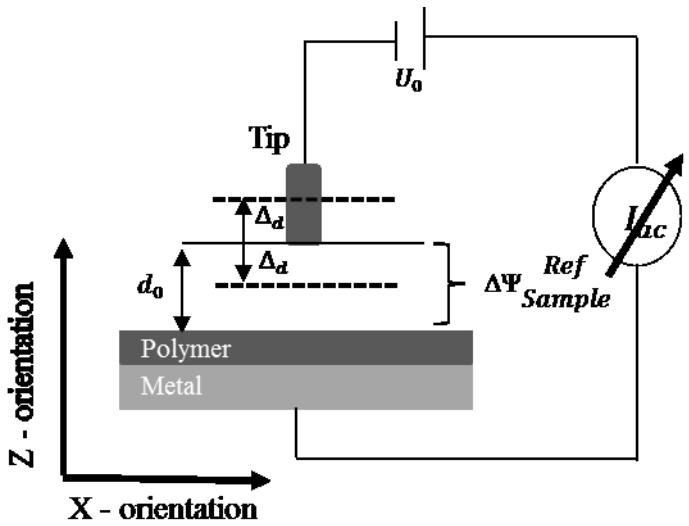

Figure 2.6 - Schematic representation of the measurement of contact potential differences with the scanning Kelvin probe

The measurement of the external potential difference between a sample and a reference electrode, which are arranged in the geometry of a parallel plate capacitor to each other, can be carried out by vibrating the reference electrode at a mean distance to the sample $\bar{d}$ and an amplitude Δd. The resultant variation of the capacitance C is given by

Equation 9

$$C = \varepsilon\varepsilon_0 \frac{A}{\bar{d} + \Delta d\ sin(\omega t)}$$

where

ε is the dielectric constant of the medium,

ε_0 the electric field constant,

ω the reference electrode frequency of vibration and

A the surface area of the reference plate.

Therefore an induced current results in the external circuit, which is given by

Equation 10

$$i_{AC} = \Delta\Psi_{Sample}^{Ref} \frac{dc}{dt}$$

$$= \Delta\Psi_{Sample}^{Ref} (\varepsilon\varepsilon_0 A \Delta d\omega) \frac{cos(\omega t)}{\left[\bar{d} + \Delta d sin(wt)\right]^2}$$

$$\approx \Delta\Psi_{Sample}^{Ref} (\varepsilon\varepsilon_0 A \Delta d\omega) \frac{cos(\omega t)}{\left(\bar{d}\right)^2}$$

for $\bar{d} \gg \Delta d$.

In the nulling SKP method, an external voltage (backing potential, V_b) is applied until a zero field state is reached, resulting in no current, then

Equation 11

$$i = (\Delta\Psi - V_b)\frac{dC}{dt},$$

with $i = 0$ for $\Delta\Psi = \mathrm{Vb}$

At this stage the backing potential is equal to the CPD.

In the present work, a distance control SKP is used, *i.e.* the distance between the SKP needle and the outer surface of the sample is simultaneously kept constant during the CPD measurements. A distance control is particularly indispensable if the roughness of the sample to be measured is in µm range, curved or if very small structures are to be measured.

The SKP sensitivity for a usual experimental setup is on the order of some µV to mV with a lateral resolution from the µm to cm range. This resolution is mainly limited by the dimensions of the Kelvin probe and by the signal-to-noise ratio of the equipment (McMurray und Williams 2002; Yee 1991; Wicinski et al. 2016). With increasing distance of the SKP needle to the sample surface, the spatial resolution of the measured potential decreases and the error width increases.

The peculiarity of the design presented in this work is that in order to measure corrosion reactions at hidden metal/polymer/glass interfaces, it is necessary to work in-situ at atmospheric pressure and under high relative humidity and to calibrate measured potentials with respect to standard potentials. Furthermore, it is necessary to be able to selectively achieve a spatial resolution of µm range as well as measuring areas of a few square millimetres in area and through relatively thick layers, polymer and glass layer thicknesses ranging from approximately 40 to 150µm.

Delamination tests

Before all measurements, the SKP instrument was calibrated to the standard hydrogen electrode using a $Cu/CuSO_4$ reference electrode, as described in (Stratmann et al. 1991). During the delamination experiments the relative humidity of the chamber was kept constant at 93%. After the preparation (Figure 2.2), the samples were left in the humid chamber for a few hours, in order to equilibrate with the water vapor of the chamber's atmosphere. After the potentials measured over the intact sample reached a steady-state value, the reservoir, which represents the initial delamination defect, was filled with a 0.5 M sodium chloride solution. At this time the delamination starts, and the SKP tip was positioned at the border next to the defect, in the middle of the polymer width. The average distance tip/sample was about 30 µm throughout all measurements (automatic height control). From this starting position, several line scans perpendicular to the defect, over the polymer and glass were made (see Figure 2.2, SKP line scan). Further measurements were performed varying the electrolyte concentration and type (at least three replicates), as well as changing the atmosphere inside the chamber (vide infra).

After the delamination tests, the samples were dried for 12-24 hours in a desiccator. The glass surface was then bonded to another metallic substrate which was immediately pulled apart

in order to remove the adhesive and the glass from the steel substrate. By doing that, the surface could be accessed and analyzed by means of X-ray photoelectron spectroscopy (XPS).

Determination of the oxygen diffusion coefficient in the bulk polymer

The SKP allows the diffusion coefficient of oxygen in the bulk polymer to be measured by varying the thickness of the coating and following potential transients after a sudden change of the oxygen activity in the atmosphere. This was reported for the first time by Leng *et al.* (Leng et al. 1998a) and the same approach is used here to obtain the diffusion coefficients of oxygen in the polymer system studied in this work.

2.4. CALIBRATION OF THE SKP

Calibration experiments have been performed to check the proportionality between the electrode potential and the Volta-potential of the polymer and glass surface. This is necessary since different interfaces were studied in this work, such as metal/polymer, metal/polymer/glass, metal/electrolyte/polymer and metal/electrolyte/polymer/glass.

2.4.1. Calibration on open and closed joint geometry

Stabilization time in SKP chamber

Before the delamination tests all samples were exposed to the SKP humid chamber in order to equilibrate with water and remove any electrostatic charging. This time for stabilization was defined by placing an open and closed joint sample (see Figure 2.3) in the SKP and measuring the potential in a point in the middle of the sample. Figure 2.7 shows the evolution of the potential over time, the potentials decrease for the open and closed joint from 0.2 $V_{(SHE)}$ to 0.1 $V_{(SHE)}$ and from 0.45 $V_{(SHE)}$ to 0.25 $V_{(SHE)}$ before they stabilize after 2 and 4 hours, respectively. The stabilization time was then defined 4 hours, so for all delamination tests the samples were placed inside the chamber for at least 4 hours before starting the test.

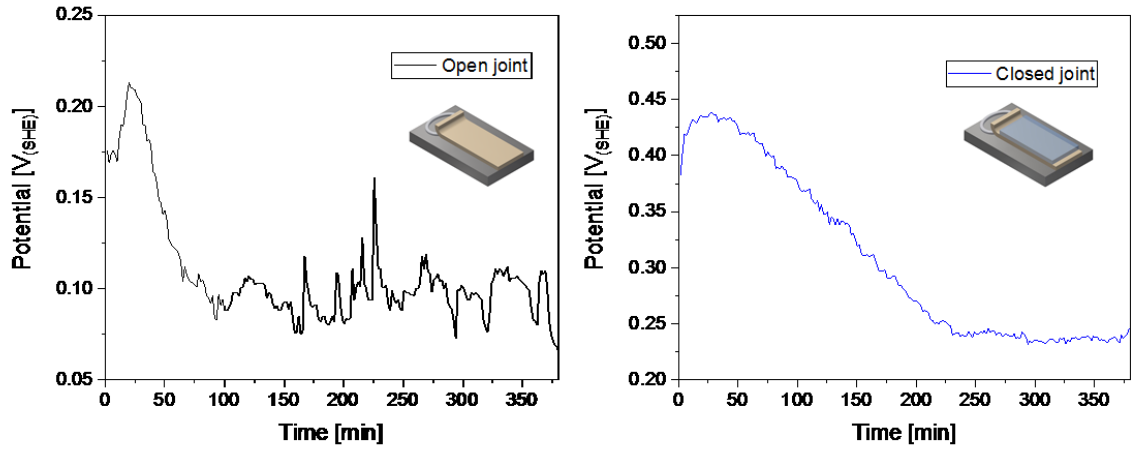

Figure 2.7 - Transient of the Volta-potential difference measured above the polymer (open joint – left) and glass (closed joint - right) covered iron surface. Point measurement in the middle of the sample. Humidity in the SKP chamber: 93%

Potential distribution without electrolyte

After the stabilization, line scans were performed over the open joint geometry without electrolyte to determine the uniformity of the potentials along the sample and to exclude any delamination occurring only due to the humidity in the chamber. Figure 2.8 shows that the potentials after 12 hours of measurement are constant and uniform over the sample length. Furthermore, after the test it was not possible to lift the film off, the polymer layer was still well adhered to the substrate.

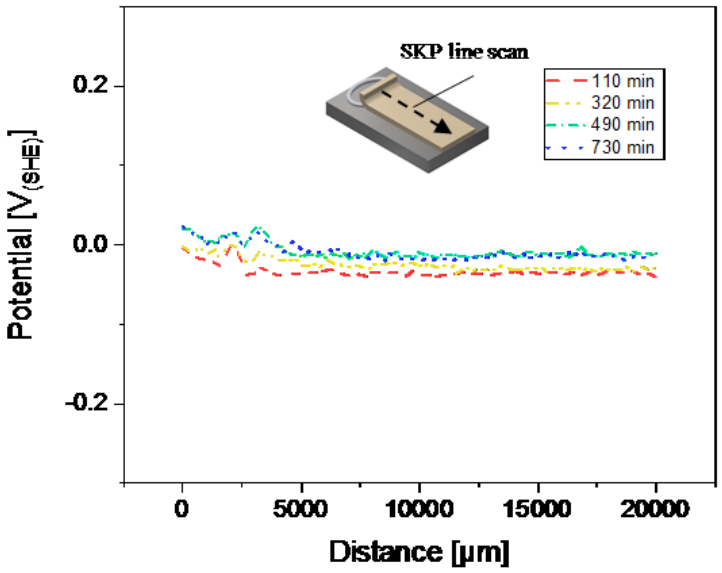

Figure 2.8 - Transient of the Volta-potential difference measured above the polymer (open joint) covered iron surface. Line scan measurement in the middle of the sample. Humidity in the SKP chamber: 93%

2.4.2. Calibration on glass

Metal/glass interface potential distribution

As already mentioned in section 1.3.2, the main required characteristics of the glasses for the SKP measurements are the small thickness (in the order of 50 to 100 µm) and the electric properties, such as low dielectric constant. Thus, some glasses were selected and their technical data is shown in Table 2-3.

Table 2-3 – Technical data and main characteristics of the glasses used in the investigation

Glasses Technical Data			
Commercial name	Type	Dielectric constant ε_r at 1 MHz	Thicknesses
D263® T eco	Borosilicate	6.7	30 and 50µm
AF32® eco	Aluminoborosilicate (alkali-free)	5.1	30 and 100µm
MEMpax®	Borosilicate	4.8	200µm

In order to assess their suitability for the SKP measurements, *i. e.* whether it is possible to measure the electrode potentials through the glasses, they were sputtered in one surface half with gold and half with chromium and the SKP line scans were performed on both sides of the glass, *i. e.* on sputtered and glass surfaces. Different values of electrode potentials are expected to be measured for the two metals. In the situation that the potentials measured over the sputtered side are similar to the potentials measured over the glass side, the glass might be considered suitable for performing the delamination tests, *i. e.* this is a hint that the SKP signal is not completely blocked by the glass.

The schematic representation of the sputtered glass sample and results of the SKP line scans are shown in Figure 2.9.

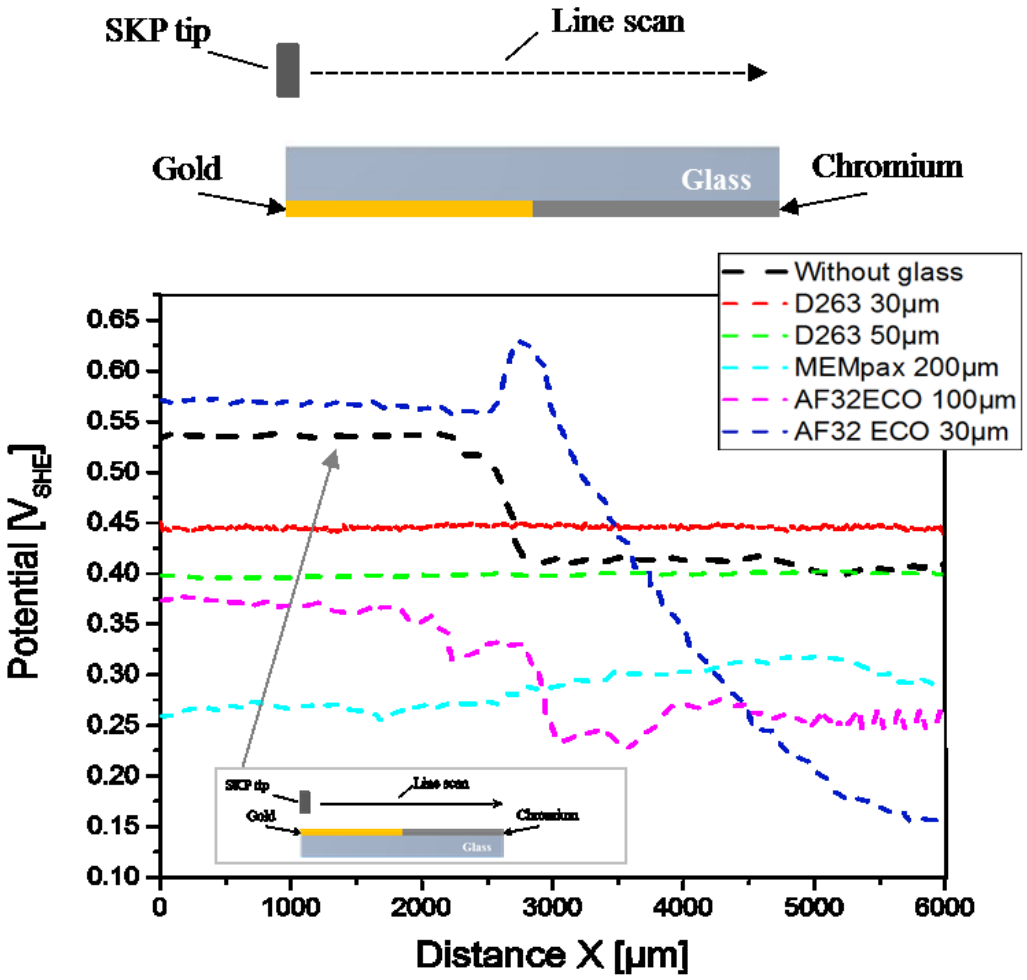

Figure 2.9 - Schematic lateral view of the sample and Volta-potential difference of sputtered gold/chromium measured above the glass surface. Line scan measurement in the middle of the sample. Humidity in the SKP chamber: 93%

The black line shows the potentials when measured over the bare metals, i.e. over the sputtered side of the sample, the electrode potentials measured for gold and chromium are in the range of 0.55 $V_{(SHE)}$ and 0.4 $V_{(SHE)}$, respectively. The potentials measured through the glasses D263® T eco and MEMpax® are constant, these glasses probably block the SKP signal which makes it impossible to measure through them. Possible reasons for this behavior are, in the case of the glass D263® T eco the dielectric constant of is probably too high (ε_r=6.7) and in the case of the MEMpax® glass it is probably too thick (200µm). In the results for the glasses AF32® eco, different values of electrode potential for the two metals are observed. AF32® eco with 100µm of thickness shifts the potentials towards more negative values. For the 30µm thickness the values of gold are nearly the same and for chromium are more negative and show a gradient pattern. The exact reason for this gradient will not be discussed in details here, this could be for instance due a non-uniform sputtering process. From the first experiments, the AF32® eco was selected as the most suitable glass and further calibration measurements are shown below.

Potential difference of metal/electrolyte/glass interfaces

In order to further assess the suitability of the AF32® eco borosilicate glass for the SKP measurements and to identify the influence of the glass on the potential difference, pieces of glass (2 x 2cm) were placed on top of $Cu/CuSO_4$ and Zn/NaCl reference electrodes (as shown in Figure 2.10) and the potentials were measured at a point in the middle of the glass.

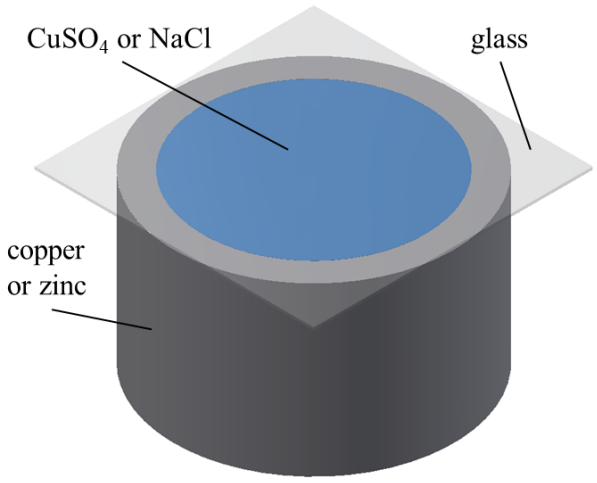

Figure 2.10 - Scheme of the experimental setup for the calibration tests

The averages of the potentials measured are presented in Figure 2.11. The electrode potential measured at the Cu/electrolyte/glass configuration is identical to the calibrated value at the Cu/electrolyte interface, 0.32 $V_{(SHE)}$. For the Zn/NaCl reference electrode, the potential

measured was -0.78 $V_{(SHE)}$ which is a typical value for free corrosion potential of an active zinc electrode (Fürbeth und Stratmann 2001a, 2001b). For the Zn/electrolyte/glass configuration, the measured potential was -0.68 $V_{(SHE)}$. These results indicate that it is indeed possible to measure the electrode potential even through the borosilicate glass layer. The small shift in the potential of around +0.1 V observed for the Zn reference electrode results from the difference between the potential at the Zn/electrolyte interface and the sum of the potentials at the Zn/electrolyte and electrolyte/glass interfaces (assuming no contribution from the outer glass/air interface). Remarkably, however, such differences cancel out (or are both negligible) in the case of Cu, indicating that the two types of cations have a different effect on the electrolyte/glass dipole potential. Since potential shifts of this order of magnitude do not impact the results of the present studies, we do not address in detail the precise reasons for the observed behavior. These could be the subject of future investigations.

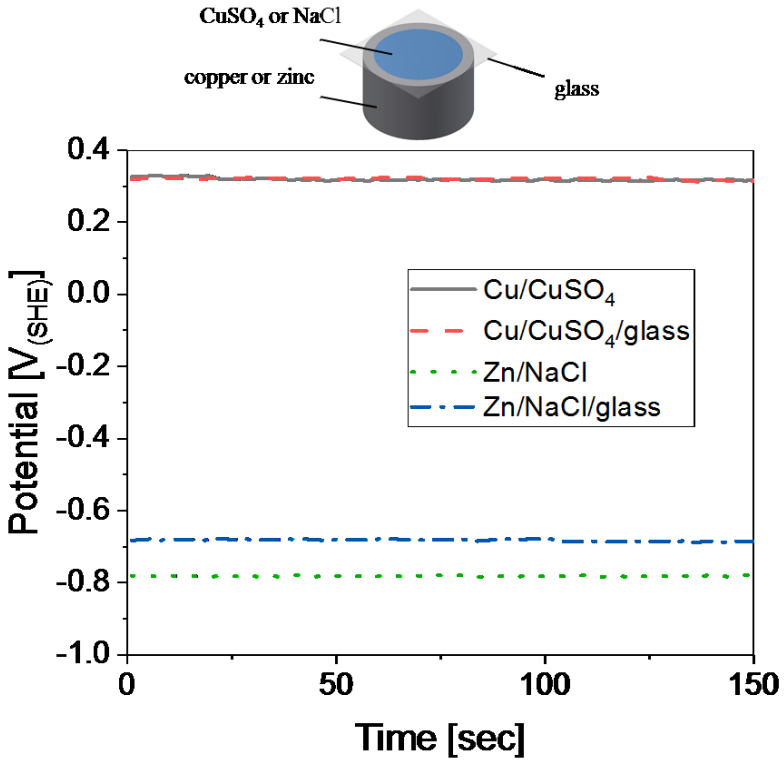

Figure 2.11 – Point measurement of the potential difference of Cu/CuSO4 and Zn/electrolyte interface with and without glass in humid air (>93% r.h.), over a time of 2.5 minutes

Height control

Further interesting analysis is to determine if the SKP tip is able to scan the transition from the polymer coated metal area to the bonded area (regions I and II from Figure 1.11, respectively). Therefore experiments were performed on two different metals, galvanized steel

and gold. Half of the sample was the bare metal and half was covered with the AF32® eco glass using a small amount of distilled water in between in order to ensure that the glass adhered to the metallic surface and that there is no air gap in between (see Figure 2.12 upper part). The SKP tip was programed to scan over bare metal first and then over the glass/water covered metal. This way the SKP tip experiences a height step of at least 50 µm and it is possible to identify if the tip does not hit the sample stopping the measurement. Figure 2.12 shows the measured potentials and topography for the galvanized steel (left) and gold (right). The SKP tip scanned the whole sample without hitting the glass and height step experienced was of 60 - 100µm. Furthermore, as expected the measured potentials on the bare metal did not differ much from the ones measured over the glass.

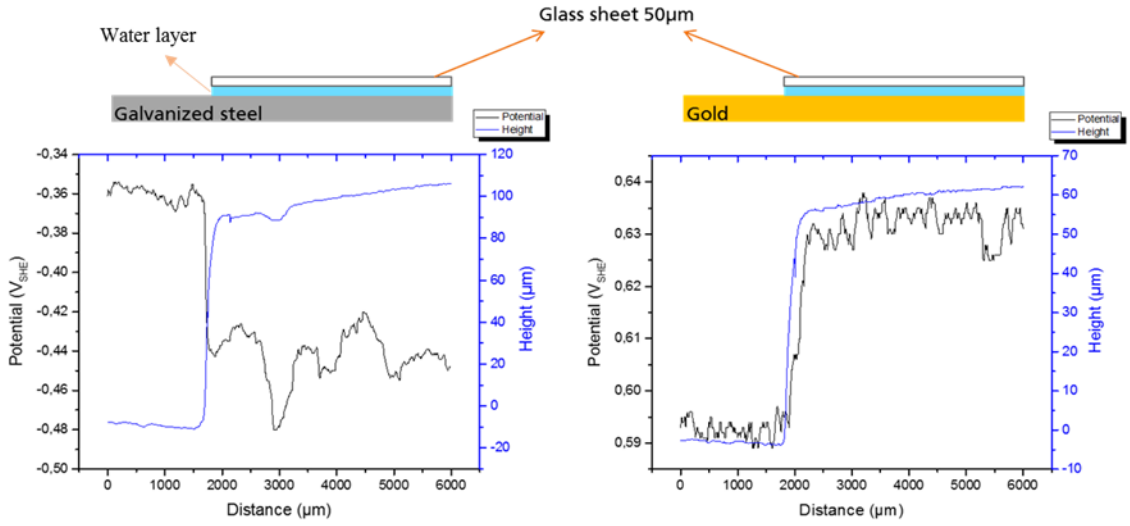

Figure 2.12 – Schematic lateral view of the samples and Volta-potential difference of galvanized steel and gold. Line scans measured over the bare metals and glass surfaces. Line scan measurement in the middle of the sample. Humidity in the SKP chamber: 93%

2.5. SUMMARY

This chapter was used to describe topics related to experimental investigations. The selection of the adhesive, the process of sample manufacturing and the experimental set-up of the tests performed were described. Also the use and measurement principle of the scanning Kelvin probe method was explained in details (Section 2.3.5). Furthermore, the measurements for the calibration of the SKP were presented in Section 2.4.

3. OPEN JOINT GEOMETRY DELAMINATION

This chapter presents the results of all experiments performed on open joint geometry samples, see Figure 3.1. The effects of electrolyte type and concentration, substrate's surface roughness and texture, and polymer thickness on the delamination of coated steel will be discussed in this chapter.

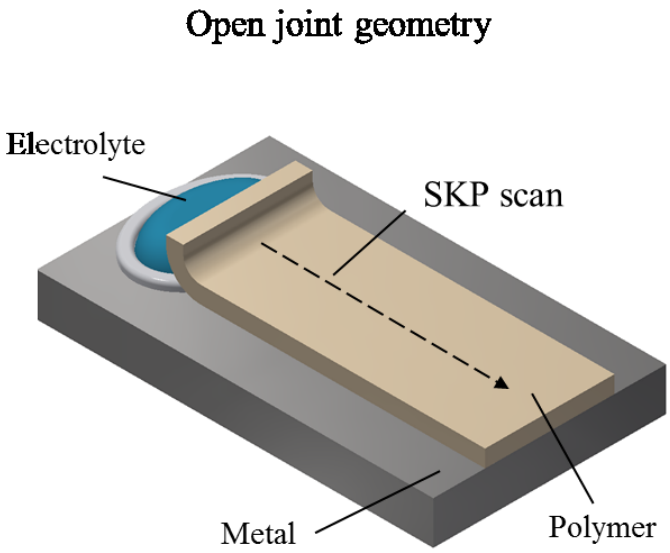

Figure 3.1 – Sketch of the open joint geometry sample

3.1. DELAMINATION OF THE POLYMER NEAR A DEFECT

The SKP delamination experiments were performed in humid air with 0.5M of NaCl at the defect of the model sample, a cathodic delamination mechanism of the iron is expected under these conditions. The typical delamination potential distribution measured with the SKP for the adhesive in an open joint geometry (region I) is presented in Figure 3.3. Similar potential profiles had been observed in delamination tests on iron and steel (Leng et al. 1998d, 1998f) and the electrochemical model that has been proposed will be used to explain the cathodic delamination process in this work.

The electrode potential was at first measured at the defect itself and its evolution with time is presented in Figure 3.2. Potential values start to decrease immediately after the addition of the electrolyte to the dry steel suface from around -0.30 $V_{(SHE)}$ to -0.65 $V_{(SHE)}$. These values stabilize after around 2 hours and are close to the ones at free corroding iron/electrolyte interfaces (Stratmann et al. 1991; Stratmann et al. 1994).

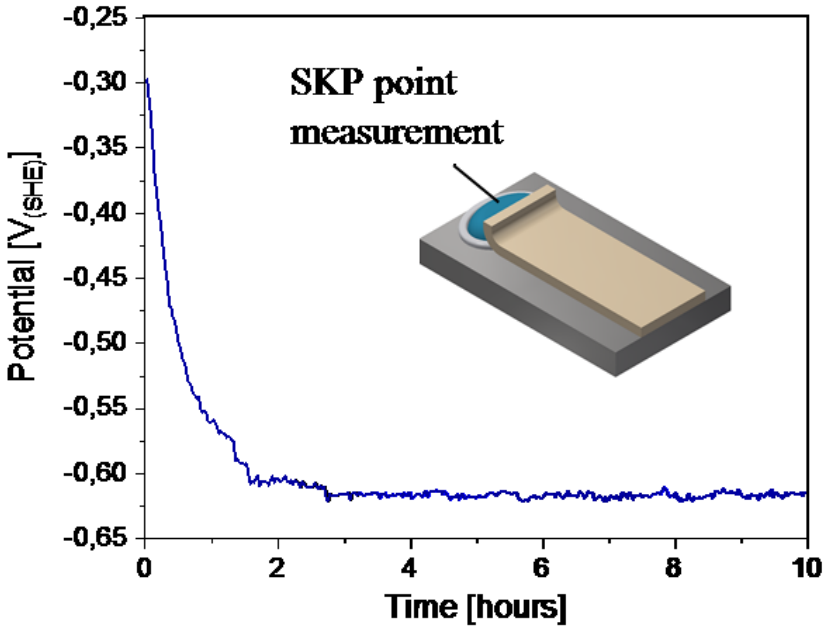

Figure 3.2 – Point measurement of the Volta potential difference above the electrolyte (0.5M NaCl) covered iron surface at the defect. Humid air atmosphere (93% r.h.)

The electrode potential of the intact polymer, *i.e.* before adding the electrolyte, is higher: around -0.05 $V_{(SHE)}$. The same applies to the values far away from the defect. The potential values of the intact polymer are given by the ratio of $[Fe^{3+}]/[Fe^{2+}]$ within the oxide layer (Stratmann und Streckel 1990a, 1990b; Stratmann et al. 1990). Some time after addition of the electrolyte, a distinct potential step of around 0.4 – 0.5 V over 500 µm becomes visible between the zone of the sample closer to the initial defect edge (lower potential) and the zone farther from the defect edge (higher potential). According to the delamination model proposed by Leng et al. (Leng et al. 1998f), this potential step marks the delamination front and moves away from the defect edge with increasing time due to the ingress of hydrated ions from the electrolyte into the adjacent polymer/metal interphase. Notably, the potential between the defect edge and the step is not constant but increases linearly with the distance. This is due to the ionic current at the delaminated interphase which produces an ohmic potential drop between the defect edge and the front of the delaminated area (Leng et al. 1998d).

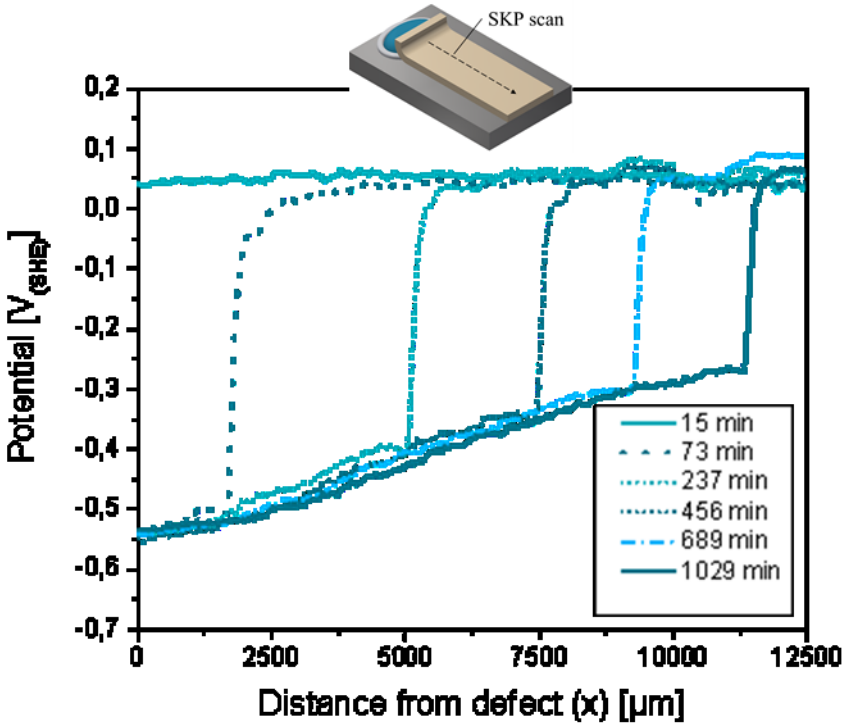

Figure 3.3 – Typical potential distributions for the coated sample (region I) in humid air (93% r.h.) for different delamination times. Electrolyte in the defect: 0.5M NaCl

After the delamination tests, a visual inspection reveals that the metallic surface at the delaminated area in region I is free of any corrosion product, meaning that the delamination is not due to anodic undermining (Leng et al. 1998f). The adhesion of the polymer film to the substrate is completely lost up to a certain distance from the defect edge and the remaining area has still good adhesion to the substrate; this can been clearly seen by lifting off the film from the substrate Figure 3.4. The position of the front of the delaminated zone matches with the position of SKP potential step, as expected.

In earlier studies (Leng et al. 1998d; Fürbeth und Stratmann 2001a; Weiss et al. 2016), attempts were made to identify the mechanisms of the bond breaking within the organic coating near the interphase. It is believed that oxidative degradation of the polymer occurs during oxygen reduction at the interface with the strong alkaline electrolyte either by hydroxide ions or by other highly reactive oxygen species generated at the metal surface. Therefore, only if oxygen diffusion is at least as fast as ion diffusion will the position of the potential step be identical to the position of the delamination front. According to Leng *et al.* (Leng et al. 1998b), a sharp step in the SKP potential would also occur at the diffusion front of ions from the electrolyte along the substrate/adhesive interface, in the early stage of galvanic coupling. However, in this case there would be concomitant diffusion of both Cl- and Na+ ions and no signature of an Ohmic

drop between the defect edge and the onset of potential step would be observed. This point will be crucial to interpret the results concerning the adhesive region covered by the glass slides in Chapter 4.

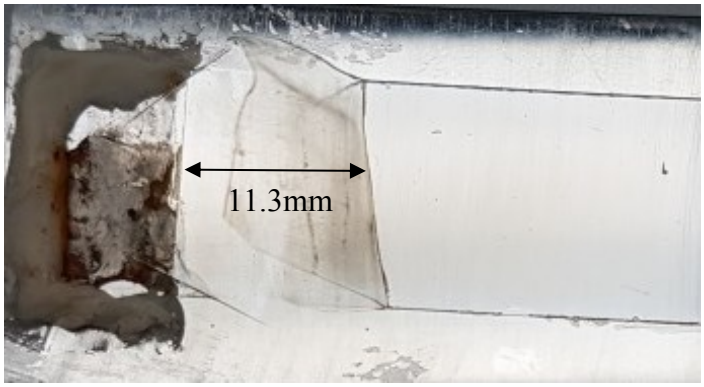

Figure 3.4 - Picture of the sample after 17 hours of delamination tests

Analysis by pH- and ion-sensitive pigments

Samples were prepared filling the adhesive with phenolphthalein or 1, 10-phenantroline pigments in order to assess the pH and the iron dissolution, respectively. Delamination tests were carried out as usual and the progress of the delamination is followed with the SKP. The samples with pH sensitive pigments showed a violet coloration (see Figure 3.5) in the areas where the potentials measured with the SKP were more negative and no coloration in the more positive values. This proves the formation of an alkaline pH at the interface metal/polymer, pH >10, and confirms the model of the oxygen reduction at the delamination front. The samples filled with 1, 10-phenantroline showed no coloration during the delamination tests, as expected no iron dissolution takes place under the polymer and agrees with the visual observation that the iron surface is non-corroded at the delaminated zone.

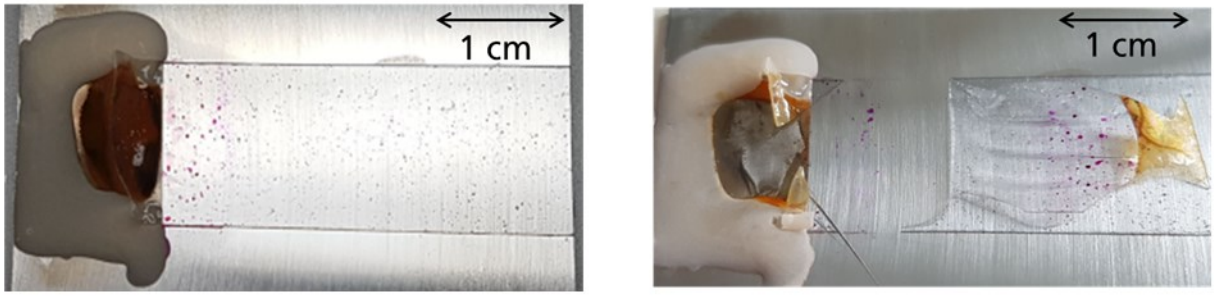

Figure 3.5 – Pictures of the samples filled with phenolphthalein after delamination. Electrolyte at the defect: 0.5M NaCl

These results are in line with the work reported by Sørensen *et al.* (Sørensen et al. 2009) showed that the underneath the coating in the delaminated regions a pH of around 13 was found, furthermore the steel surface was not corroded.

3.1.1. Delamination kinetics of the open joint – region I

In order to understand the time dependence of the delamination reaction, the delaminated distances were obtained from the graphs in Figure 3.3, and defined as the value of the x axis in correspondence of the potential at about half of the SKP step. Figure 3.6 gives a typical plot of the delaminated distances (x_{del}) versus the square root of time ($\sqrt{t_{del}}$) and the calculated delamination rate constants *A* (slope) of the curves fitted with Equation 12.

Equation 12

$$x_{del} = A\sqrt{t_{del}}$$

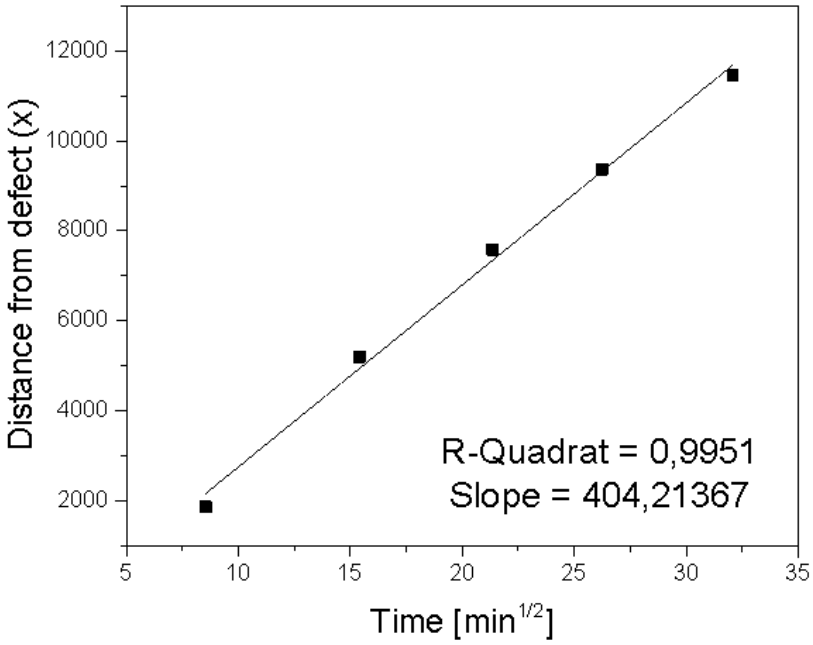

Figure 3.6 – Plot of the delaminated distance (x_{del}) vs. square root of time ($\sqrt{(t_{del})}$)

The delamination process is transport-controlled, since the delaminated distance varies linearly with the square root of time. This indicates that no diffusion perpendicular to the coating can be the rate-determining step of the delamination, as this diffusion path does not depend on the distance to the defect. As it will be made clear in the following sections, this is related to the mobility of ions for region I (Leng et al. 1998f; Sørensen et al. 2010c).

3.1.2. *Effect of electrolyte type and concentration*

Influence of the electrolyte type

In order to gain a detailed insight into the mechanism of the delamination reaction, additional experiments were performed changing the type and concentration of the electrolyte. Figure 3.7 summarizes the averages and standard deviation of the delamination rate constant *A* (Equation 12) in region I obtained for different electrolyte types with same concentration (0.5M).

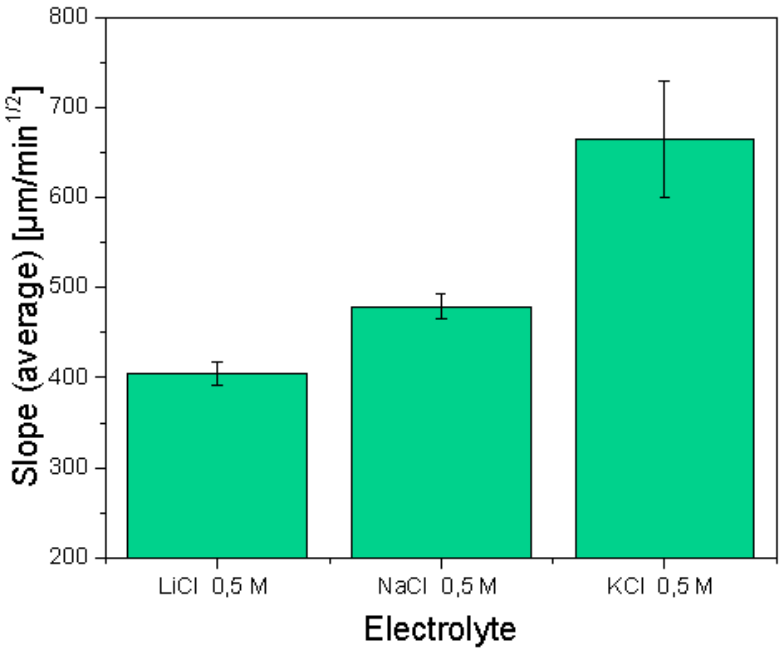

Figure 3.7 – Delamination kinetics for samples whose defects have been filed with a 0.5M solution of LiCl, NaCl or KCl - Delamination rate constant A (Equation 12) for different samples, whose defects have been filled with solutions of LiCl, NaCl, KCl and $NaClO_4$ in concentrations of 0.5 and 1M

It can be clearly seen that in region I there is a dependence of the delamination rate on the type of cation, in the sequence $Li^+ < Na^+ < K^+$. This is consistent with the size of the radii of the hydrated alkali cations and their diffusion in bulk electrolytes, where smaller hydrated cations will diffuse faster. Therefore the mobility of cations differs strongly between K^+ and Li^+, with the hydrated Li^+ ion being the slowest due to the large and strongly bound hydration shell which clearly exceeds the size of the hydration shell of the other alkali ions (Hamann und Vielstich 2005).

Influence of the electrolyte concentration

The effect of the electrolyte concentration in the delamination rate was also investigated. Figure 3.8 presents the average and standard deviation of the slopes *A* calculated from different concentrations of sodium chloride solution (0.1, 0.5 and 1M). In all cases straight lines were observed in the √time-plots, the slopes increased in the sequence 0.1 M < 0.5 M < 1 M, as expected. This shows that the delamination strongly depends on the ionic strength of cations within the electrolyte. However, according to (Leng et al. 1998f) these results also demonstrate that the slope of the straight line cannot be interpreted only by the mobility of the cation, as the mobility does not depend on the concentration. It is more likely that instead of the mobility, the slope is given by some type of permeation coefficient (product of concentration and mobility). This dependency of the concentration on the delamination rate was also observed in studies of the delamination of epoxy from mild steel (Bi und Sykes 2016).

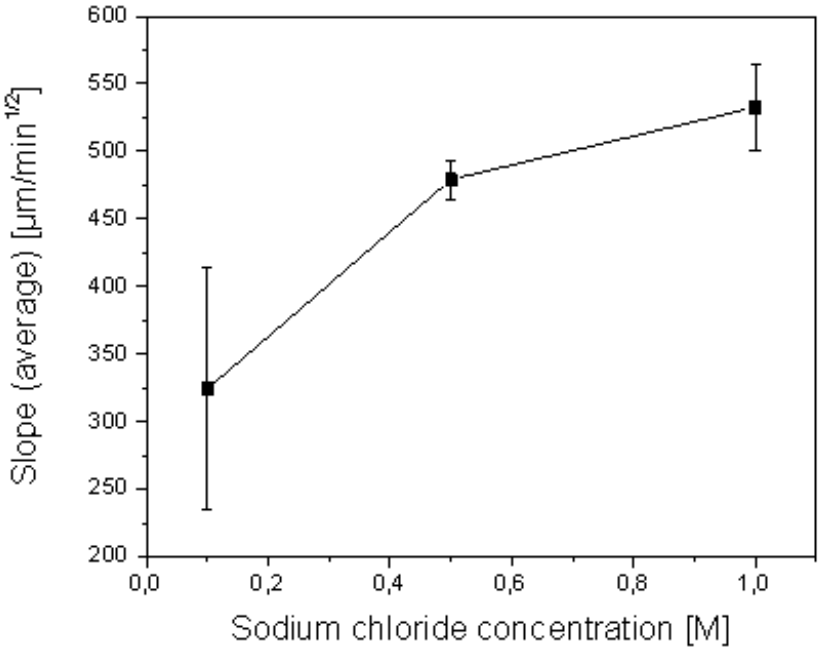

Figure 3.8 – Delamination kinetics as a function of the ionic strength of NaCl within the defect

Figure 3.9 presents the results for the KCl solutions, varying the concentrations (0.1, 0.5 and 1M). For concentrations up to 0.5M the behaviour was similar as observed for NaCl solutions, increasing the salt concentration decreases the delamination rate. However, for more concentrated solution (1M), the delamination rate decreased for KCl.

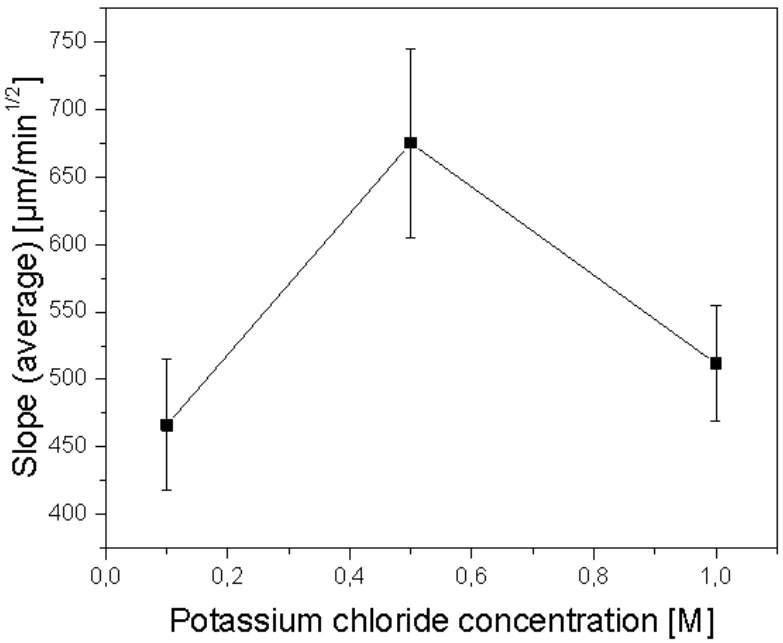

Figure 3.9 – Concentration of potassium chloride vs. the slope.

The reduction in the delamination rate for the higher ionic strength in the KCl solution may be explained by the lower rate of corrosion, which subsequently will reduce the electrical potential gradient, which controls the rate of transport of cations to the cathodic areas. Similar results were also found by Sorensen et al. (Sørensen et al. 2010b), the authors immersed coated iron samples for 9 weeks in different KCl concentrations and observed a decrease in the delamination rate for more concentrated solutions.

3.1.3. Effect of the substrate surface preparation on delamination

In order to obtain further insights on the influence of the substrate surface preparation on the delamination different roughness and textures were studied. The values of roughness were analysed by means of laser scanning confocal microscopy (LSCM). In this work the root mean square surface roughness, R_q, was used as a roughness parameter in order to compare with values from the literature used by Khun and Frankel (Khun und Frankel 2013). Detailed description of roughness parameters as measured by stylus instruments can be found in ISO 4287 (ISO 4287:1997).

Figure 3.10 shows the topography of the directionally abraded steel substrates with different roughness obtained by using different grit papers (80, 500 and 1200 grit paper). In the LSCM images blue represents valleys and red represents peaks.

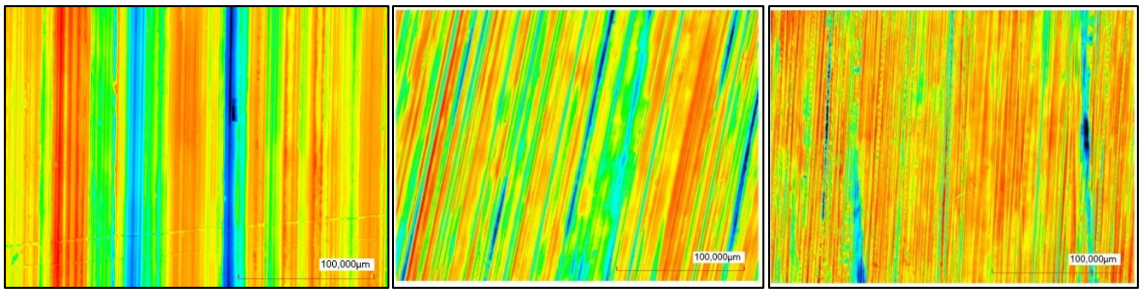

Figure 3.10 - Surface topographies of directionally abraded steel substrates (from left to right: 80, 500 and 1200 grit)

From the LSCM topography, the values of root-mean-square surface roughness (R_q) were obtained and are presented in the Table 3-1 below. The smoother surface (1200 grit paper) shows values of R_q = 48 nm whereas the rougher surface (80 grit paper) has R_q = 275 nm.

Table 3-1- Root mean square surface roughness (R_q) values

Abrasive paper grit	R_q (nm)
80	275
500	71
1200	48

Influence of the surface roughness

If the rate of cathodic delamination is controlled by diffusion of cations along the coating/steel interface, the delamination rate should also depend on the substrate's roughness (Sørensen et al. 2009). Delamination tests were performed on samples with varying surface roughness showed in Table 3-1. Cathodic delamination was observed for all the surface roughnesses, the potential profiles were similar to those shown previously and the slopes (A) obtained are plotted in Figure 3.11. The cathodic delamination rates are shown to decrease significantly with increased R_q value up to around 70nm. For rougher surfaces the decrease was less pronounced. The underlying steel substrate with the smoothest surface (48 nm) had the fastest coating delamination.

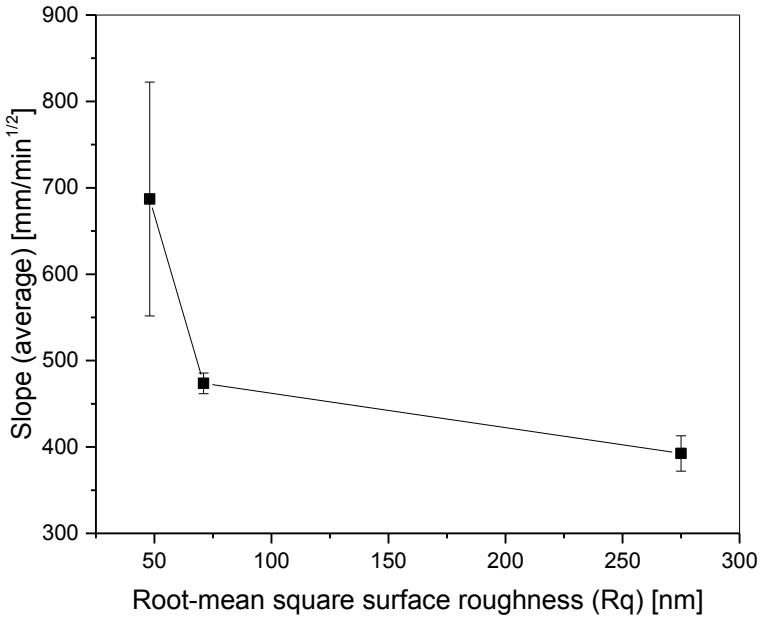

Figure 3.11 – Slope averages and standard deviation vs. root mean square surface roughness. Electrolyte at the defect: NaCl 0.5M

These results are in agreement literature, Khun and Frankel (Khun und Frankel 2013) showed that for very smooth surfaces with R_q values of around 10 to 50 nm there is a steep decrease in the delamination rate, whereas for surfaces with R_q from 50 to 300 nm this decrease is less pronounced. They explained this behaviour by the larger bonding area in the rougher surfaces and more mechanical interlocking promoting the adhesion between the coating and steel substrate. As a result, the promoted adhesion significantly reduces the delamination rate by reducing the degradation of the polymer/metal interface during the cathodic delamination progress.

Influence of the abrading orientation

SKP measurements were made on samples with abrading orientations either parallel or perpendicular to the delamination direction to understand the effect of surface texture on the cathodic delamination. Figure 3.12 presents the slopes obtained from the potential profiles for the samples with different textures abraded with different grit papers (500 and 80). The results show that delamination is faster on the steel substrate with parallel surface scratches than on the one with perpendicular surface scratches. For the rougher surface, paper grit 80, the texture effect on delamination is more evident. Similar behavior was reported in literature for an epoxy coated steel (Khun und Frankel 2013), the authors attributed this behavior to the geometric

constraints, where delamination up the side of polishing grooves is more difficult than along the groove valleys.

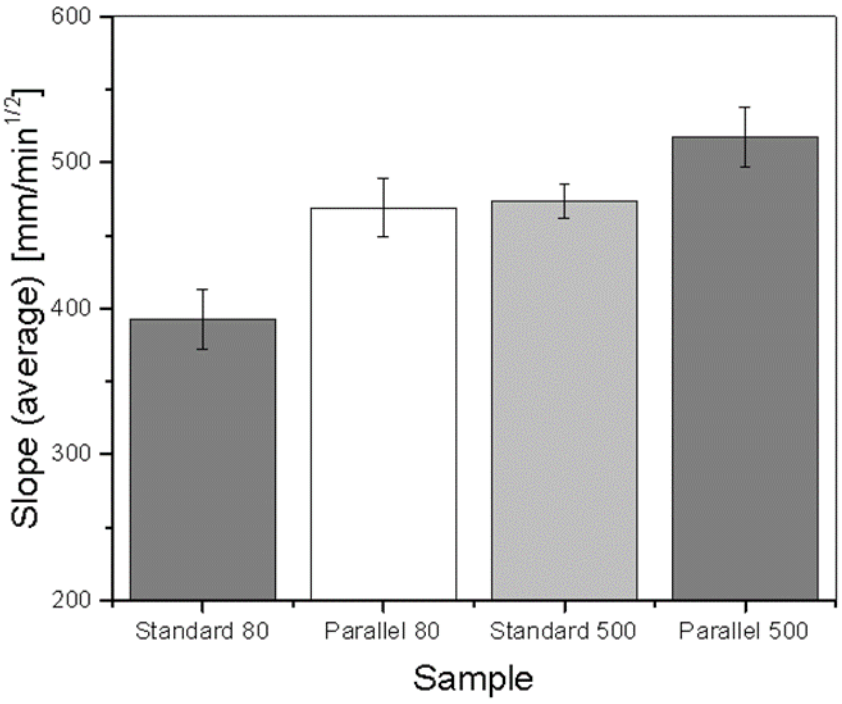

Figure 3.12 – Slope averages and standard deviation of the different abraded orientations. Electrolyte at the defect: NaCl 0.5M

3.1.4. Effect of the coating thickness on delamination

The influence of the coating thickness on the delamination kinetics was also investigated. The diffusion of oxygen through the coating thickness is necessary to support cathodic delamination, however, this should not affect the kinetics as it was already proven to be controlled by the transport of cations along the metal/polymer interface. SKP measurements were performed on samples of varying coating thickness, Figure 3.13 shows the plot of the obtained slopes *A* vs. the coating thickness. As expected, the delamination rate does not depend significantly on the film thickness. This supports the idea that the diffusion of oxygen in the direction perpendicular to delamination does not control the delamination rate for thickness up to 120µm for the studied polymer system. This is, however, not true for all coating systems, for instance for the polybutadiene coating studied by Leidheiser *et al.* the delamination rate decreased with increasing the coating thickness. In this case the delamination rate was determined by the diffusion of oxygen through the coating thickness.

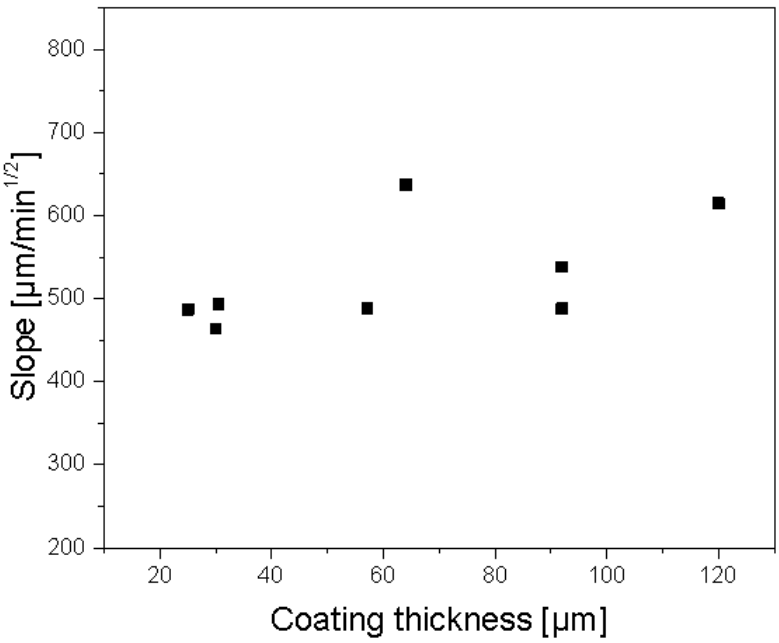

Figure 3.13 – Slopes obtained by the delamination experiments with different coating thicknesses. Electrolyte at the defect: 0.5M NaCl

3.2. SUMMARY

The delamination of the coated steel was followed by means of SKP presenting typical potential distributions for the cathodic delamination mechanism. The transport of sodium ions from a defect in the coating to the cathodic areas was found to be the rate-determining step for the coating system studied. The apparent diffusion coefficient of sodium ions in the ultrathin aqueous layer at the coating–steel interface was calculated.

The effects of electrolyte type and concentration, substrate's surface roughness and texture, and polymer thickness on the cathodic delamination of coated steel samples were investigated using SKP with the following conclusions drawn:

i) the delamination rate is controlled by the diffusion of the hydrated ions into the interface and decreases in the sequence KCl > NaCl > LiCl,

ii) increasing the concentration of NaCl 0.1 M to 1 M increases the delamination rate, whereas for KCl the delamination rate increases for concentrations up to 0.5 M and decreases for higher concentratios,

iii) increased steel substrate roughness dramatically decreased the cathodic delamination of the coating due to the increased interactions between the coating and substrate associated with increased surface areas,

iv) the surface texture clearly shows the significant effect on the cathodic delamination rate, which was faster in the direction of parallel abrasion lines than perpendicular to the lines due to the barrier effect of groove side walls compared to groove valleys,

v) the delamination rate was not influenced by varying the coating thickness from 20 to 120μm, this reinforces the transport-controlled process by the transport of cations at the interface and not by the oxygen diffusion through the coating thickness.

4. CLOSED JOINT GEOMETRY DELAMINATION

The section 4.1 presents the results of the experiments performed on closed joint geometry samples (see Figure 4.1) and the effects of electrolyte type and concentration and atmosphere oxygen partial pressure on the delamination of bonded steel. Section 4.1.4 shows the study of water and oxygen diffusion in the bulk polymer, sodium ion diffusion in the bulk electrolyte and the in-plane diffusion assigned to oxygen and sodium ions at the polymer/substrate interface. Part of this chapter was published by Andreon et al. (Andreon et al. 2019).

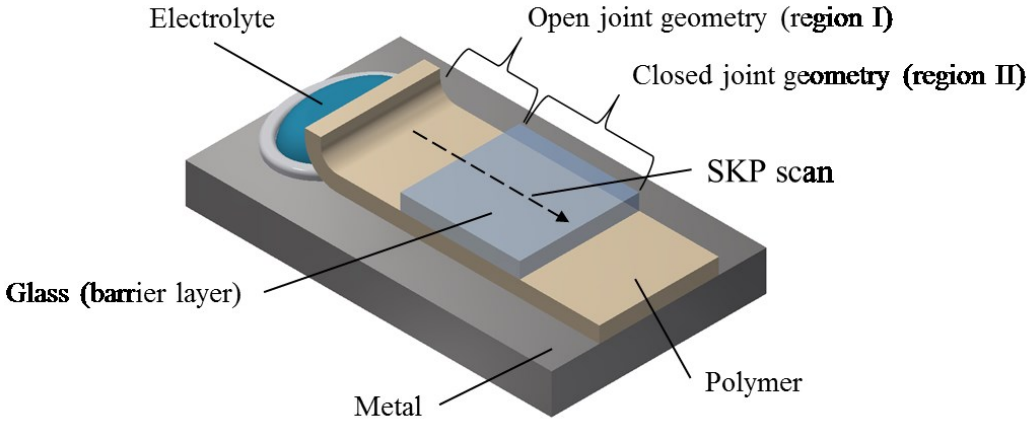

Figure 4.1 - Sketch of the sample with open (region I) and closed (region II) joint geometry

4.1. DELAMINATION OF THE POLYMER NEAR A DEFECT

The samples were prepared in a way (Figure 4.2) that the sample can be divided in two regions Region I represents the open joint geometry and region II the closed joint geometry (where the adhesive is covered by the glass). The SKP delamination tests were performed under similar conditions as for the open joint geometry in order to allow comparisons. The results of delamination tests are illustrated in Figure 4.2 and are divided in two regions of the sample. The Volta potential is measured as a function of the distance from the defect at different times. The time is related to the moment when the electrolyte is added to the defect; the SKP line scan is started immediately afterwards.

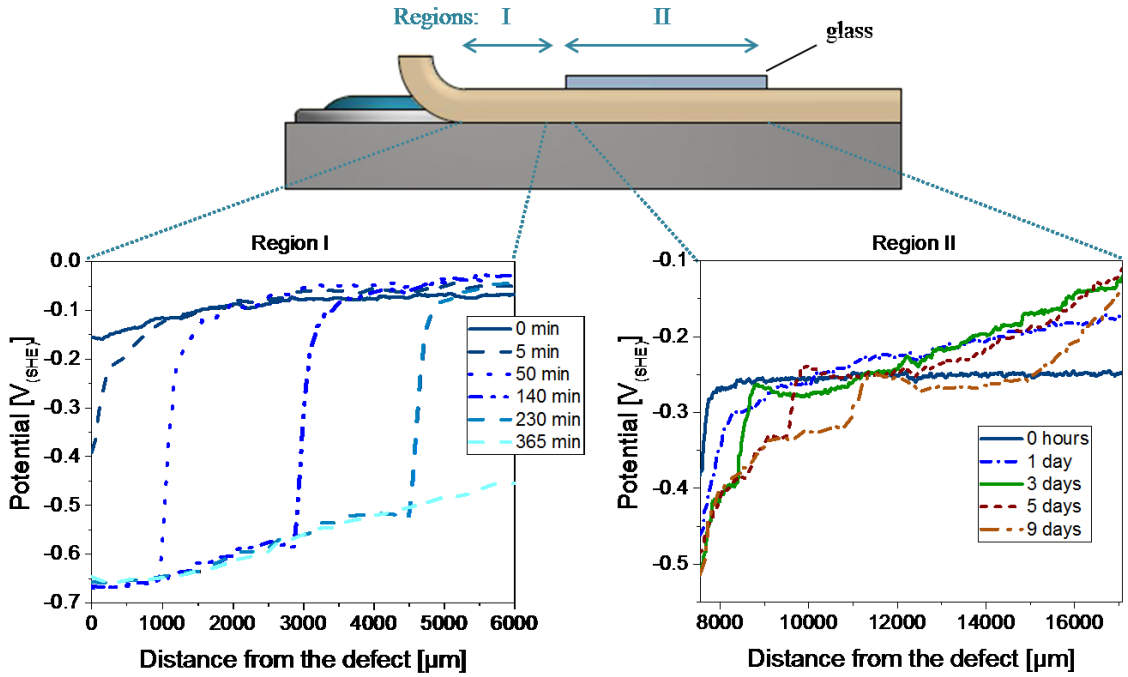

Figure 4.2 – Top part: lateral view of the sample (schematic representation), showing the regions I and II, representing a coated and a joint geometry, respectively. Bottom part: typical potential distributions for the coated sample (region I, left side) and bonded sample (region II, right side) in humid air (>95% r.h.) for different delamination times. Electrolyte in the defect: 0.5M NaCl(aq). Adapted from (Andreon et al. 2019)

Figure 4.2 (bottom, right) shows the measured potential distribution across the adhesive joint under the glass barrier layer (region II). The potential underneath the glass, before addition of the electrolyte, present a constant value of about -0.25 $V_{(SHE)}$. At the very edge of the glass, however, the potential decreases very sharply, a fact which we attribute to the SKP tip scans transitioning from region I to II and experiencing a height step of around 30 µm at the glass border.

After the addition of the electrolyte, the potential at the infiltrated glass border drops to a value of about -0.5 $V_{(SHE)}$ and still presents an initial sharp increase due to similar edge effects as before. With progressing time (days) the potential profiles start displaying an ohmic drop which we attribute to the presence of a galvanic current between the glass edge and an advancing delamination front underneath the glass. The position of such front is clearly indicated by a sharp potential step of about 100 mV/µm which shifts to larger and larger distances away from the defect edge as time progresses.

Although the potential distribution for the infiltrated area is in essence similar to the one observed for region I, two major differences can be identified. First, prior to adding the electrolyte to the defect, the rest potential under the glass is about 150 mV more negative in comparison with region I without electrolyte. Second, after adding the electrolyte to the defect, the potential profile at the intact part (far from the defect) does not remain constant but shifts up and down with time in a nonlinear manner.

As it will be proven later in this work, this behaviour most probably results from the (slow) diffusion of oxygen from the atmosphere along the substrate/polymer interphase, which locally changes the superficial oxidation states of the substrate's oxide layer by chemisorption (Hausbrand et al. 2008).

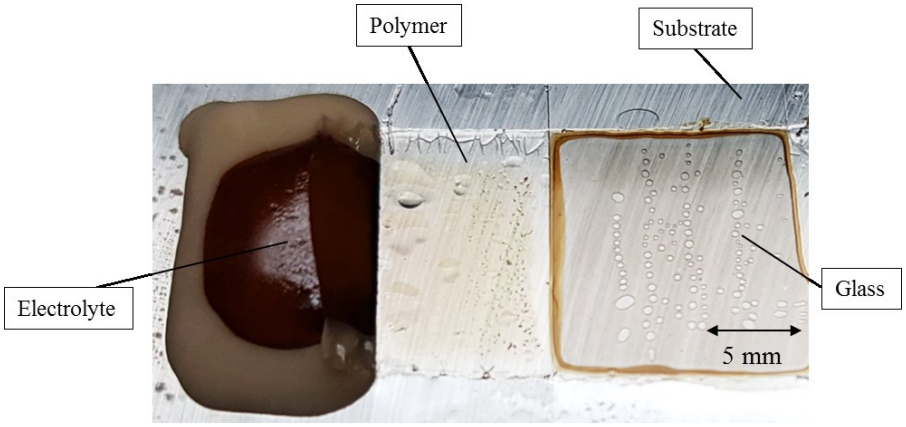

Figure 4.3 – Picture of the sample after 9 days of delamination tests. Adapted from (Andreon et al. 2019)

Corrosion products could be observed only in region II up to a distance of 0.7 mm from the infiltrated border of the glass (see sample picture, Figure 4.3). After drying the sample, the adhesive and glass were removed from the metallic substrate by bonding the glass to a third substrate which was then pulled apart. The fracture was mainly interfacial, taking place between the adhesive and the steel substrate. Often the fracture was interfacial, taking place between the adhesive and the steel substrate. However, mixed adhesive and cohesive failure was also observed for some of the tested samples. When this was the case, the position of the transition from purely interfacial to cohesive failure was identical to the position of the potential step measured with SKP. A representative example in shown in Figure 4.4, which presents the potential distribution after 5 days of delamination along with pictures of the sample before and after removing the adhesive and glass from the metallic substrate. This indicates that oxygen diffusion underneath the glass barrier is at least as fast as ion diffusion (see below). This type

of failure is characteristic from cathodic disbondment occurring in adhesive joints aged in corrosive environments, e.g. immersed in water (Gledhill und Kinloch 2006; Davis und Watts 1996; Weiss et al. 2016; Kinloch et al. 2007).

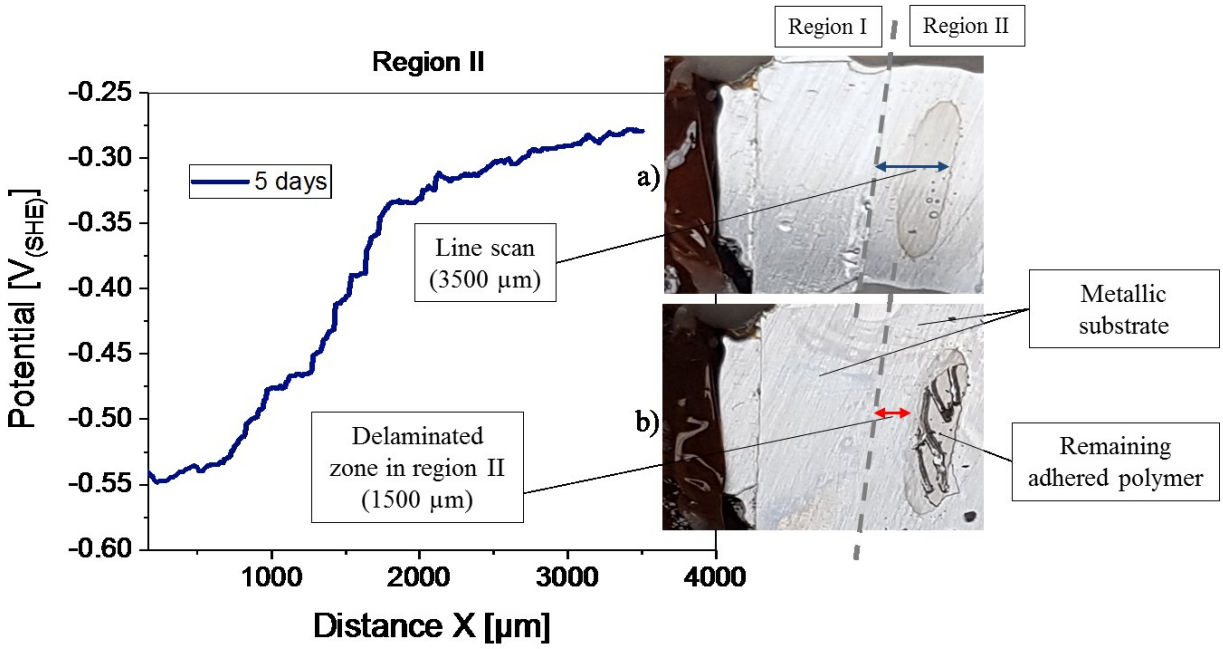

Figure 4.4 - Correlation between the SKP potential profile in region II after 5 days of adding the electrolyte to the defect (0.5M NaCl) and the pictures before (a)) and after (b)) removal of the polymer and glass. Adapted from (Andreon et al. 2019)

Surface scan

It is also interesting to analyse the 2D shape of the advancing delamination front. Therefore a surface scan was performed over the half of the glass surface. Figure 4.5 shows the scanned area of the sample and the typical two-dimensional potential profiles measured with the SKP over the region II after 75 and 140 hours of delamination, left and right hand side, respectively. The potentials are similar to the ones observed in Figure 4.2 and Figure 4.4, they also show the presence of a delamination front advancing towards far away from the defect. The shape of the delamination front is however not linear but has a concave shape, *i.e.* in the middle of the sample ($Y = 0$) the front advances slower, whereas in the borders of the glass ($Y > 0$) delamination advances faster. Furthermore, the shape of the advancing delamination front is similar to the fracture pattern observed in Figure 4.4. This behaviour is expected, once oxygen diffusion from the glass sides along the interphase for region II is believed to be the delamination rate controlling step.

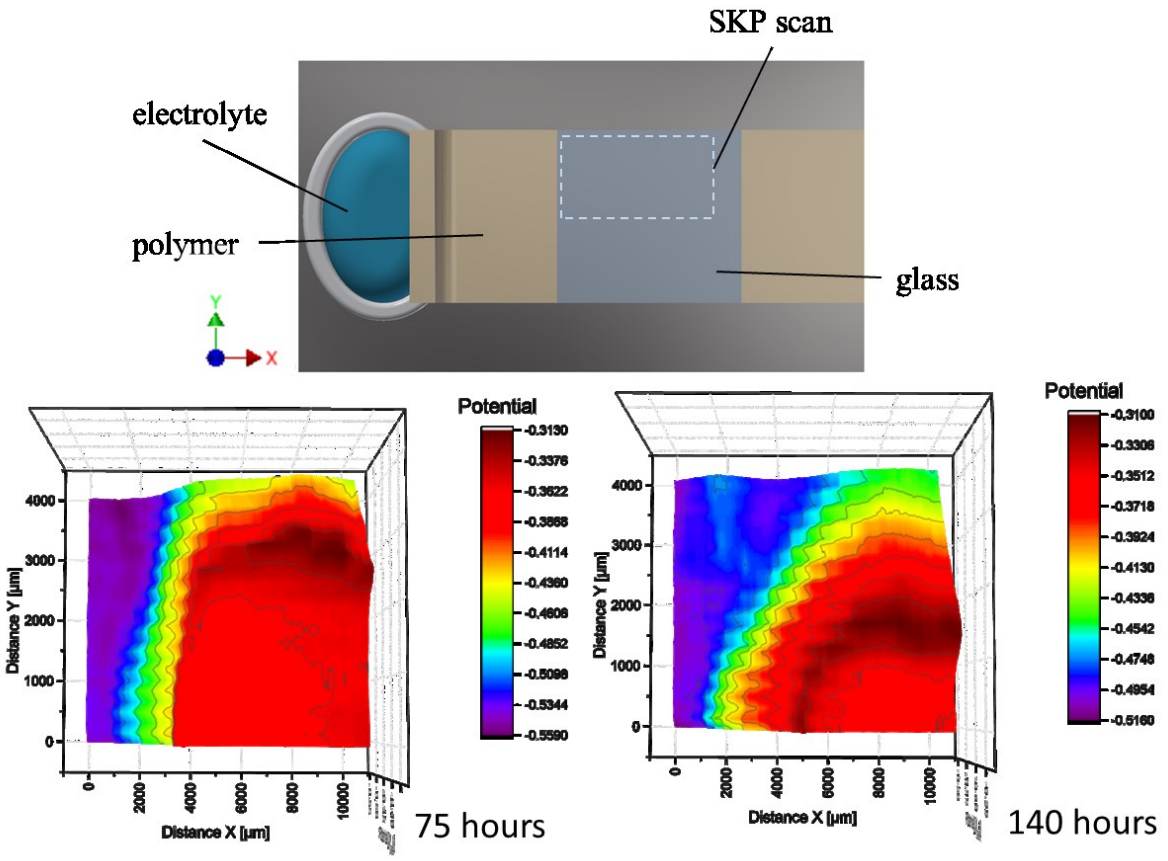

Figure 4.5 - Top part: superior view of the sample (schematic representation), showing the scanned region (in region II). Bottom part: typical two-dimensional potential distributions for the region II after different delamination times, 75 (left side) and 140 hours (right side). Electrolyte in the defect: 0.5M NaCl(aq); color code for potential as legend

4.1.1. Delamination kinetics of the closed joint – region II

In both regions the delamination process is transport-controlled, since the delaminated distance varies linearly with the square root of time. The slope A is equal to $2\sqrt{D}$, where D is the in-plane diffusion coefficient limiting the delamination. In region II diffusion is about hundred times slower than in region I, D presented values of 9.4 10^{-6} cm^2/s and 8.4 10^{-8} cm^2/s in regions I and II, respectively. Furthermore, the diffusion coefficient value has similar magnitude as reported in literature for coated steel with different epoxy systems (1.5 10^{-7} cm^2/s (Wapner et al. 2006), 6.4 10^{-7} cm^2/s (Leng et al. 1998f)).

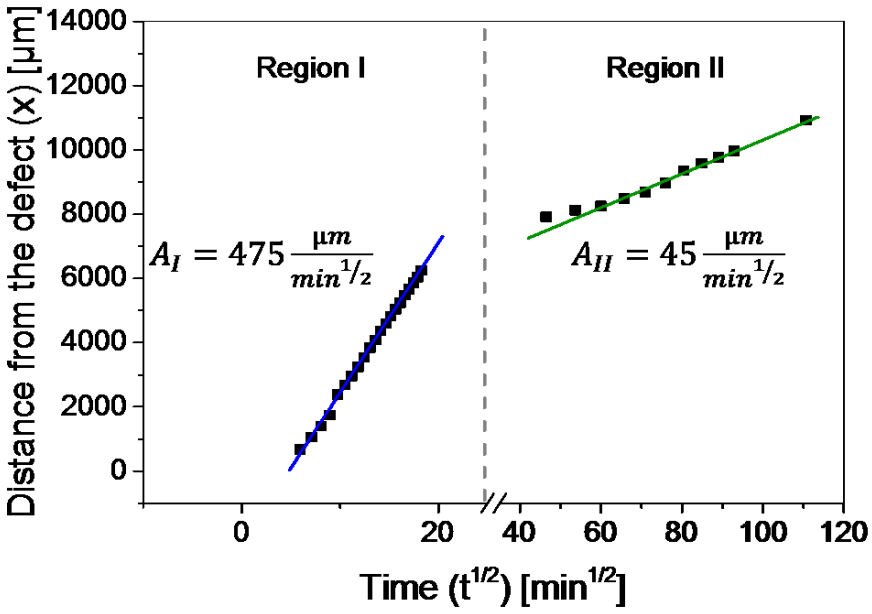

Figure 4.6 – Plot of the delaminated distance (x_{del}) vs. square root of time ($\sqrt{t_{del}}$). Adapted from (Andreon et al. 2019)

4.1.2. Effect of electrolyte type and concentration

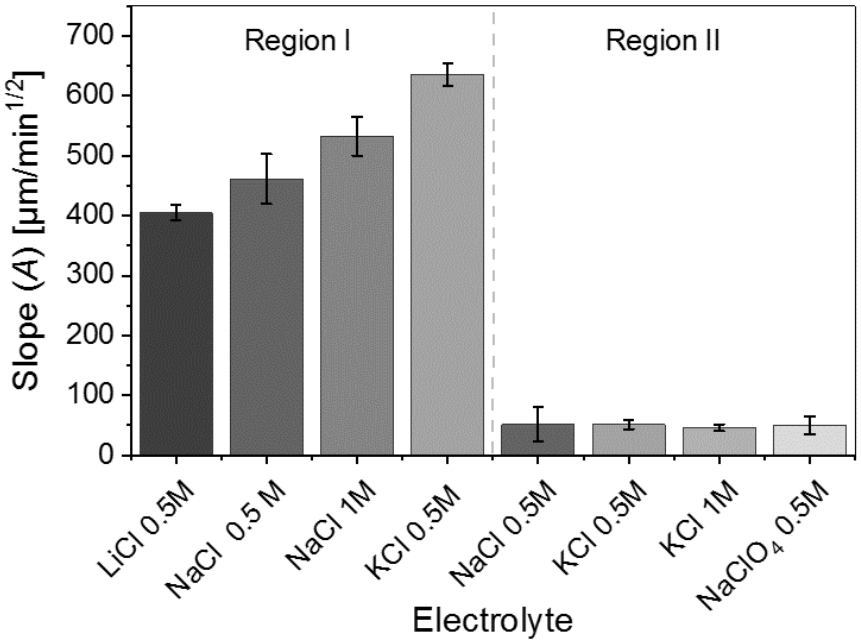

Figure 4.7 – Delamination rate constant A (Equation 12) for different samples, whose defects have been filled with solutions of LiCl, NaCl, KCl and $NaClO_4$ in concentrations of 0.5 and 1M. Some of the values were obtained from chapter 3.

The slopes A were also calculated for samples whose defects have been covered by LiCl, NaCl, KCl and $NaClO_4$ solutions in concentrations of 0.5 and 1M. For comparison, Figure 4.7 displays the results obtained for the open joint geometry (from Figure 3.7 and Figure 3.8) and the results of Region II. As already discussed in chapter 5, the type and concentration of the electrolytes strongly influences the delamination kinetics for the open joint geometry. In region II, instead, there is no detectable trend of the delamination rate constant with different cation types (Na^+ to K^+), anion types (Cl^- to ClO_4^-) and electrolyte concentrations (0.5 and 1M). Therefore, it can be concluded that neither the cations nor the anions transport along the interphase is the determining step for the delamination rate in region II. It also confirms that the sharp potential step in the SKP profiles is due to the presence of a true delamination front, and not to the diffusion front of the cations. A possible limiting step for the delamination in region II is the slow diffusion of oxygen or water molecules from the atmosphere along the substrate/polymer interphase. In addition, the decreased oxygen activity leads to a reduction of the iron oxide layer at the delaminated region. This reduction may also take place as the cathodic partial reaction, instead of purely oxygen reduction (Leng et al. 1998a). Wint et al. (Wint et al. 2016) observed a reduced rate in the delamination of a coated steel after changing the atmosphere from oxygen to nitrogen. They suggested that autoreduction of iron occurs, allowing the delamination to continue even in absence of oxygen.

4.1.3. Chemical analysis of the interfaces by XPS

XPS measurements were carried out after removing the adhesive and glass to reveal the ion distribution at the steel substrate's surface. XPS line scans were performed in steps of approx. 2000 µm, with measuring spot sizes of 400 µm x 400 µm. Figure 8 displays the SKP potential profile of the sample after 9 days (from Figure 4.2) and the corresponding Na^+ and Cl^- amount in atomic %, as measured with XPS. The amount of Na^+ is much higher in region I, around 12 at%, while Cl^- amounts to less than 1 at%. In region II, no chlorine ions were found, and the sodium amount decreases from approx. 13.4 at the glass edge to 0 at% after about 3300 µm. Reference XPS spectra collected on the bare steel surface did not detect the presence of Na^+ or Cl^- ions. On the pure polymer (adhesive) surface, only 0.1 at% of Na^+ could be detected. Therefore, the sodium found at the delaminated area is not due to contamination of the sample. The XPS results clearly supports the assumption made on the basis of the SKP data, that the presence of Na^+ ions is responsible for the more negative potentials values in both region I and II. In particular, the results confirm that the SKP potential step is located at the forefront of the diffusion region of cations from the electrolyte.

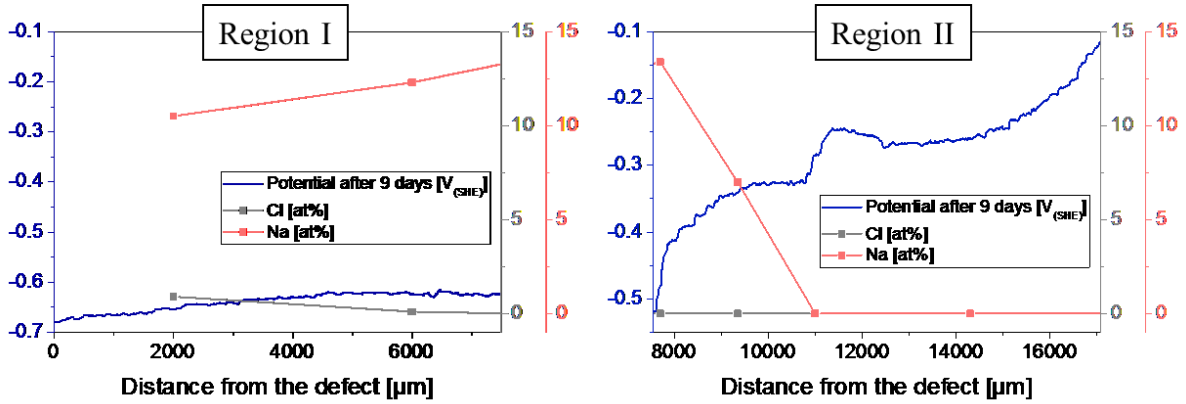

Figure 4.8 – Correlation between the SKP potential profiles in regions I and II after 9 days (same data as in Figure 4.2) and the amount of Na^+ or Cl^- ions measured with XPS after removal of the polymer and glass. The local resolution of each XPS datapoint is about 120 µm. Adapted from (Andreon et al. 2019)

4.1.4. Effect of the oxygen partial pressure on the Volta potential

Within the stability range of the type of oxide layer covering the iron surface (FeO, Fe_3O_4, Fe_2O_3), and especially at the oxide surface, the ratio of $[Fe^{3+}]/[Fe^{2+}]$ decreases with decreasing oxygen activity in the atmosphere (Cornell und Schwertmann 2003), lowering the Fermi level in the oxide. Furthermore, at the very terminal surface, the absence of oxygen might lift the band-bending induced by chemisorption. This can be directly observed with SKP because it measures the changes in the Fermi level of the outermost layer (Leng et al. 1998a; Hausbrand et al. 2008). Data obtained in previous studies (Leng et al. 1998a; Posner et al. 2009) showed that by decreasing the partial pressure of oxygen (P_{O_2}) from 0.2 bar to nearly 0 bar the SKP potential of the coated iron surface decreases from about -0.1 $V_{(SHE)}$ up to values of -0.45 $V_{(SHE)}$, which is the potential of an iron surface in an electrolyte free of oxygen.

In order to understand the potential differences measured for region II in Figure 4.2, it is helpful to consider the situation regarding the oxygen supply that exists for the closed joint geometry. Volta potential measurements were thus performed at the intact region (in the middle of the sample) over the polymer/glass changing the oxygen partial pressure. Figure 4.9 demonstrates that by changing the partial pressure of oxygen in atmosphere from P_{O_2}= 0.02 bar to P_{O_2}= 0.2 bar the potential increase quickly from -0.55 $V_{(SHE)}$ to 0 $V_{(SHE)}$ in region I, and slowly from -0.42 $V_{(SHE)}$ to -0.20 $V_{(SHE)}$ in region II. It is reasonable to assume that, due to the geometric constraints, the oxygen concentration in region II is smaller than in region I.

Consequently, at least at the very surface of the oxide layer, the ratio of $[Fe^{3+}]/[Fe^{2+}]$ within in region II is expected to be lower than in region I. Thus, the more negative potential values observed for the intact region II could be attributed to the surface coverage of absorbed oxygen and the redox-properties of the iron oxide layer under nearly anoxic conditions.

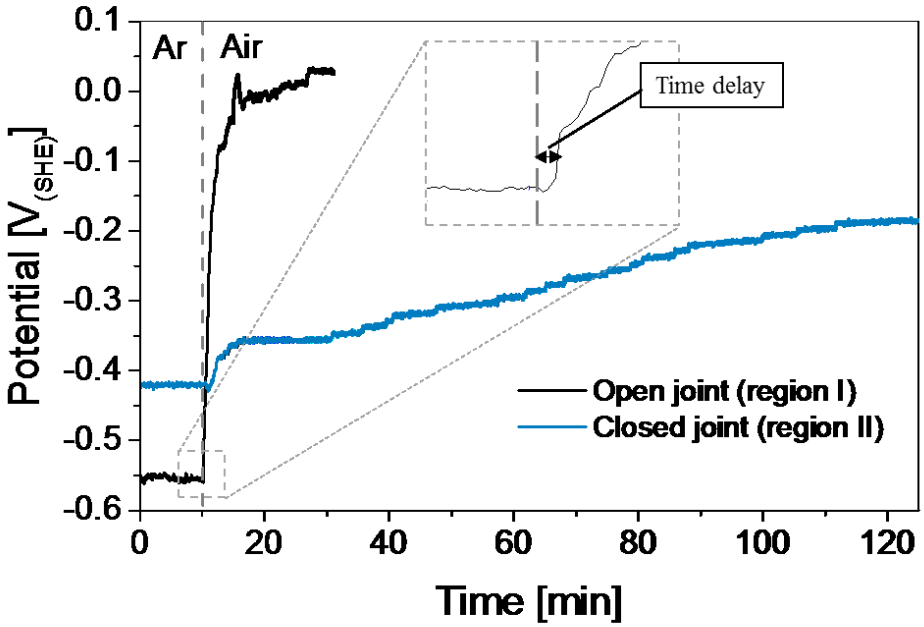

Figure 4.9 – Potential difference after exchanging the atmosphere from water saturated argon (time = 0) to water saturated air (time = 10 minutes). Measurements taken from one point in regions I and II before adding the electrolyte. Zoomed: time delay (breakthrough time) between atmosphere change and potential rise for region I. Adapted from (Andreon et al. 2019)

In region I, oxygen ingress takes place from the entire adhesive surface, quickly diffusing across the adhesive in direction perpendicular to the substrate's plane, along a path of about 30 µm. This is why a nearly constant potential plateau is observed before addition of the electrolyte (see Figure 4.2 left, 0 minutes). In region II, the glass barrier forces diffusion of oxygen to take place along the metal/polymer interphase, along a path as long as 5 mm. Therefore, at any given point in time, a (negative) gradient in its concentration is expected, with a corresponding decrease of the $[Fe^{3+}]/[Fe^{2+}]$ ratio with larger and larger distances from the glass edges, both the left one at about 7700 µm (at the electrolyte side) and the right one at about 16500 µm. This is in fact consistent with the concave shape of the SKP potential profile (Figure 4.2 and Figure

4.8, right-hand sides), which decreases slightly just after the potential step at the delamination front and increases again at larger distances.

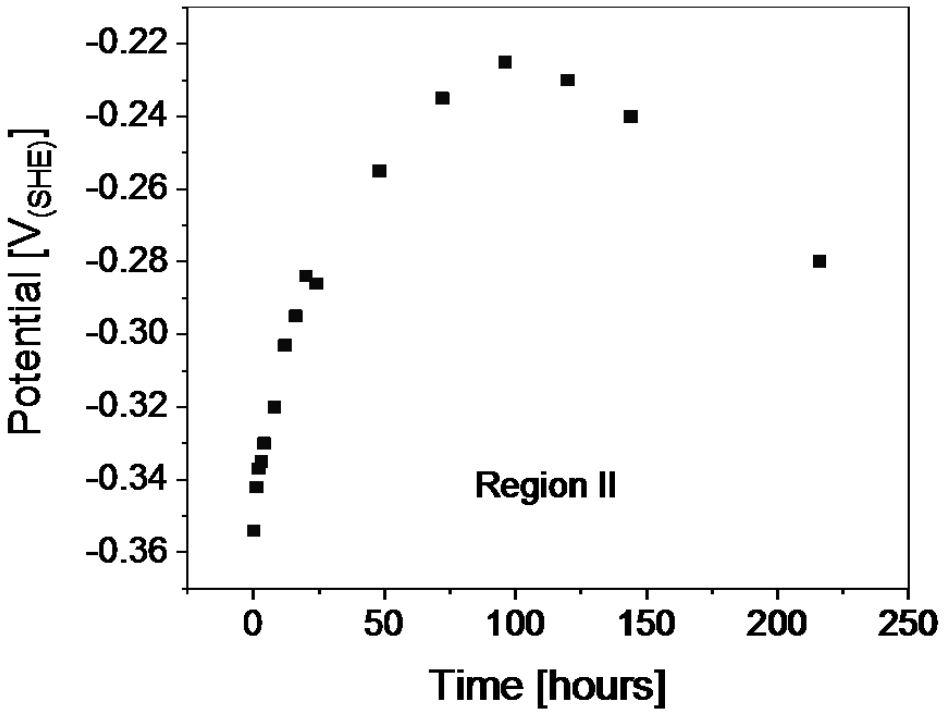

Figure 4.10 – Potentials from Figure 4.2 at the distance 16500 µm from the defect vs. √time. Adapted from (Andreon et al. 2019)

The time-dependency of the SKP potential in region II at a fixed point well beyond the delamination front (16500 µm) is reported in Figure 4.10 (from the same dataset as in Figure 4.2). In the first 100 hours the potential increases, after that a maximum is reached and a decrease is observed. These findings are in line with previous results reported in the literature (Leng et al. 1998a), where the galvanic current at a metal/polymer interface was observed first to increase and, after long exposure to corrosive media, to strongly decrease. While a precise explanation remains unclear at the present stage, we can tentatively interpret the results in the following way. Initially, there is an increase in the oxygen ingress and diffusion from the glass edges in the direction parallel to the sandwiched structure (with respect to the scheme in Figure 4.2, top). The subsequent decrease could be caused by (i) oxygen consumption at the advancing delamination front; (ii) the formation of corrosion products around the border of the glass, providing an additional anodic drive force (Figure 3.4); (iii) cation diffusion along the outer border of the glass. We note that diffusion of cations under the glass beyond the delamination front does not occur, as proven by the XPS measurements in Figure 4.8.

4.2. DETERMINATION OF DIFFUSION COEFFICIENTS

4.2.1. Diffusion of oxygen in the bulk polymer

The potential transient measured at the open joint geometry after increasing the oxygen activity shows a little time delay (shown in the insert of Figure 4.9) between the change of the activity and the onset of the potential upward slope. This time delay occurs due to the mixing time (t_{mix}), *i.e.* the time required for the atmosphere to be exchanged, and due to the oxygen diffusion time (t_{diff}) through the polymer thickness. Figure 4.11 shows a linear relation between the time delay (breakthrough time) and the square of the polymer thickness d^2. The intercept is the mixing time. The diffusion coefficient (D_{O_2}) can be derived from the slope of the plot using Equation 13 (Leng et al. 1998a; Crank 1976).

Equation 13

$$D_{O_2} = \frac{d^2}{20 t_{diff}}$$

The resulting value is $D_{O_2} = 4.8x10^{-8}\,\frac{cm^2}{s}$, which is comparable to the coefficient reported by Leng *et al.* on an Epoxy system (Leng et al. 1998a). Furthermore, the diffusion coefficient is identical to the value obtained from the free standing films tested with a gas permeability tester ($D_{O_2} = 4.79x10^{-8}\,\frac{cm^2}{s}$).

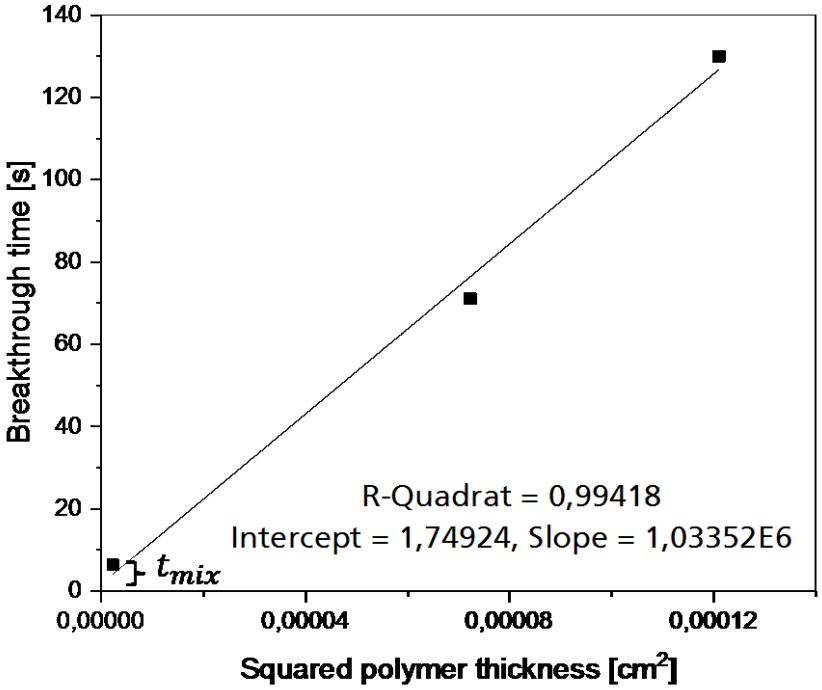

Figure 4.11 – Breakthrough time after exchanging the atmosphere from water saturated argon to air (see Figure 4.11) as function of the square of the polymer thickness. Adapted from (Andreon et al. 2019)

4.2.2. Diffusion of water in the bulk polymer

In order to investigate the water uptake of the bulk polymer, a free-standing film was measured by means of DVS. Figure 4.12 shows typical time evolutions of the net percent change in mass (based on dry mass) for two independent measurements, together with the humidity change in the DVS. The sorption/desorption profiles for both samples show relatively high mass uptakes, around 20 to 25% with respect to the dry mass. Fitting of the curves leads to an average water vapor diffusion coefficient $D_{H_2O} = 1.5x10^{-7}\,\frac{cm^2}{s}$. Comparable coefficients were reported in literature for a similar polymer system (Goossens et al. 2004).

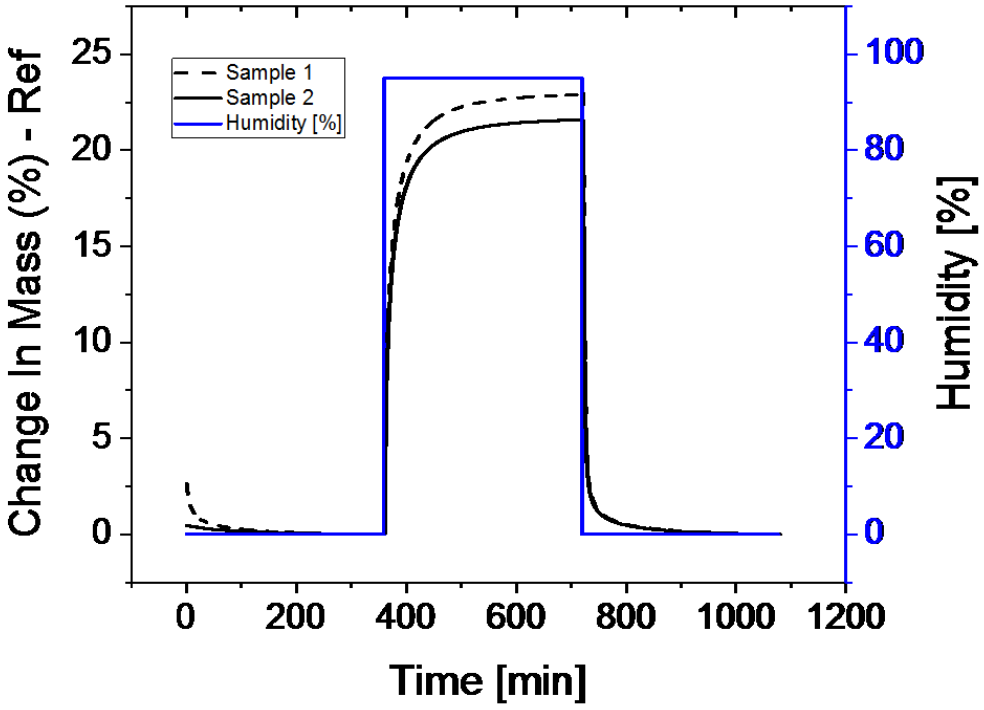

Figure 4.12 – Sorption/desorption cycle for two adhesive film samples showing water sorption kinetics at 20°C. Black lines (left axis): relative mass change; blue line (right axis): relative humidity change. Adapted from (Andreon et al. 2019)

4.2.3. Diffusion of sodium ions at the interface iron/polymer

Table 4-1 shows a comparison of the diffusion coefficients for water and oxygen in the bulk polymer, sodium ion in the bulk electrolyte and the in-plane diffusion coefficients assigned to oxygen and sodium ions at the polymer/substrate interface, as estimated from the data in Figure 4.2 (see above). In the latter, the electrical field gradient modifies the mobility of the sodium ions, however, for simplification, we considered purely diffusive transport (Leng et al. 1998e).

The results indicate that water is present at a high concentration in the polymer and can permeate faster than oxygen through the coating. This allows the electrochemical processes to occur and indicates that water diffusion is not the rate-determining step for the delamination process. The calculated diffusion coefficient of sodium ions for region I is smaller than that literature values for aqueous electrolytes, this agrees with the idea that the ions diffuse along the interface in a gel-like polymer layer rather than in a bulk electrolyte (Leng et al. 1998e; Grundmeier et al. 1998). In addition, the calculated diffusion coefficient for the oxygen in region II are in the same order of magnitude as for the oxygen in the bulk polymer. This, again,

corroborates the fact that oxygen diffusion might control the rate of delamination for this polymer system in the close joint geometry.

Table 4-1 - Diffusion coefficients for water and oxygen in the bulk polymer, sodium ion in the bulk electrolyte and the in-plane diffusion coefficients assigned to the sodium ions at the interface

Specie/medium	**Diffusion coefficient** $\left(\frac{cm^2}{s}\right)$	**Method (temperature)**
Water in bulk polymer	$D_{H_2O} = 1.5x10^{-7}$	DVS (20°C)
Oxygen in bulk polymer	$D_{O_2} = 4.8x10^{-8}$	SKP and permeability tester (24°C)
Oxygen at the interface - Region II	$D_{Na} = 8.4x10^{-8}$	Calculated diffusion coefficient (20 – 24°C)
Hydrated sodium ions at the interface - Region I	$D_{Na} = 9.4x10^{-6}$	Calculated diffusion coefficient (20 – 24°C)
Sodium ions in bulk electrolyte	$D_{Na} = 1.5x10^{-5}$	From reference (25°C) (Leng et al. 1998e; Fell und Hutchison 1971)

4.3. DELAMINATION OF THE POLYMER NEAR A DEFECT – WITHOUT REGION I

Samples were prepared without region I in order to further understand the mechanisms of delamination occurring in a closed joint geometry where not only the cations but also the anions from the defect have access to the interphase. Figure 4.13 shows the schematic representation of the sample and the line scan position of the SKP delamination tests. The tests were performed under similar conditions as for the samples with regions I and II (Section 4.1).

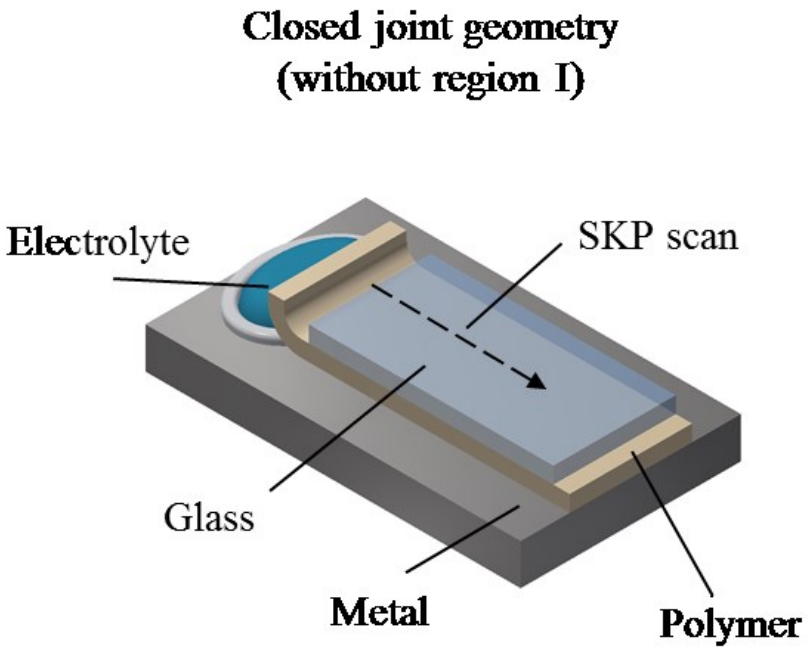

Figure 4.13 – Top part: lateral view of the sample (schematic representation), showing the SKP line scan

The results of delamination tests are illustrated in Figure 4.14. The Volta potential is measured as a function of the distance from the defect at different times. The time is related to the moment when the electrolyte is added to the defect. The measured potential distribution is similar as the one measured in Region II across the adhesive joint under the glass barrier layer (Figure 4.2). Before the addition of the electrolyte, the potential presents a constant value of about -0.25 $V_{(SHE)}$. After the addition of the electrolyte, the potential at the infiltrated glass border drops to a value of about -0.5 $V_{(SHE)}$, with progressing time (days) the potential profiles start displaying an ohmic drop. The delamination front for this sample presents a potential step of about 50 mV/μm which shifts away from the defect as time progresses.

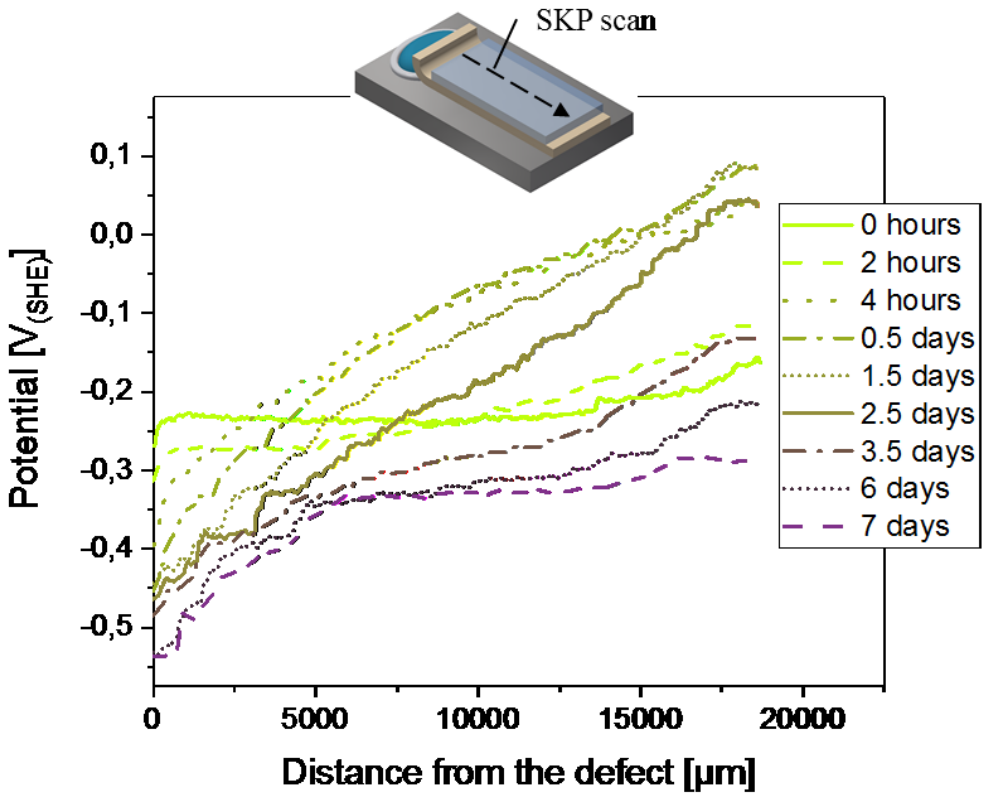

Figure 4.14 - Bottom part: typical potential distributions for the sample without region I in humid air (>95% r.h.) for different delamination times. Electrolyte in the defect: 0.5M NaCl(aq)

The time dependence of the delamination reaction for this sample (obtained from Figure 4.14) is shown in Figure 4.15. The delamination process is transport-controlled, since the delaminated distance varies linearly with the square root of time. The in-plane diffusion coefficient was calculated using the delamination rate constant *A* (slope) of the curve fitted with Equation 12 and has a value of 1.1 10^{-7} cm^2/s. The diffusion coefficient value has similar magnitude as the one calculated for region II in section 4.1 (8.4 10^{-8} cm^2/s).

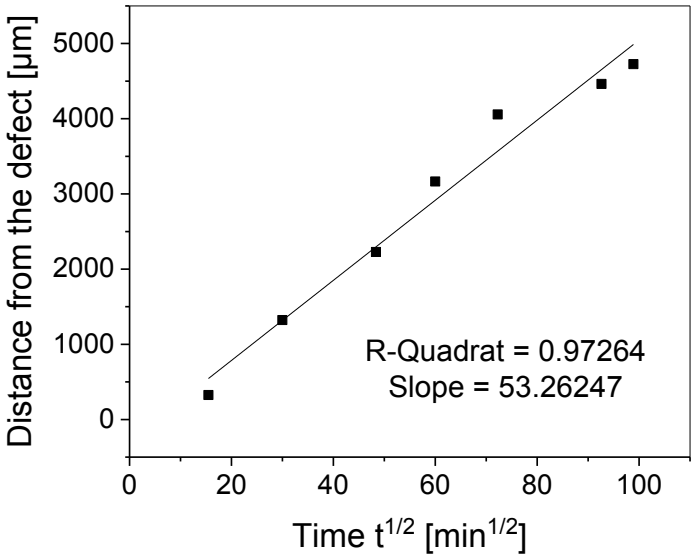

Figure 4.15 - Plot of the delaminated distance (x_{del}) vs. square root of time ($\sqrt{(t_{del})}$)

Figure 4.16 shows the picture of the sample after 7 days of delamination tests. Contrary to the observed for the samples with region I, corrosion products are now observed under the glass in a region of around 4mm near the defect. The real active interface shown in the SKP potential profile after 7 days in Figure 4.14 is larger than the rusted area observed in the picture, around 5mm vs. 4mm respectively.

Figure 4.16 - Picture of the sample after 7 days of delamination tests

Furthermore, the oxide colours change from green to orange/red-brown. It is known that in the presence of oxygen the dehydrated corrosion product of iron is thought to be principally haematite (red), this corrosion product may change in the absence of oxygen to become partly or fully either magnetite (black) or fourgerite (green rust) (Watson et al. 2014). Green rusts are a group of Fe^{II} – Fe^{III} hydroxy compounds which are formed under anoxic conditions (Cornell

und Schwertmann 2003). These observations suggest that the delamination mechanism of this type of sample might be anodic undermining instead of cathodic delamination. For iron substrates, green rust is stable in the anodic site as a result of the low oxygen concentration. The iron oxide identification supports the mechanism of differential aeration (Saraby-Reintjes 1972) where the anodic site is the advancing delamination front and the oxygen reduction takes place outside the joint, *e.g.* at the defect. To further verify this assumption, surface analyses were performed and the results will be discussed in the following chapter.

4.3.1. Chemical analysis of the interfaces by XPS

After removing the adhesive and glass, XPS measurements were carried out in two samples, delaminated using 0.5M of NaCl and KCl as electrolytes. Figure 4.17 shows the ion distribution on the steel substrates (Cl^- and Na^+ or K^+ amount in atomic %) and the SKP potential profile of the sample after 7 days. As expected, no Na^+ was found for the sample using KCL as electrolyte and no K^+ was found for the sample delaminated with NaCl. On both samples the presence of approx. 12 at% of chlorine ions supports the assumption of anodic undermining mechanism. Furthermore, cations were detected only in smaller amounts and near the defect (at x<5000µm). Two delamination fronts can be observed for both samples and the SKP potential steps are located at the forefront of the migration region of the anions and cations from the electrolyte. This might be associated to a change in the mechanism after certain time of exposure, e.g. from anodic undermining to cathodic delamination. The literature shows that that the SKP is able to detect this transition (Doherty und Sykes 2004; Fürbeth und Stratmann 2001b).

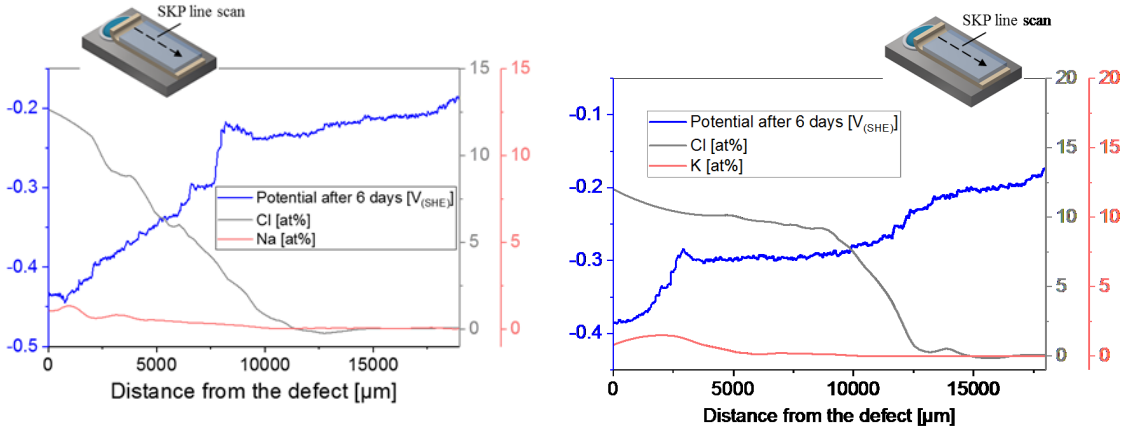

Figure 4.17 - Correlation between the SKP potential profiles in the closed joint geometry (without region I) after 7 days and the amount of Na^+, K^+ or Cl^- ions measured with XPS after removal of the polymer and glass. The local resolution of each XPS datapoint is about 120 µm. Electrolytes: NaCl (left), KCl (right)

4.4. SUMMARY

The delamination of the bonded joint steel was followed by means of SKP. The potential distributions of the buried interface polymer/metal were measured using a thin glass as barrier layer. For the closed joint geometry it was found that it is not the transport of sodium ions from a defect into the interface that controls the delamination rate but the ingress of oxygen. Therefore, the delamination rate was found to decrease in around 100 times when compared to the open joint geometry.

The diffusion coefficients of for water and oxygen in the bulk polymer and the in-plane diffusion coefficient assigned to oxygen at the polymer/substrate interface were calculated from the experiments. Furthermore, the effects of the joint geometry on the delamination mechanisms were presented and will be discussed in detail in the following section.

5. DISCUSSIONS AND OUTLOOK

In this chapter **Section 5.1** contains the discussion of the presented results from previous sections including the models proposed for the delamination mechanisms in closed joint geometries. **Section 5.2** provides an assessment of the novel contributions of the present work to the research field of delamination of adhesive joints and concluding remarks are made to evaluate whether the research objectives were accomplished. Finally, some suggestions for future topics of research that could widen the present study are given in **Section 5.3**.

5.1. DISCUSSIONS

The primary objective of this work was to study the kinetics of electrochemical processes that take place in an adhesively bonded joint under corrosive conditions. These processes are detectable by means of scanning Kelvin probe method and well described in literature for coated metals. However, this method has not yet been applied for closed joint geometries, mainly because finding a suitable barrier layer which allows the SKP measurements is extremely challenging. Therefore, a crucial achievement of this work was to demonstrate that a thin borosilicate glass does not block nor significantly influences in the SKP signal, thus allowing the measurements of the processes occurring at the buried interphase polymer/metal.

The open joint delamination tests results (shown in chapter 3) demonstrated that the cathodic delamination mechanism proposed in literature by Leng *et al.* (Leng et al. 1998f) occurs also for the coating system in the present study and served as base for comparison with the closed joint geometry and for understanding the mechanisms occurring in this type of geometry. First, as water, oxygen and cations are essential for the electrochemical processes to take place in the cathodic delamination mechanism, it is interesting to have a deeper look on the permeability of those species in the adhesive (Acronal) and in different diffusion paths. The diffusion coefficients of hydrated sodium ions, water and oxygen (from Table 4-1) and the transport paths are displayed in Figure 5.1.

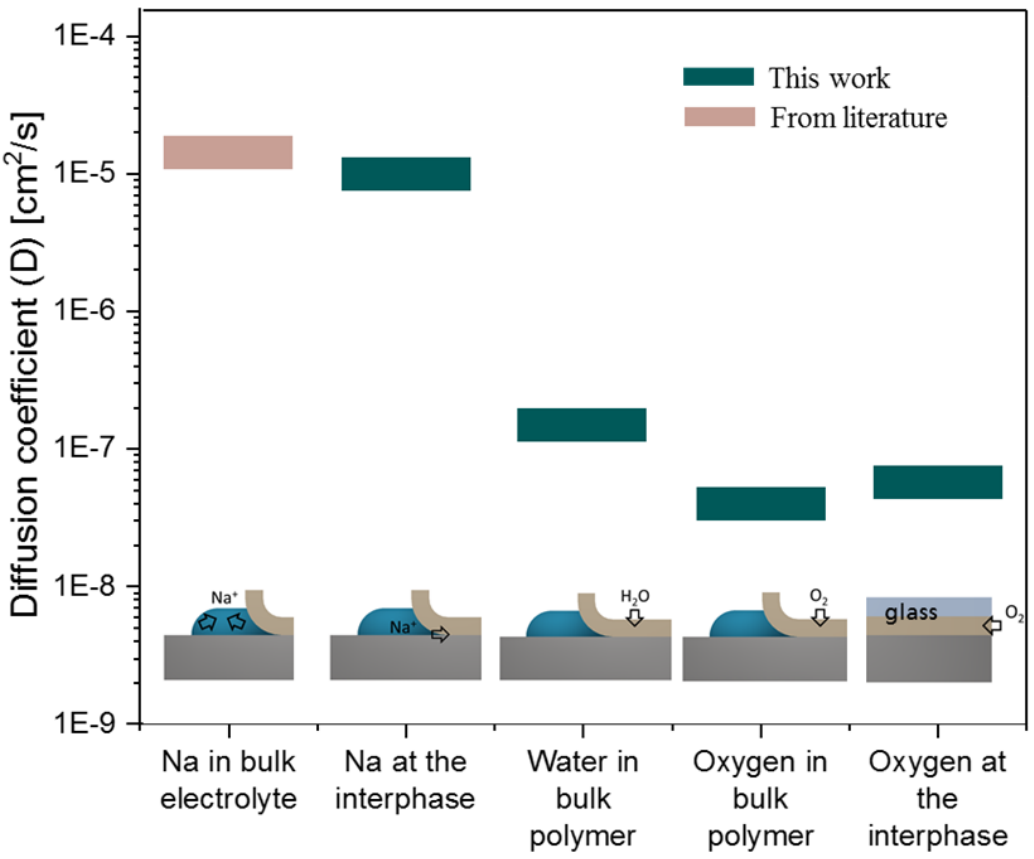

Figure 5.1 – Measured diffusion coefficients of hydrated sodium, water and oxygen vs. the transport path, data from Table 4-1. Literature: (Fell und Hutchison 1971)

Although the transport of hydrated sodium ions along the adhesive/metal interface in an open joint is around 100 times faster than the transport of water and oxygen through the adhesive, the results in chapter 3 showed that the delamination is still controlled by the ingress of hydrated sodium ions along the adhesive/metal interface. It was previously shown in Figure 4.12 that Acronal reaches saturation (25%) after the first hour of exposure to humid atmosphere and in Figure 4.11 that oxygen reaches the metallic surface through the polymer in 1 - 2 min. Thus, as the delamination tests are performed after few hours of stabilization in the SKP chamber at 93% r.h. (see Figure 2.7), when the delamination starts the polymer is already saturated with water, as well as oxygen is already available at the interphase. Here the different diffusion paths play an important role, while water and oxygen are able to quickly reach the interphase through the thin adhesive layer (around 30µm of thickness), cations have to be transported from the defect into the interphase. Even if Na^+ or Cl^+ were able to diffuse through the coating thickness, this transport would be too slow as the usual diffusion coefficients of ions in bulk polymer are in

the order of 10^{-13} cm^2/s (Sørensen et al. 2010c). These findings are in agreement with the cathodic delamination mechanism proposed by Leng *et al.* (Leng et al. 1998f).

Now for the closed joint geometry, not only ions but also water and oxygen have to be transported along the interphase adhesive/metal. The diffusion coefficient of oxygen through the adhesive obtained by means of permeability tests have the same order of magnitude of the diffusion coefficient of oxygen along the interphase, calculated from the SKP tests. Besides that, water diffuses faster than oxygen (at least for Acronal), those are further evidences that the delamination rate is controlled by the diffusion of oxygen along the interphase for the closed joint geometry.

Barrier to oxygen diffusion

It is interesting to understand the delamination behavior when no oxygen is allowed to diffuse from the glass edges. Therefore, further experiments were performed on a sample with sealed glass edges in order to avoid (or at least reduce) oxygen ingress into the interphase. Figure 5.2 displays the sample sketch with the barrier around the glass edges created with an epoxy paste and the potential distribution of the line scans performed over 6 days. First, a nonlinear decrease of potentials starting from around 0.1 $V_{(SHE)}$ is observed near the defect and after some time the potentials values reach a plateau of around -0.5 $V_{(SHE)}$. It is remarkable that no delamination front is detected, the possible explanation for this could be that the oxygen present under the glass at the beginning of the experiment will be consumed at the glass edge ($x = 0$) until when no oxygen is available anymore. Indeed, the more negative potential values (-0.5 $V_{(SHE)}$) observed are an indication that the joint interface is probably anoxic (behavior shown in section 4.1.4). One could speculate that, as there is nearly no potential difference between the defect and the intact area, the driving force for the delamination is ceased and delamination will probably not advance, or will advance with a strongly decreased rate. An additional interpretation is that probably oxygen does not diffuse from the glass edge next to the defect and as the other edges are sealed no oxygen is available for the cathodic partial reaction, therefore no delamination is observed in this case.

These analyses indicate how crucial the oxygen permeability in the polymer and the transport paths are for the long-term stability of an adhesive joint.

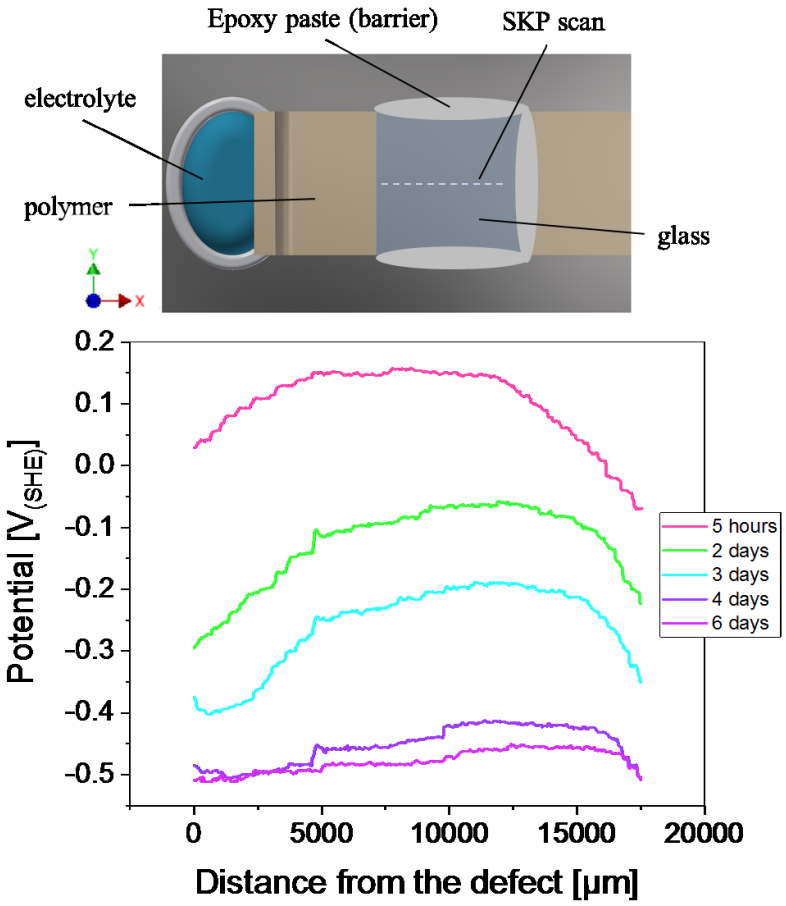

Figure 5.2 - Top part: superior view of the sample (schematic representation), showing the sealed parts of the sample (in region II). Bottom part: potential distribution of the line scans in region II after different delamination times. Electrolyte in the defect: 0.5M NaCl(aq)

Cathodic delamination vs. anodic undermining

Based on the electrochemical model for the cathodic delamination of coatings proposed by Leng e*t al.* (Leng et al. 1998f) and based on the delamination tests results of chapters 3 and 4, models for the corrosion mechanisms occurring in closed joint geometries are summarised schematically in Figure 5.3 and Figure 5.4, for geometries with and without region I respectively.

In the sample configuration with region I, the cathodic delamination mechanism takes place. When the electrolyte is added to the defect there is a formation of a galvanic couple between the defect and the intact interface. The metal dissolution occurs at the defect (anode) and is balanced by oxygen reduction occurring at the intact polymer/substrate interface (cathode), which results in an alkaline electrolyte. Thus, at the interface, no anodic metal dissolution is possible either due to the presence of the polymer or due to the presence of the alkaline

electrolyte. The defect becomes acidic and this pH-shift stabilizes the electrochemical element. In region I oxygen diffuses though the polymer and, as a result of the oxygen reduction occurring at the interphase, there is an excess of negative charges (OH- ions). The loss of adhesion between the polymer and the substrate is believed to be due to the reaction products from the oxygen reduction reaction (Wroblowa 1992; Grundmeier et al. 1998). Due to the negative charges excess, cations then migrate from the defect to the delaminated region and this transport of cations controls the delamination rate for region I (coating). Once delamination reaches the region II its velocity is hindered in around 100 times as previously shown in Figure 4.6. The cations continue advancing from region I towards region II, however the glass acts as a barrier layer and therefore oxygen cannot be transported through the polymer thickness. In region II oxygen has to be supplied from the glass edges, thus oxygen diffusion along the interface is the delamination controlling step for this type of joint geometry.

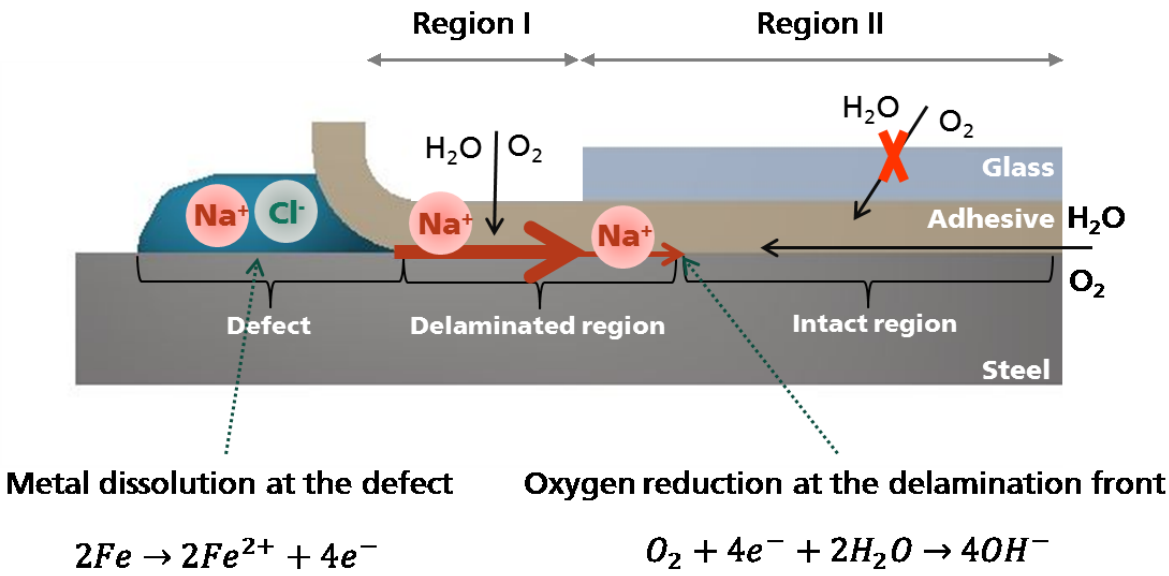

Figure 5.3 – Schematic illustration of the mechanism of cathodic delamination

For the joint geometry without region I the delamination mechanism suggested is the anodic undermining (see Figure 5.4). Here it is believed that the galvanic element is driven by an oxygen concentration cell, in this case the electrodes are in contact with different oxygen concentrations; the electrode in contact with the lower oxygen concentration becomes the anode, the electrode in contact with the higher oxygen concentration becomes the cathode (Saraby-Reintjes 1972). Being the lower oxygen concentration at the interface and the higher concentration in the defect, the defect becomes now the cathode and the delamination front the anode.

The excess of negative charges resulting from the oxygen reduction in the defect, leads to migration of Cl- ions in the direction of the anode (polymer/metal interface). The presence of Cl- ions at the delaminated region was confirmed in the already shown XPS results in Figure 4.17. It is important to note that migration of the chlorides and activation of the interface follows the dependence of square root of time (Nazarov et al. 2018). This behavior was observed in the present work, as shown previously in Figure 4.15.

As a first step of the anodic undermining the chloride ions migrate from the defect along the interface without significant rusting. Following this transport of anions occurs the metal or metal oxide dissolution beneath the polymer. This dissolution is usually green rust as it is stable in low oxygen concentrations and the iron oxide identification supports the mechanism of differential aeration (Cornell und Schwertmann 2003).

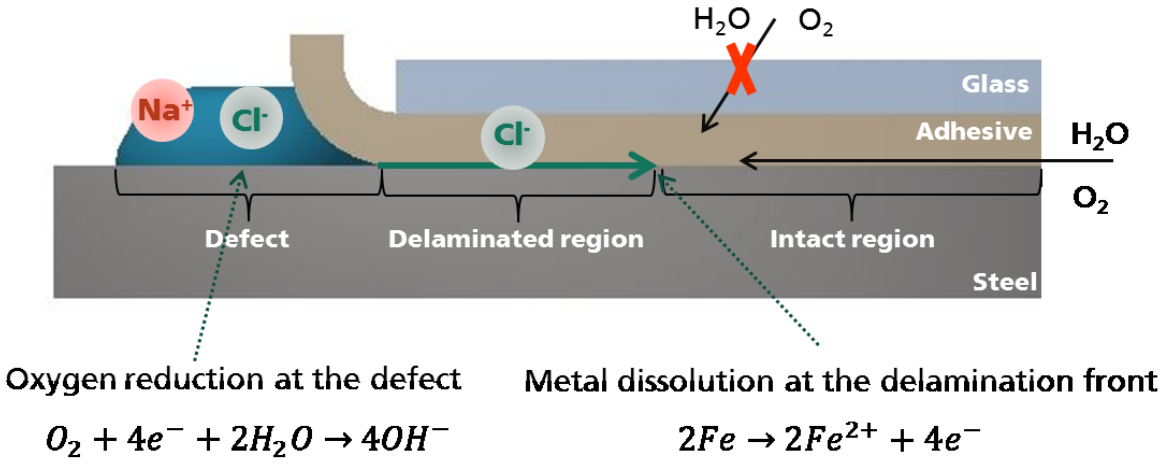

Figure 5.4 – Schematic illustration of the mechanism of anodic undermining

After longer delamination times, cations also migrate through the interphase, following the migration of anions. This is shown in the correlation of chemical analysis vs. potentials measured with the SKP in Figure 5.5 (from Figure 4.17), where the concentration of chlorine correlates well with the first potential jump which limits the anodic area, whereas the concentration of potassium correlates well with the second potential jump. The area between the two potential jumps could be a local cathode leading to the migration of positive charges (K^+) to compensate the formation of hydroxyl ions from the oxygen reduction.

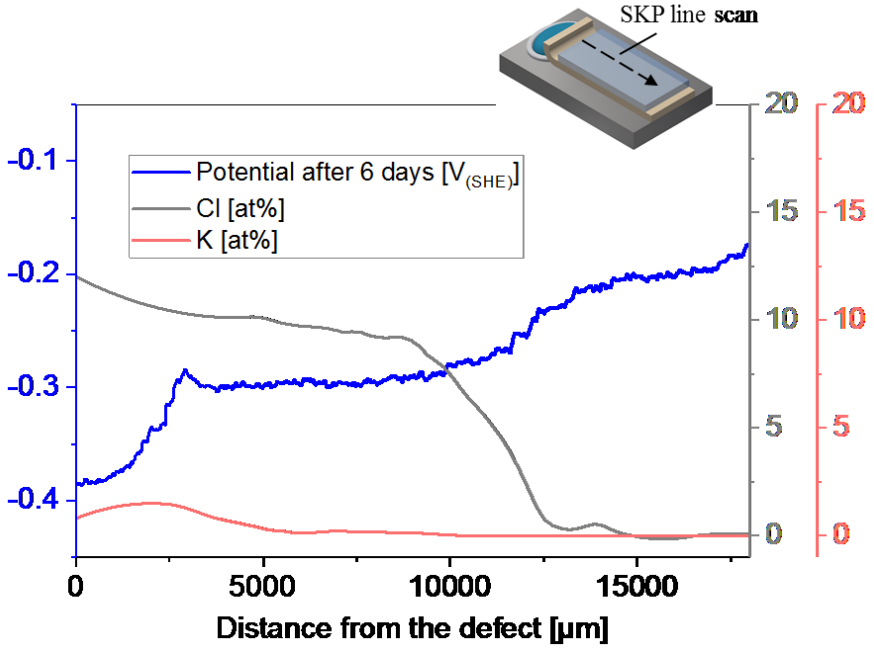

Figure 5.5 - Correlation between the SKP potential profiles in the closed joint geometry (without region I) after 7 days and the amount of K^+ or Cl^- ions measured with XPS after removal of the polymer and glass (from Figure 4.17)

Joint design guidelines

Based on the findings of this work, guidelines for the design of steel/Acronal bonded joints will be recommended in this section. In a summary, it was shown for this adhesive system that two delamination mechanisms can take place; the cathodic delamination mechanism occurs when there is an excess of adhesive outside of the joint (here named region I), this excess prevents the Cl^- ions to reach the adhesive joint interphase. Whereas anodic undermining occurs when there is no adhesive excess outside of the joint (*i.e.* geometry without region I). In this case not only cations but also anions have access to the joint interphase and, due to the differential aeration cell formation, the reduction of oxygen takes place outside the joint and therefore the Cl^- ions migrate from the defect to the metal/polymer interphase where metal dissolution and rusting takes place.

In general this excess of adhesive outside of the joint, could be correlated with the fillet (see Figure 1.5 and Figure 1.6), which is usually used in the joint design to improve the joint strength and corrosion resistance. It should, therefore, be considered during design that the use or not of fillets could lead, when the joint is exposed to corrosive media, to a change in the delamination mechanism, *e.g.* from cathodic delamination (filleted) to anodic undermining (unfilleted). These joint geometries are sketched in Figure 5.6, designs *B* and *D*, respectively.

Furthermore, from the results presented in Figure 5.2 a useful design recommendation in the case of the filleted joint, is the sealing of the other joint edges (design *A* from Figure 5.6). This could discontinue the delamination as it advances from the fillet and reaches the joint interface. The aforementioned approach, however, is in theory probably not helpful in the case of the unfilleted joints (design *C* from Figure 5.6) once the delamination mechanism is the anodic undermining. In this case the oxygen reduction takes place outside the joint, so the delamination would probably advance even with the joint edges sealed.

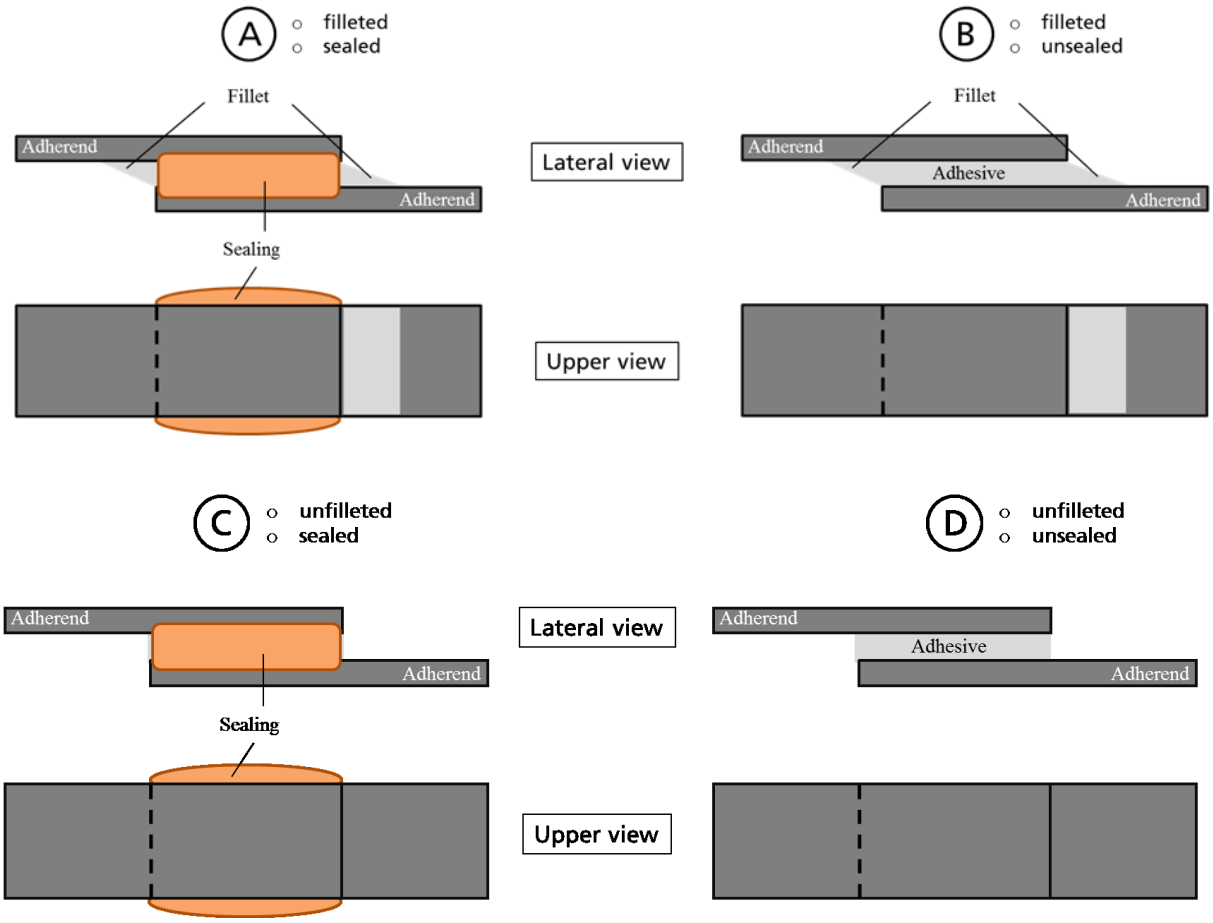

Figure 5.6 – Design of filleted and unfilleted joints

The summary of the design types and the possible corrosion behavior are presented in

Table 5-1 below. It is important to mention that although these guidelines are useful for understanding how the corrosion mechanisms are influenced by different joint geometries, corrosion development is determined by the complete system, *i. e.* the combination of materials properties and environmental conditions. Therefore, further investigations are needed for the design of bonded components with other adhesive/substrate materials, geometries and environmental conditions.

Table 5-1 - Summary of design types and the corrosion behavior

Design type	Delamination mechanism	Adherend rusting
A	Cathodic delamination (might be possible to avoid)	Outside the joint
B	Cathodic delamination	Outside the joint
C	Anodic undermining	Inside the joint
D	Anodic undermining	Inside the joint

Epoxy System

A delamination test was performed in a closed joint geometry using an unmodified epoxy system in order to assess the usability of this method for assessing the delamination with other adhesive systems. Figure 5.7 shows the sample sketch, the line scan and potential profiles measured with the SKP. It is possible to see the delamination front advancing with delamination time, however, the absolute potential values are more negative when compared with the Acronal system. Furthermore, the delamination rate is slower for the Epoxy system, after 7 days the delamination front shows a displacement of only 750µm while for the Acronal (sample from Figure 4.2) the delamination front advanced 3000µm after the same time frame. Also, the plot of the delaminated distance vs. the square root of time in Figure 5.8 shows that the slope of the fitted line is 5.7µm/min$^{1/2}$, while for the Acronal system it is 45µm/min$^{1/2}$ (value from Figure 4.6).

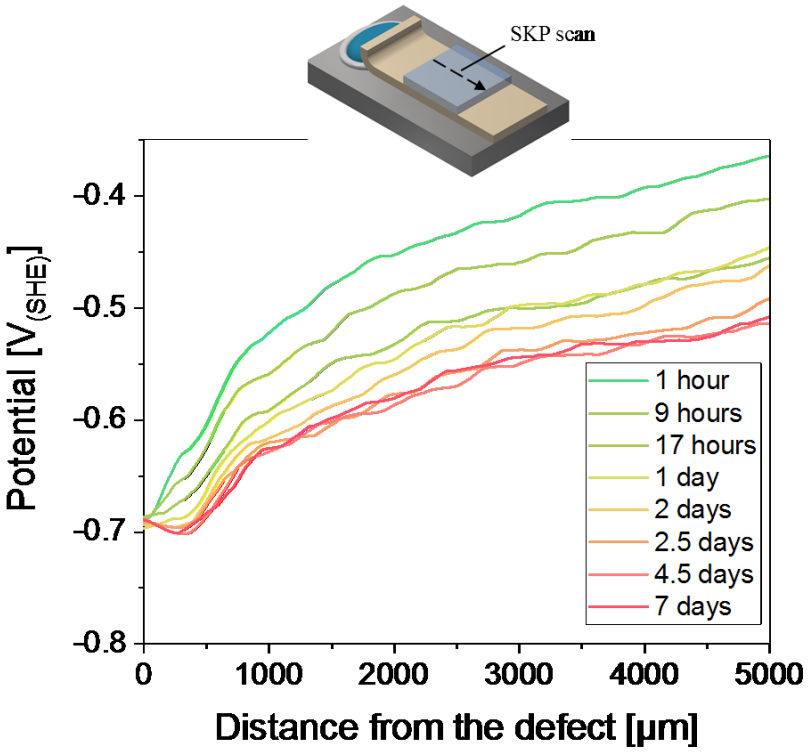

Figure 5.7 - Typical potential distributions for the epoxy system sample without region I in humid air (>95% r.h.) for different delamination times. Electrolyte in the defect: 0.5M NaCl(aq)

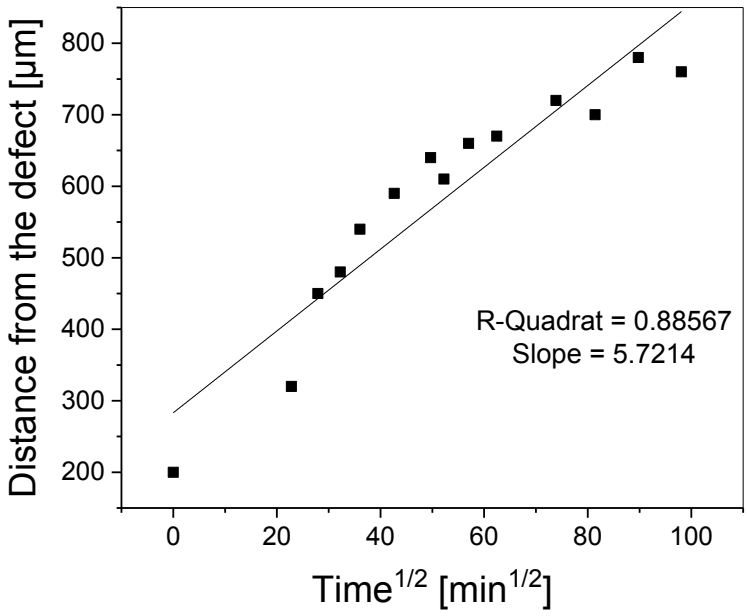

Figure 5.8 - Plot of the delaminated distance (x_{del}) vs. square root of time ($\sqrt{(t_{del})}$)

In principle, the method can be useful to have a fast first assessment on the delamination kinetics of different adhesive systems. However, additional delamination tests and/or surface analyses are required for further detailed information of the type of mechanisms taking place.

SKP vs. Immersion tests

Immersion tests are common for assessing the corrosion resistance of coatings and adhesive joints (Sørensen et al. 2010b; Kinloch et al. 2000), it is thus interesting to compare the new methodology described in this work with the usual immersion tests. Sørensen *et al.* (Sørensen et al. 2010b) evaluated the extent of the cathodic delamination in coated and bonded samples by immersion tests. Figure 5.9 shows the results obtained by the authors vs. the results obtained in the present work. Although the literature results were obtained for a different adhesive system (epoxy), the delamination kinetics are comparable. For the closed joint the delamination rate is reduced in around 100 times in comparison to open joint geometry for both studies.

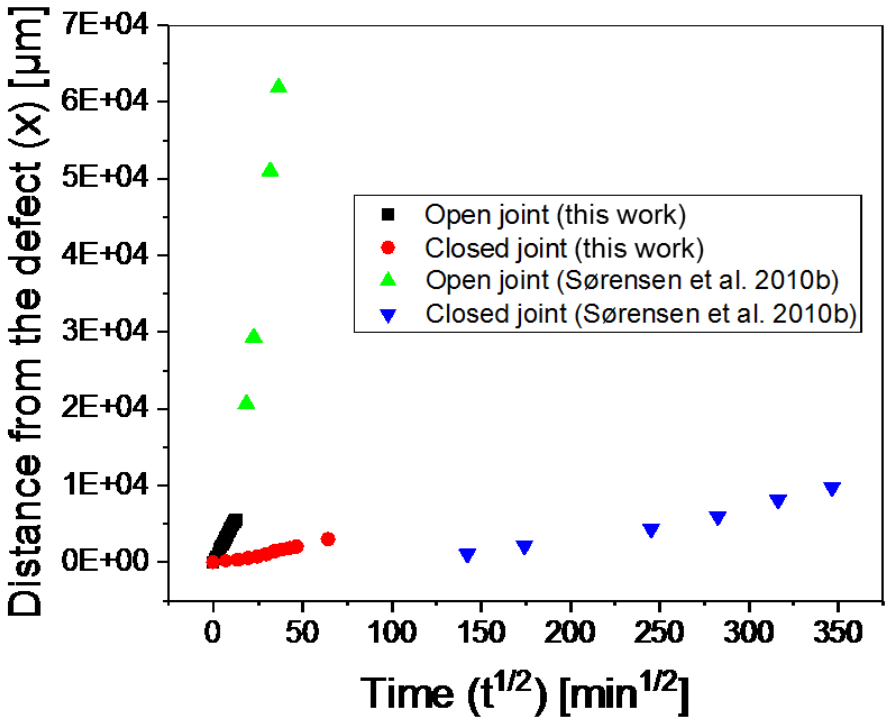

Figure 5.9 - Plot of the delaminated distance (x_{del}) vs. square root of time ($\sqrt{(t_{del})}$), data in black and red from Figure 4.6 (Acronal) and in green and blue from reference (epoxy system) (Sørensen et al. 2010b) . Electrolytes: NaCl 0.5M (this work) and KCl 0.5M (Sørensen et al. 2010b)

Some advantages and disadvantages of the SKP tests vs. immersion tests are summarized in Table 5-2 and will be discussed as follows.

Table 5-2 – Comparison SKP delamination tests vs. immersion tests.

	SKP delamination tests	**Immersion tests (Sørensen et al. 2010b)**
Test duration	5 – 10 days	3 months
Number of samples	2	10
Results evaluation (e.g. delaminated distance)	no further tests required	mechanical tests required
Early stage information	✓	✗
Measurements complexity	sophisticated and delicate	robust and versitale

The first remarkable point is the test duration difference among the two testing methods, immersion tests took around 3 months while the SKP results were obtained in 5 – 10 days. Furthermore, the SKP delamination tests required 2 samples only, whereas the results from literature each point in the diagram correspond to one sample, totalizing 10 samples. Another unique advantage of the SKP method is the possibility to obtain early stage information, the first micrometers of delamination can be detected already in the first days of measurement. Besides, the results obtained with the SKP are straight forward, meaning that the delaminated distance can be directly obtained by the SKP potential curves, while for the immersion tests further mechanical tests have to be performed.

Although the SKP method shows several advantages in correlation to immersion tests, the drawback is that it is a very delicate and complex technique. In addition, it is so far only suitable for really thin adhesive and barrier layers, while immersion tests are quite robust and versatile in this regard.

5.2. NOVEL CONTRIBUTIONS OF THE PRESENT RESEARCH WORK

In this study the applicability of the SKP technique was confirmed for the analysis of the ageing of organic adhesives bonded to metallic substrates, in line with previous literature (Leng et al. 1998c). With respect to previous studies, it was possible to monitor *in situ* the advancement of

a delamination at a metal/adhesive joint interphase in a closed geometry, realized with an adhesive layer sandwiched between a metal substrate and a thin borosilicate glass layer.

The evolution of the potential profiles across the entire joint region and the delamination kinetics were derived quantitatively from SKP measurements. The ingress of cations at the adhesive/metal interphase was investigated, revealing that the transport of cations at the interphase is the delamination-rate determining step for open adhesive coating. This is not the case for closed joint geometries, in which the delamination reaction is rather limited by the ingress and availability of oxygen at the delamination front in case of cathodic delamination. Furthermore, depending on the geometry of the joint, the delamination mechanism might change from cathodic delamination to anodic undermining.

5.3. SUGGESTIONS FOR FUTURE RESEARCH

The presented new approach can be a powerful tool to reveal early-stage information on time dependent development of ageing processes and provides the groundwork for future studies assessing the ageing mechanisms occurring in adhesively bonded joints exposed to corrosive media.

Since the present research revealed the delamination mechanisms occurring in one water based adhesive system bonded to steel, future studies should focus in other joint systems and geometries. For instance, the so called bondline corrosion (W.Brockmann, O.-D.Hennemann, H.Kollek, C.Matz 1986) is the typical delamination mechanism occurring in bonded aluminium when exposed to corrosive media. Supplementary insights on this mechanism could be obtained using the presented new approach.

In terms of further validation of the proposed method for the analysis of the delamination of bonded joints, for future research it could be interesting have a deeper understanding on the correlations among the proposed method with other types of ageing tests, such as the commonly performed immersion tests.

6. References

Abrahami, Shoshan T.; Hauffman, Tom; M.M. de Kok, John; Terryn, Herman; Mol, Johannes M.C. (2017): Adhesive Bonding and Corrosion Performance Investigated as a Function of Aluminum Oxide Chemistry and Adhesives. In: *CORROSION* 73 (8), S. 903–914. DOI: 10.5006/2391.

Adams, Robert D. (2005): Adhesive bonding. Science, technology and applications. Boca Raton, FL, Cambridge: CRC Press. Online verfügbar unter http://search.ebscohost.com/login.aspx?direct=true&scope=site&db=nlebk&db=nlabk&AN=137811.

Adams, Robert D.; Comyn, John; Wake, William C. (1997): Structural adhesive joints in engineering. 2. ed. London: Chapman & Hall.

DIN EN 923, 2016-03: Adhesives - Terms and definitions.

Al-Harthi, Mamdouh; Loughlin, Kevin; Kahraman, Ramazan (2007): Moisture diffusion into epoxy adhesive: testing and modeling. In: *Adsorption* 13 (2), S. 115–120. DOI: 10.1007/s10450-007-9011-y.

Andreon, B.; Guenther, B. L.; Cavalcanti, W. L.; Colombi Ciacchi, L.; Plagemann, P. (2019): On the use of scanning Kelvin probe for assessing in situ the delamination of adhesively bonded joints. In: *Corrosion Science*.

Bajaj, P.; Goyal, Meenakshi; Chavan, R. B. (1994): Synthesis and characterization of methacrylic acid–ethyl acrylate copolymers. In: *J. Appl. Polym. Sci.* 53 (13), S. 1771–1783. DOI: 10.1002/app.1994.070531307.

Bautista, A. (1996): Filiform corrosion in polymer-coated metals. In: *Progress in Organic Coatings* 28 (1), S. 49–58. DOI: 10.1016/0300-9440(95)00555-2.

Beber, V. C.; Fernandes, P.H.E.; Schneider, B.; Brede, M.; Mayer, B. (2017): Fatigue lifetime prediction of adhesively bonded joints. An investigation of the influence of material model and multiaxiality. In: *International Journal of Adhesion and Adhesives* 78, S. 240–247. DOI: 10.1016/j.ijadhadh.2017.08.007.

DIN EN ISO 12944-5, 2018-06: Beschichtungsstoffe - Korrosionsschutz von Stahlbauten durch Beschichtungssysteme - Teil 5: Beschichtungssysteme.

Bi, Huichao; Sykes, John (2016): Cathodic delamination of unpigmented and pigmented epoxy coatings from mild steel. In: *Progress in Organic Coatings* 90, S. 114–125. DOI: 10.1016/j.porgcoat.2015.10.002.

Bischof, C.; Bauer, A.; Possart, W.; Kapelle, R.; Schulze, R. D. (1989): Zur Adhäsion in Metall-Polymer-Grenzschichten und ihrer praktischen Nutzung. In: *Acta Polym.* 40 (3), S. 214–221. DOI: 10.1002/actp.1989.010400309.

Brémont, M.; Brockmann, W. (1996): Comparison of the Degradation Mechanisms of Zinc-Coated Steel, Cold-Rolled Steel, and Aluminium/Epoxy Bonded Joints. In: *The Journal of Adhesion* 58 (1-2), S. 69–99. DOI: 10.1080/00218469608014400.

Cambier, S. M.; Verreault, D.; Frankel, G. S. (2014): Raman Investigation of Anodic Undermining of Coated Steel During Environmental Exposure. In: *CORROSION* 70 (12), S. 1219–1229. DOI: 10.5006/1358.

Camp, J. B.; Darling, T. W.; Brown, Ronald E. (1991): Macroscopic variations of surface potentials of conductors. In: *Journal of Applied Physics* 69 (10), S. 7126–7129. DOI: 10.1063/1.347601.

Cappadonia, Marcella; Doblhofer, Karl; Jauch, Matthias (1988): The Electrical State of an Ion-Exchange Membrane Surface after Emersion from Liquid Electrolytes. In: *Berichte der Bunsengesellschaft für physikalische Chemie* 92 (8), S. 903–908. DOI: 10.1002/bbpc.198800218.

Ceresana (2017): Market Study: Adhesives - World. Constance, Germany. Online verfügbar unter https://www.ceresana.com/en/market-studies/industry/adhesives-world/.

Cornell, Rochelle M.; Schwertmann, Udo (2003): The Iron Oxides. Structure, Properties, Reactions, Occurences and Uses. 2nd, Completely Revised and Extended ed. Weinheim: Wiley-VCH. Online verfügbar unter http://www.myilibrary.com/?id=56077.

Crank, John (1976): The mathematics of diffusion. 2. ed., reprint. Oxford: Clarendon Press.

Davis, G. D.; Whisnant, P. L.; Venables, J. D. (1995): Subadhesive hydration of aluminum adherends and its detection by electrochemical impedance spectroscopy. In: *Journal of Adhesion Science and Technology* 9 (4), S. 433–442. DOI: 10.1163/156856195X00374.

Derjaguin, B. V.; Smilga, V. P. (1967): Electronic Theory of Adhesion. In: *Journal of Applied Physics* 38 (12), S. 4609–4616. DOI: 10.1063/1.1709192.

Dillard, David A. (2010): Advances in structural adhesive bonding. Boca Raton, Fla, Oxford: Woodhead Pub. Ltd (Woodhead Publishing Series in Welding and Other Joining Technologies). Online verfügbar unter http://site.ebrary.com/lib/alltitles/docDetail.action?docID=10654043.

DIN 50035:2012-09.

Ding, Yifu; Liu, Mojun; Li, Shanjun; Zhang, Shuyong; Zhou, Wei-Fang; Wang, Bo (2001): Contributions of the Side Groups to the Characteristics of Water Absorption in Cured Epoxy Resins. In: *Macromol. Chem. Phys.* 202 (13), S. 2681–2685. DOI: 10.1002/1521-3935(20010901)202:13<2681::AID-MACP2681>3.0.CO;2-E.

Doblhofer, K.; Armstrong, R. D. (1988): Membrane-type coatings on electrodes. In: *Electrochimica Acta* 33 (4), S. 453–460. DOI: 10.1016/0013-4686(88)80162-2.

Doherty, M.; Sykes, J. M. (2004): Micro-cells beneath organic lacquers: a study using scanning Kelvin probe and scanning acoustic microscopy. In: *Corrosion Science* 46 (5), S. 1265–1289. DOI: 10.1016/j.corsci.2003.09.016.

Ebnesajjad, Sina; Landrock, Arthur (2015): Adhesives technology handbook. 3. ed. Amsterdam: Elsevier/William Andrew.

F. M. Fowkes, in R. L. Patrick,. Treatise on Adhesion and Adhesives (1967). In: *M. Dekker Inc., New York* (Vol. 1).

Fell, Christopher J. d.; Hutchison, H. Peter. (1971): Diffusion coefficients for sodium and potassium chlorides in water at elevated temperatures. In: *J. Chem. Eng. Data* 16 (4), S. 427–429. DOI: 10.1021/je60051a005.

Fowkes, F. M. (1964): Attractive forces at interfaces. In: *Industrial & Engineering Chemistry* (Vol. 56), S. 40–52.

Fürbeth, W.; Stratmann, M. (1995): Investigation of the delamination of polymer films from galvanized steel with the Scanning Kelvinprobe. In: *Analytical and bioanalytical chemistry* 353 (3-4), S. 337–341. DOI: 10.1007/s0021653530337.

Fürbeth, W.; Stratmann, M. (2001a): The delamination of polymeric coatings from electrogalvanised steel – a mechanistic approach. In: *Corrosion Science* 43 (2), S. 207–227. DOI: 10.1016/S0010-938X(00)00047-0.

Fürbeth, W.; Stratmann, M. (2001b): The delamination of polymeric coatings from electrogalvanized steel – a mechanistic approach. In: *Corrosion Science* 43 (2), S. 229–241. DOI: 10.1016/S0010-938X(00)00048-2.

Fürbeth, W.; Stratmann, M. (2001c): The delamination of polymeric coatings from electrogalvanized steel – a mechanistic approach. In: *Corrosion Science* 43 (2), S. 243–254. DOI: 10.1016/S0010-938X(00)00049-4.

ISO 4287:1997: Geometrical Product Specifications (GPS) -- Surface texture: Profile method -- Terms, definitions and surface texture parameters.

Gledhill, R. A.; Kinloch, A. J. (2006): Environmental Failure of Structural Adhesive Joints. In: *The Journal of Adhesion* 6 (4), S. 315–330. DOI: 10.1080/00218467408075035.

Good, Robert J. (1964): Theory for the Estimation of Surface and Interfacial Energies. In: Frederick M. Fowkes (Hg.): Contact Angle, Wettability and Adhesion, Bd. 43. [Place of publication not identified]: AMERICAN CHEMICAL SOCIETY (Advances in Chemistry Ser, No. 43), S. 74–87.

Good, Robert J. (1975): Spreading pressure and contact angle. In: *Journal of Colloid and Interface Science* 52 (2), S. 308–313. DOI: 10.1016/0021-9797(75)90205-2.

Goossens, E.L.J; van der Zanden, A.J.J; van der Spoel, W.H (2004): The measurement of the moisture transfer properties of paint films using the cup method. In: *Progress in Organic Coatings* 49 (3), S. 270–274. DOI: 10.1016/j.porgcoat.2003.10.008.

Grundmeier, G.; Jüttner, K.; Stratmann, Martin (2006): Novel Electrochemical Techniques in Corrosion Research. In: R. W. Cahn, P. Haasen und E. J. Kramer (Hg.): Materials Science and Technology, Bd. 144. Weinheim, Germany: Wiley-VCH Verlag GmbH & Co. KGaA, S. 2986.

Grundmeier, G.; Reinartz, C.; Rohwerder, M.; Stratmann, M. (1998): Corrosion properties of chemically modified metal surfaces. In: *Electrochimica Acta* 43 (1-2), S. 165–174. DOI: 10.1016/S0013-4686(97)00221-1.

Grundmeier, G.; Stratmann, M. (2005): ADHESION AND DE-ADHESION MECHANISMS AT POLYMER/METAL INTERFACES. Mechanistic Understanding Based on In Situ Studies of Buried Interfaces. In: *Annu. Rev. Mater. Res.* 35 (1), S. 571–615. DOI: 10.1146/annurev.matsci.34.012703.105111.

Habenicht, Gerd (2006): Kleben. Grundlagen, Technologien, Anwendungen. 5., erweiterte und aktualisierte Auflage (VDI-Buch). Online verfügbar unter http://dx.doi.org/10.1007/3-540-31223-4.

Habenicht, Gerd (2016): Kleben - erfolgreich und fehlerfrei. Handwerk, Praktiker, Ausbildung, Industrie. 7., überarbeitete und aktualisierte Auflage. Wiesbaden: Springer Vieweg. Online verfügbar unter http://dx.doi.org/10.1007/978-3-658-14696-2.

Hamann, Carl H.; Vielstich, Wolf (2005): Elektrochemie. 4., vollständig überarbeitete und aktualisierte Auflage. Weinheim: Wiley-VCH-Verlag GmbJ &Co. KGaA. Online verfügbar unter http://deposit.ddb.de/cgi-bin/dokserv?id=2615658&prov=M&dok_var=1&dok_ext=htm.

Hausbrand, R.; Stratmann, M.; Rohwerder, M. (2008): The Physical Meaning of Electrode Potentials at Metal Surfaces and Polymer/Metal Interfaces: Consequences for Delamination. In: *J. Electrochem. Soc.* 155 (7), C369. DOI: 10.1149/1.2926589.

Heil, H.; Steiger, J.; Karg, S.; Gastel, M.; Ortner, H.; Seggern, H. von; Stößel, M. (2001): Mechanisms of injection enhancement in organic light-emitting diodes through an Al/LiF electrode. In: *Journal of Applied Physics* 89 (1), S. 420–424. DOI: 10.1063/1.1331651.

Heinz, William F.; Hoh, Jan H. (1999): Relative Surface Charge Density Mapping with the Atomic Force Microscope. In: *Biophysical Journal* 76 (1), S. 528–538. DOI: 10.1016/S0006-3495(99)77221-8.

Ilie, A.; Hart, A.; Flewitt, A. J.; Robertson, J.; Milne, W. I. (2000): Effect of work function and surface microstructure on field emission of tetrahedral amorphous carbon. In: *Journal of Applied Physics* 88 (10), S. 6002–6010. DOI: 10.1063/1.1314874.

Jacobs, H. O.; Knapp, H. F.; Müller, S.; Stemmer, A. (1997): Surface potential mapping: A qualitative material contrast in SPM. In: *Ultramicroscopy* 69 (1), S. 39–49. DOI: 10.1016/S0304-3991(97)00027-2.

Kelvin (2009): V. Contact electricity of metals. In: *The London, Edinburgh, and Dublin Philosophical Magazine and Journal of Science* 46 (278), S. 82–120. DOI: 10.1080/14786449808621172.

Khun, N. W.; Frankel, G. S. (2013): Effects of surface roughness, texture and polymer degradation on cathodic delamination of epoxy coated steel samples. In: *Corrosion Science* 67, S. 152–160. DOI: 10.1016/j.corsci.2012.10.014.

Kinloch, A. J. (1980): The science of adhesion. In: *J Mater Sci* 15 (9), S. 2141–2166. DOI: 10.1007/BF00552302.

Kinloch, A. J. (1982): The science of adhesion. In: *J Mater Sci* 17 (3), S. 617–651. DOI: 10.1007/BF00540361.

Kinloch, A. J.; Korenberg, C. F.; Tan, K. T.; Watts, J. F. (2007): Crack growth in structural adhesive joints in aqueous environments. In: *J Mater Sci* 42 (15), S. 6353–6370. DOI: 10.1007/s10853-006-1181-6.

Kinloch, A.J; Little, M.S.G; Watts, J.F (2000): The role of the interphase in the environmental failure of adhesive joints. In: *Acta Materialia* 48 (18-19), S. 4543–4553. DOI: 10.1016/S1359-6454(00)00240-8.

Kohlrausch, F. (2014): Praktische physik. Zum gebrauch fr unterricht, forschung und technik volume 3. [Place of publication not identified]: Morgan Kaufmann.

Koley, G.; Spencer, M. G. (2001): Surface potential measurements on GaN and AlGaN/GaN heterostructures by scanning Kelvin probe microscopy. In: *Journal of Applied Physics* 90 (1), S. 337–344. DOI: 10.1063/1.1371941.

Kropka, Jamie M.; Adolf, Douglas B.; Spangler, Scott; Austin, Kevin; Chambers, Robert S. (2015): Mechanisms of degradation in adhesive joint strength. Glassy polymer thermoset bond in a humid environment. In: *International Journal of Adhesion and Adhesives* 63, S. 14–25. DOI: 10.1016/j.ijadhadh.2015.07.014.

Leblanc, Patrick P.; Frankel, G. S. (2004): Investigation of Filiform Corrosion of Epoxy-Coated 1045 Carbon Steel by Scanning Kelvin Probe Force Microscopy. In: *J. Electrochem. Soc.* 151 (3), B105. DOI: 10.1149/1.1641038.

Lee, Lieng-Huang (1994): Molecular Bonding and Adhesion at Polymer-Metal Interphases. In: *The Journal of Adhesion* 46 (1-4), S. 15–38. DOI: 10.1080/00218469408026646.

Legghe, Elise; Aragon, Emmanuel; Bélec, Lénaïk; Margaillan, André; Melot, Denis (2009): Correlation between water diffusion and adhesion loss: Study of an epoxy primer on steel. In: *Progress in Organic Coatings* 66 (3), S. 276–280. DOI: 10.1016/j.porgcoat.2009.08.001.

Leidheiser, H.; Deck, P. D. (1988): Chemistry of the metal-polymer interfacial region. In: *Science (New York, N.Y.)* 241 (4870), S. 1176–1181. DOI: 10.1126/science.241.4870.1176.

Leidheiser, Henry (1982): Corrosion of Painted Metals—A Review. In: *CORROSION* 38 (7), S. 374–383. DOI: 10.5006/1.3581899.

Leidheiser, Henry; Wang, Wendy; Igetoft, Lars (1983): The mechanism for the cathodic delamination of organic coatings from a metal surface. In: *Progress in Organic Coatings* 11 (1), S. 19–40. DOI: 10.1016/0033-0655(83)80002-8.

Lenderink, Hermen Jan Willem (1995): Filiform corrosion of coated aluminium alloys. A study of mechanisms. @Delft, Techn. Univ., Diss. : 1995. Delft: Univ.

Leng, A.; Streckel, H.; Hofmann, K.; Stratmann, M. (1998a): The delamination of polymeric coatings from steel Part 3. Effect of the oxygen partial pressure on the delamination reaction and current distribution at the metal/polymer interface. In: *Corrosion Science* 41 (3), S. 599–620. DOI: 10.1016/S0010-938X(98)00168-1.

Leng, A.; Streckel, H.; Hofmann, K.; Stratmann, M. (1998b): The delamination of polymeric coatings from steel Part 3: Effect of the oxygen partial pressure on the delamination reaction and current distribution at the metal/polymer interface. In: *Corrosion Science* 41 (3), S. 599–620. DOI: 10.1016/S0010-938X(98)00168-1.

Leng, A.; Streckel, H.; Stratmann, M. (1998c): The delamination of polymeric coatings from steel. Part 1. Calibration of the Kelvinprobe and basic delamination mechanism. In: *Corrosion Science* 41 (3), S. 547–578. DOI: 10.1016/S0010-938X(98)00166-8.

Leng, A.; Streckel, H.; Stratmann, M. (1998d): The delamination of polymeric coatings from steel. Part 1: Calibration of the Kelvinprobe and basic delamination mechanism. In: *Corrosion Science* 41 (3), S. 547–578. DOI: 10.1016/S0010-938X(98)00166-8.

Leng, A.; Streckel, H.; Stratmann, M. (1998e): The delamination of polymeric coatings from steel. Part 2. First stage of delamination, effect of type and concentration of cations on delamination, chemical analysis of the interface. In: *Corrosion Science* 41 (3), S. 579–597. DOI: 10.1016/S0010-938X(98)00167-X.

Leng, A.; Streckel, H.; Stratmann, M. (1998f): The delamination of polymeric coatings from steel. Part 2: First stage of delamination, effect of type and concentration of cations on delamination, chemical analysis of the interface. In: *Corrosion Science* 41 (3), S. 579–597. DOI: 10.1016/S0010-938X(98)00167-X.

Lu, Zhiguo; Wang, Peichung; Lin, Jianping; Wang, Liying; Li, Gang (2011): Effect of moisture content in uncured adhesive on static strength of bonded galvanized DP600 steel joints. In: *International Journal of Adhesion and Adhesives* 31 (4), S. 202–208. DOI: 10.1016/j.ijadhadh.2011.01.004.

Marcus, P. (2002): Corrosion mechanisms in theory and practice. 2nd ed., rev. and expanded. New York: Marcel Dekker (Corrosion technology, 17).

Mathakiya, Ismail; Rao, P. V. C.; Rakshit, A. K. (2001): Synthesis and characterization of styrene-acrylic ester copolymers. In: *J. Appl. Polym. Sci.* 79 (8), S. 1513–1524. DOI: 10.1002/1097-4628(20010222)79:8<1513::AID-APP190>3.0.CO;2-I.

McCafferty, E. (2010): Corrosion Under Organic Coatings. In: Edward McCafferty (Hg.): Introduction to Corrosion Science. New York, NY: Springer Science+Business Media LLC, S. 403–425.

McMurray, H. N.; Williams, G. (2002): Probe diameter and probe–specimen distance dependence in the lateral resolution of a scanning Kelvin probe. In: *Journal of Applied Physics* 91 (3), S. 1673–1679. DOI: 10.1063/1.1430546.

Nazarov, A.; Thierry, D. (2010): Influence of Electrochemical Conditions in a Defect on the Mode of Paint Corrosion Delamination from a Steel Surface. In: *CORROSION* 66 (2), 025004-025004-10. DOI: 10.5006/1.3319661.

Nazarov, Andrej; Le Bozec, Nathalie; Thierry, Dominique (2018): Assessment of steel corrosion and deadhesion of epoxy barrier paint by scanning Kelvin probe. In: *Progress in Organic Coatings* 114, S. 123–134. DOI: 10.1016/j.porgcoat.2017.09.016.

Orihuela, M. F.; Somoza, A. M.; Colchero, J.; Ortuño, M.; Palacios-Lidón, E. (2017): Localized charge imaging with scanning Kelvin probe microscopy. In: *Nanotechnology* 28 (2), S. 25703. DOI: 10.1088/1361-6528/28/2/025703.

Pethrick, Richard A. (2014): Design and ageing of adhesives for structural adhesive bonding – A review. In: *Proceedings of the Institution of Mechanical Engineers, Part L: Journal of Materials: Design and Applications* 229 (5), S. 349–379. DOI: 10.1177/1464420714522981.

Pfeiffer, M.; Leo, K.; Karl, N. (1996): Fermi level determination in organic thin films by the Kelvin probe method. In: *Journal of Applied Physics* 80 (12), S. 6880–6883. DOI: 10.1063/1.363757.

ISO 15105-1:2007: Plastics — Film and sheeting — Determination of gas-transmission rate — Part 1: Differential-pressure methods.

Posner, R.; Giza, G.; Marazita, M.; Grundmeier, G. (2010): Ion transport processes at polymer/oxide/metal interfaces under varying corrosive conditions. In: *Corrosion Science* 52 (5), S. 1838–1846. DOI: 10.1016/j.corsci.2010.01.034.

Posner, R.; Santa, M.; Grundmeier, G. (2011): Wet- and Corrosive De-Adhesion Processes of Water-Borne Epoxy Film Coated Steel. In: *J. Electrochem. Soc.* 158 (3), C29. DOI: 10.1149/1.3525239.

Posner, R.; Wapner, K.; Stratmann, M.; Grundmeier, G. (2009): Transport processes of hydrated ions at polymer/oxide/metal interfaces: Part 1. Transport at interfaces of polymer coated oxide covered iron and zinc substrates. In: *Electrochimica Acta* 54 (3), S. 891–899. DOI: 10.1016/j.electacta.2008.06.074.

Salerno, Marco; Dante, Silvia (2018): Scanning Kelvin Probe Microscopy. Challenges and Perspectives towards Increased Application on Biomaterials and Biological Samples. In: *Materials (Basel, Switzerland)* 11 (6). DOI: 10.3390/ma11060951.

Saraby-Reintjes, A. (1972): The differential aeration cell. In: *Journal of Electroanalytical Chemistry and Interfacial Electrochemistry* 37 (1), S. 357–360. DOI: 10.1016/S0022-0728(72)80240-7.

Shouldice, Grant T.D.; Vandezande, Gerald A.; Rudin, Alfred (1994): Practical aspects of the emulsifier-free emulsion polymerization of styrene. In: *European Polymer Journal* 30 (2), S. 179–183. DOI: 10.1016/0014-3057(94)90157-0.

Silva, Lucas F. M.; Sato, Chiaki (Hg.) (2013): Design of Adhesive Joints Under Humid Conditions. Berlin, Heidelberg, s.l.: Springer Berlin Heidelberg (Advanced Structured Materials, 25). Online verfügbar unter http://dx.doi.org/10.1007/978-3-642-37614-6.

Silva, Lucas Filipe Martins da; Öchsner, Andreas; Adams, Robert D. (2011a): Handbook of adhesion technology. Berlin: Springer (Springer Reference).

Silva, Lucas Filipe Martins da; Öchsner, Andreas; Adams, Robert D. (2011b): Handbook of adhesion technology. Berlin: Springer (Springer Reference).

Sørensen, P. A.; Dam-Johansen, K.; Weinell, C. E.; Kiil, S. (2010a): Cathodic delamination of seawater-immersed anticorrosive coatings. Mapping of parameters affecting the rate. In: *Progress in Organic Coatings* 68 (4), S. 283–292. DOI: 10.1016/j.porgcoat.2010.03.012.

Sørensen, P. A.; Dam-Johansen, K.; Weinell, C. E.; Kiil, S. (2010b): Cathodic delamination of seawater-immersed anticorrosive coatings: Mapping of parameters affecting the rate. In: *Progress in Organic Coatings* 68 (4), S. 283–292. DOI: 10.1016/j.porgcoat.2010.03.012.

Sørensen, P. A.; Dam-Johansen, K.; Weinell, C. E.; Kiil, S. (2010c): Cathodic delamination: Quantification of ionic transport rates along coating–steel interfaces. In: *Progress in Organic Coatings* 68 (1-2), S. 70–78. DOI: 10.1016/j.porgcoat.2009.08.018.

Sørensen, P. A.; Kiil, S.; Dam-Johansen, K.; Weinell, C. E. (2009): Influence of substrate topography on cathodic delamination of anticorrosive coatings. In: *Progress in Organic Coatings* 64 (2-3), S. 142–149. DOI: 10.1016/j.porgcoat.2008.08.027.

Stratmann, M.; Feser, R.; Leng, A. (1994): Corrosion protection by organic films. In: *Electrochimica Acta* 39 (8-9), S. 1207–1214. DOI: 10.1016/0013-4686(94)E0038-2.

Stratmann, M.; Streckel, H. (1990a): On the atmospheric corrosion of metals which are covered with thin electrolyte layers—I. Verification of the experimental technique. In: *Corrosion Science* 30 (6-7), S. 681–696. DOI: 10.1016/0010-938X(90)90032-Z.

Stratmann, M.; Streckel, H. (1990b): On the atmospheric corrosion of metals which are covered with thin electrolyte layers—II. Experimental results. In: *Corrosion Science* 30 (6-7), S. 697–714. DOI: 10.1016/0010-938X(90)90033-2.

Stratmann, M.; Streckel, H.; Feser, R. (1991): A new technique able to measure directly the delamination of organic polymer films. In: *Corrosion Science* 32 (4), S. 467–470. DOI: 10.1016/0010-938X(91)90126-A.

Stratmann, M.; Streckel, H.; Kim, K. T.; Crockett, S. (1990): On the atmospheric corrosion of metals which are covered with thin electrolyte layers-iii. the measurement of polarisation curves on metal surfaces which are covered by thin electrolyte layers. In: *Corrosion Science* 30 (6-7), S. 715–734. DOI: 10.1016/0010-938X(90)90034-3.

Taylor, D.M (2000): Developments in the theoretical modelling and experimental measurement of the surface potential of condensed monolayers. In: *Advances in Colloid and Interface Science* 87 (2-3), S. 183–203. DOI: 10.1016/S0001-8686(99)00044-5.

ASTM D1434: Test Method for Determining Gas Permeability Characteristics of Plastic Film and Sheeting.

Venables, J. D. (1984): Adhesion and durability of metal-polymer bonds. In: *J Mater Sci* 19 (8), S. 2431–2453. DOI: 10.1007/BF00550796.

Vojuckij, Sergej S. (1963): Autohesion and Adhesion of High Polymers. Interscience Publishers, New York, London, Sidney.

W.Brockmann, O.-D.Hennemann, H.Kollek, C.Matz (1986): Adhesion in bonded aluminium joints for aircraft construction. In: *International Journal of Adhesion and Adhesives*, S. 115–143.

Wapner, K.; Stratmann, M.; Grundmeier, G. (2006): In situ infrared spectroscopic and scanning Kelvin probe measurements of water and ion transport at polymer/metal interfaces. In: *Electrochimica Acta* 51 (16), S. 3303–3315. DOI: 10.1016/j.electacta.2005.09.024.

Watson, T. M.; Coleman, A. J.; Williams, G.; McMurray, H. N. (2014): The effect of oxygen partial pressure on the filiform corrosion of organic coated iron. In: *Corrosion Science* 89, S. 46–58. DOI: 10.1016/j.corsci.2014.08.004.

Weiss, J.; Voigt, M.; Kunze, C.; Sánchez, J. HuacujaE.; Possart, W.; Grundmeier, G. (2016): Ageing mechanisms of polyurethane adhesive/steel interfaces. In: *International Journal of Adhesion and Adhesives* 70, S. 167–175. DOI: 10.1016/j.ijadhadh.2016.06.009.

Wicinski, Mariusz; Burgstaller, Wolfgang; Hassel, Achim Walter (2016): Lateral resolution in scanning Kelvin probe microscopy. In: *Corrosion Science* 104, S. 1–8. DOI: 10.1016/j.corsci.2015.09.008.

Wicks, Zeno W. (2007): Organic coatings. Science and technology. 3rd ed. Hoboken, N.J: Wiley-Interscience. Online verfügbar unter http://site.ebrary.com/lib/alltitles/docDetail.action?docID=10278501.

Williams, G.; N. McMurray, H.; Hayman, D.; C. Morgan, P. (2001a): Time-lapse potentiometric imaging of active filiform corrosion using a scanning Kelvin probe technique. In: *PhysChemComm* 4 (6), S. 26. DOI: 10.1039/b100835h.

Williams, Geraint; Grace, Richard (2011): Chloride-induced filiform corrosion of organic-coated magnesium. In: *Electrochimica Acta* 56 (4), S. 1894–1903. DOI: 10.1016/j.electacta.2010.09.005.

Williams, Geraint; McMurray, H.Neil (2003): The mechanism of group (I) chloride initiated filiform corrosion on iron. In: *Electrochemistry Communications* 5 (10), S. 871–877. DOI: 10.1016/j.elecom.2003.08.008.

Williams, Geraint; Neil McMurray, H.; Worsley, David A. (2001b): Latent Fingerprint Detection Using a Scanning Kelvin Microprobe. In: *J. Forensic Sci.* 46 (5), 15103J. DOI: 10.1520/JFS15103J.

Wroblowa, H. S. (1992): Intermediate products of atmospheric oxygen reduction and the integrity of metal—organic coating interface. In: *Journal of Electroanalytical Chemistry* 339 (1-2), S. 31–40. DOI: 10.1016/0022-0728(92)80443-8.

Yee, Shelgon (1991): Application of a Kelvin Microprobe to the Corrosion of Metals in Humid Atmospheres. In: *J. Electrochem. Soc.* 138 (1), S. 55. DOI: 10.1149/1.2085578.

Zhang, Fan; Wang, Hui-Ping; Hicks, Christina; Yang, Xin; Carlson, Blair E.; Zhou, Qing (2013): Experimental study of initial strengths and hygrothermal degradation of adhesive joints between thin aluminum and steel substrates. In: *International Journal of Adhesion and Adhesives* 43, S. 14–25. DOI: 10.1016/j.ijadhadh.2013.01.001.

Zisman, W. A_. (1963): Influence of constitution on adhesion. In: *Industrial & Engineering Chemistry* (Vol.55, No. 10), S. 18–38.

In the dissertation the results from the supervision of the following students' works are included:

- Barbara Luiza Guenther, "*Study of the coating thickness, surface preparation, electrolyte type and concentration influence on the delamination of coated steel*", 2018.

Curriculum Vitae

Barbara Priscila Andreon

Place of birth: Indaial, Brazil
E-Mail: baandreon@gmail.com

EDUCATION

Jul 2015 – Dec 2019	**Doctoral work** performed at Fraunhofer IFAM and at University of Bremen, Bremen - Germany
Sep 2015 – Jun 2016	**European Adhesive Engineer** specialization course at Fraunhofer IFAM, Bremen - Germany
May 2008 – Feb 2014	**Materials Engineer** – graduated at Federal University of Santa Catarina (UFSC), Florianopolis – Brazil
	Bachelor thesis concluded at *Bundesanstalt für Materialforschung und –prüfung* (BAM), Berlin – Germany

PROFESSIONAL CARRER

Jun 2015 – Dec 2019 — Doctoral candidate at **Fraunhofer IFAM**, Bremen - Germany

Research in the Adhesive Bonding Technology and Surfaces department

- PhD work in the topic of ageing of adhesives
- Acquisition of European funding – Horizon 2020

Aug 2017 – currently — Lead of Research and Innovation at **WearHealth UG**, Bremen - Germany

Work in the topic of Industry 4.0 - wearables and AI for the safety of workers

- Acquisition of European and German funding
- Business development in Germany, France and Spain
- Industry 4.0, IoT, wearables, AI, machine learning

May 2013 – Jan 2014 — Intern at **Bundesanstalt für Materialforschung und –prüfung, (BAM)** Berlin - Germany

Bachelor thesis and internship in the topic of corrosion and electrochemistry

- November 2013 - Awarded with the first prize in the poster competition of the Annual Meeting of the GfKORR – *Gesellschaft für Korrosionsschutz e. V.*

May 2011 – Sep 2012 — Intern at **Fraunhofer-Gesellschaft IFAM**, Bremen – Germany

Internship in 2 departments of the institute:

- Shaping and Functional Materials
- Adhesive Bonding Technology and Surfaces

Mai 2010 – Sep 2010	Intern at **Bosch Rexroth**, Pomerode – Brazil

Internship in the R&D department

- Quality control of the surface treatment process
- Development of the capability of the process

LANGUAGES

Portuguese: Primary language / English: Fluent / German: Advanced

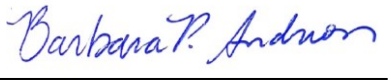

Bremen, November 2019 Barbara Priscila Andreon